Stochastic Optimal Control of Spacecraft

by

Eric Daniel Gustafson

A dissertation submitted in partial fulfillment
of the requirements for the degree of
Doctor of Philosophy
(Aerospace Engineering)
in The University of Michigan
2010

Doctoral Committee:

Professor Daniel J. Scheeres, Chair
Professor Pierre T. Kabamba
Professor N. Harris McClamroch
Professor Demosthenis Teneketzis

“Always keep Ithaca in your mind.
To arrive there is your ultimate goal.
But do not hurry the voyage at all.
It is better to let it last for many years;
and to anchor at the island when you are old,
rich with all you have gained on the way,
not expecting that Ithaca will offer you riches.

Ithaca has given you the beautiful voyage.
Without her you would have never set out on the road.
She has nothing more to give you.

And if you find her poor, Ithaca has not deceived you.
Wise as you have become, with so much experience,
you must already have understood what Ithacas mean.”

excerpt from *Ithaca*, by C.P. Cavafy

To Allison, my parents, and Allison's parents.

Thank you for all of your support.

Acknowledgments

I'd like to begin by thanking my advisor, Professor Daniel Scheeres. Had my advisor been any less patient, there may not have been a dissertation in which to thank him. Even though Professor Scheeres moved on to an endowed chair at the University of Colorado at Boulder during my studies, he was willing to keep me as a student here at Michigan. For this, I am extremely grateful.

Although there is no doubt that all professors and teachers I have had along the way have contributed to my education, I would like to specifically thank a few that stand out. First, I am very thankful for the other members of my committee: Professor McClamroch, Professor Kabamba, and Professor Teneketzis. I have learned a great deal from these excellent teachers. Another excellent professor who has had a lasting impact on me is Professor Howell at Purdue University.

Also, I am very thankful to Dr. Marci Paskowitz-Possner, Dr. Chandeok Park, and Dr. Ryan Park. Each of these former students of Professor Scheeres was responsible for educating me in some way.

During my undergraduate studies at Purdue, I was fortunate to be a Co-op student at the NASA Glenn Research Center. The "SPACE Team" gave so much knowledge, wisdom and insight that I will always feel indebted to them. Thank you, Ann Delleur, Jeff Hojnicki, Tom Kerslake, Dave McKissock, Tony Jannette, and Carlos Rodriguez. Also at Glenn, I had the privilege of working many other great people; Clint Ensworth, Dale Stalnaker, Bruce Manners, Dave Hoffman, John Riehl, Dr. Les Balkanyi, and others.

I also spent a summer at the Aerospace Corporation, where I worked with Dr. Jim

Gidney, Dr. Eric Campbell, Priya Sheth, Dr. Lael Woods, Dr. Mike Menn, Dr. Sante Scuro, John Cox, and others. Thank you all for the opportunity to learn so much from you! This is another group of people to which I feel indebted for all of their support and encouragement.

Also, I'd be remiss if I didn't thank the Michigan Space Grant Consortium for providing partial funding for my research.

Some of the best times I've had during graduate school have been spent with my colleagues; particularly with Dr. Andy Klesh and Dr. Amor Menezes. We've been called the "three amigos," but we all know we're closer to the "three stooges." Andy, Amor and I started graduate school at the same time; we then took classes together, took our quals together, beat our heads against walls together, and constantly learned from each other. They even stood in my wedding.

Along with Andy and Amor, I'd like to thank the rest of our office as well. To Erin Farbar, Pat Trizila, Dr. Nick Bisek, Matt Bennet, Chang-Kwon Kang, Dr. Emre Sozer, Jinhui Zhao, Jeremy Hanke, and the rest of the bunch: you are all awesome. It's been a pleasure sharing the converted lab space/office with you.

To the future generation of Flight Dynamics and Controls students – it's been an honor to work with all of you. Many thanks to Sara Spangelo and John Springmann, who have taken over my responsibilities on the RAX team.

Finally, my wife, Allison Craddock, has been infinitely patient and understanding while still knowing when to occasionally prod me. Thank you for "moving to my freaking state."

Table of Contents

List of Figures

Figure

List of Tables

Table

List of Appendices

Appendix

Abstract

This dissertation studies the influence of uncertainty on spacecraft control. The sources of the uncertainty are either imperfect state measurements or stochastic acceleration due to thruster noise. First, we analyze the impact of uncertainty in state measurements on the long-term cost of controlling an unstable periodic system. Under a specific procedure for updating control laws, we show that for unstable systems, there is an optimal time to perform updates in order to minimize the long-term cost per unit time.

Second, we consider the effect of stochastic acceleration due to thruster noise, which results in multiplicative noise on the control. Feedback control laws are obtained by numerically solving the stochastic Hamilton-Jacobi-Bellman equation using the spectral method. The optimal feedback control law for realistic noise levels is shown to differ significantly from the deterministic control. This suggests that trajectory planning would benefit from the inclusion of these stochastic effects.

Finally, we show that Taylor series expansions can be also be used to solve the stochastic Hamilton-Jacobi-Bellman equation under the fairly nonrestrictive assumption that the expansion is performed about an equilibrium point and that the gradient of the value function about the expansion point is zero. The Taylor series approach produces a system of ordinary differential equations describing the evolution of the coefficients in the power series. We show that in steady-state, a proper Taylor series may not exist, and that the proper solution is obtained through a Frobenius series expansion.

Chapter 1
Introduction

This dissertation studies the effects of uncertainty on the optimal control of spacecraft using low-thrust propulsion systems. Low-thrust electric propulsion systems are an enabling technology for several space missions including Deep Space 1, SMART-1, and Dawn. The primary benefit of electric propulsion is a dramatic reduction in propellant mass, and therefore mission cost, due to the high exhaust velocity of the thruster as compared to chemical propulsion. The necessary drawback of low thrust is that the thrusters must operate for long periods of time to achieve mission goals. This long thrusting time allows for uncertainty and stochastic effects to play a significant role in the dynamical evolution of a thrusting spacecraft.

We study these effects in two parallel approaches; in the first, we consider deterministic dynamics, but imperfect state measurements. Our goal is then to determine how to optimally update feedback control laws to minimize long-term cost. In the second approach, we assume perfect state knowledge, but allow for stochastic dynamics resulting from thruster noise. In this case, the problem is to derive the optimal feedback control law considering that increasing thruster force results in increased thrust fluctuations. In either case, knowledge of the future, conditioned on information in the present, is uncertain.

The initial motivation for this work was the desire to expand on Renault and Scheeres' work dealing with optimal timing of impulsive correction maneuvers for libration point orbiters [1]. Our extension was to consider the case of continuous control.

Additional motivation was drawn from experiments performed by Reid et al. [2], which

characterized the variations in thrust level for a Hall thruster. It is clear that significant discharge current fluctuations of about 10%-20% about the mean occur in the discharge chamber up to high frequencies (greater than 10^5 Hz). These current fluctuations are directly proportional to thrust variations. This suggests that analyzing the control force as stochastic, rather than deterministic, could be a more appropriate modelling approach.

1.1 Contributions and Outline

The following list is a summary of the primary contributions of this research:

- Development of a general theory that describes how best to schedule updates to the control law for unstable systems with continuous control and imperfect, discrete measurements.
- Analysis of *stochastic* optimal feedback control laws for spacecraft using the Spectral Method to numerically solve the stochastic Hamilton-Jacobi-Bellman equation.
- Taylor series (time-varying) and Frobenius (steady-state) series solutions of the stochastic Hamilton-Jacobi-Bellman equation.

The structure of the dissertation is as follows: Chapter 2 discusses the results for the case of imperfect measurements and deterministic dynamics. This approach uses tools familiar to aerospace engineers: Gaussian covariance propagation, deterministic optimal feedback control laws, dynamical systems theory, etc. The contribution of this chapter is the development of a general theory that describes how best to schedule updates to the control law for unstable systems with continuous control and imperfect, discrete measurements. The theory is applied to control about the relative equilibria and halo orbits in the Hill Three-Body Problem (H3BP).

Chapter 3 deals with our approach to numerically solving the optimal feedback control law for the stochastic case. We begin the chapter with some background information on stochastic calculus and proper stochastic modeling, which is typically unfamiliar to aerospace engineers. The remainder of the chapter discusses the solution method we use, the spectral method, and applications again to the H3BP. The primary contribution of this chapter is not the theoretical development or solution method, but the analysis of stochastic

optimal feedback control laws for spacecraft, which, to our knowledge, has not yet been performed. The result is a strong argument that control laws for spacecraft using noisy low-thrust propulsion are more properly developed in a stochastic framework instead of the standard deterministic one.

The final contribution of the dissertation is presented in Chapter 4, which describes an alternate approach to the stochastic optimal control problem. While Chapter 3 takes a global approach with the spectral method, Chapter 4 takes a local approach using Taylor series expansions. The contributions are the conditions under which these expansions are feasible, as well as applications to the Hill Restricted Three-Body Problem equilibrium points. Also, we develop the steady state solutions using Frobenius expansions.

1.2 Relevant Publications

The following publications are related to the subject matter of this dissertation.

- Gustafson, E. D. and Scheeres, D. J., "Optimal Timing of Control-Law Updates for Unstable Systems with Continuous Control," *Journal of Guidance, Control, and Dynamics*, Vol. 32, No. 3, May-June 2009, pp. 878–887.
- Gustafson, E. D. and Scheeres, D. J., "Spacecraft Stochastic Optimal Control," *AIAA/AAS Spaceflight Mechanics Meeting*, No. AAS 10-109, 2010.
- Gustafson, E. D. and Scheeres, D. J., "Optimal Timing of Control Law Updates for Unstable Systems with Continuous Control," *American Control Conference*, 2008. **Awarded Best Paper in Session Award.**
- Gustafson, E. D. and Scheeres, D. J., "Dynamically Relevant Local Coordinates for Halo Orbits," *Astrodynamics Specialist Conference*, 2008.
- Gustafson, E. D. and Scheeres, D. J., "Optimal Control of Uncertain Trajectories Using Continuous Thrust," *AIAA/AAS Spaceflight Mechanics Meeting*, 2007.

1.3 Deterministic, Uncertain, and Stochastic Systems

Deterministic Systems Astrodynamic systems are typically modeled with ordinary differential equations to describe how the positions and velocities of objects evolve under the influence of Newtonian gravity and other deterministic forces [8]. A primary concern of space mission design is the optimization of spacecraft trajectories to minimize fuel

consumption. Deterministic optimal control has a rich, well-established history and has been successfully applied to many space missions. Tools such as Pontryagin's Maximal Principle have provided the basis for many numerical approaches to efficiently solve for deterministic optimal control [9]. The Maximal Principle results in a Hamiltonian system, and Chan, et al. [10] have shown that Hamiltonian Systems theory may be used to obtain series solutions to the optimal feedback control law. The remarkable aspect of this approach is that truncation of the dynamics at a given order results in the terms of the true control law at that order. For example, if the dynamics are truncated at n-th order, then the resulting n-th order approximate control law will be the n-th order terms of the Taylor series expansion of the full nonlinear control law.

In practical applications, however, deterministic analysis is typically not sufficient. For example, spacecraft orbit maintainance and targeting require the analysis of state uncertainty. Often times, preliminary analysis will be performed in a deterministic framework, then uncertainty will be "superimposed" on top of the solution in an open-loop fashion.

Uncertain Systems The next level of realism past deterministic systems in to assume uncertainty throughout the analysis. In this approach, statistical maneuvers and targeting correction costs can be estimated *a priori*. An example of the benefits of this approach are given in the work by Renault and Scheeres [1], in which the authors estimate the cost of controlling a spacecraft in an unstable system using impulsive control.

When considering natural dynamics (uncontrolled dynamics), recent advances in uncertainty propagation have been made by Park and Scheeres [11], where the evolution of uncertainty distributions is computed using high order expansions of the dynamics. Also, their work develops the concept of "Nonlinear Statistical Targeting," *i.e.*, how to best target a future state given the uncertainties in the current state. The uncertainty analysis in this dissertation is limited to the linear case; however, the concepts developed by Park and Scheeres could be used to extend these results.

Stochastic Systems One further step of realism is to consider stochastic forces on the spacecraft. The source of such a random force could be natural, such as atmospheric drag, or it could be due to thruster noise. To our knowledge, the inclusion of thruster noise in the computation of optimal control laws has not been performed prior to this work. Despite this, the analysis of noisy control is very interesting, and is a field of active research. When the control itself is a source of noise, the optimal controller must balance increasing control against minimizing uncertainty.

The primary goal of considering stochastic accelerations in the control law design is to achieve better expected performance. We show that an optimal stochastic controller can outperform its deterministic counterpart for the systems studied. Although we restrict ourselves to fairly simple systems, the results are encouraging, and suggest that stochastic controllers also have a significant benefit when applied to more realistic spacecraft models.

Ultimately, the most realistic analysis would consider the combination of uncertain measurements *and* stochastic dynamics simultaneously, but this is left as future work.

Chapter 2

Uncertain Optimal Control: Control Law Update Timing

In this chapter, we describe a method to analyze the average (or ensemble) cost of optimal control near a periodic unstable trajectory. Specifically, we focus on control of the time-varying linear system resulting from linearizing the full dynamics about a nominal periodic trajectory. We consider a specific control strategy to take into account the finite horizon of the continuous control and uncertainty in the estimate of the state. This analysis is of direct application to the determination of mission operations for halo orbiters and for the budgeting of statistical fuel costs, especially for spacecraft in the highly unstable Earth-Moon system.

Previously, Renault and Scheeres [1] conducted a similar study of optimal statistical control which considered the placement of impulsive control maneuvers near an unstable equilibrium point. The results of this paper serve to reinforce key results in Renault and Scheeres such as the correlation between optimal control maneuver timing and the characteristic time of the instability of a system. Also, trends derived in Scheeres' previous work [12] concerning the qualitative impact of the update time on control cost using impulsive maneuvers are developed here for the continuous control case, and shown to be similar.

The control force and system dynamics are assumed to be deterministic, and the state estimates are assumed to have a Gaussian probability distribution. The Gaussian assumption is justified for this analysis because spacecraft uncertainties are almost always reported according to Gaussian statistics; more detailed information is not typically available. Additionally, this allows for the availability of analytical control laws for linear systems with

state uncertainty. Further analysis could be performed under non-Gaussian statistics. All system uncertainty is assumed to be adequately described by uncertainties in the estimation of the state. In addition, it is worthwhile to note that we focus on optimally updating control laws in the presence of uncertainty, not optimal control per se.

The motivation for these control law updates is as follows:

1. At some time t_1, we have an estimate of the state with a certain uncertainty level. The uncertainties at this point can be viewed as the steady-state uncertainties of an estimation process.

2. Based on the estimate of the state at t_1, we choose and implement a controller which would nominally cause the state to converge to the target state at time t_2 (in the absence of uncertainty).

3. At time t_2, error exists again due to uncertainties at time t_1.

This process repeats, and therefore there is a statistical cost associated with the steady-state control. It is also similar to the actual process used in spacecraft trajectory control [12]. To estimate this statistical cost, we evaluate the expected cost of the control from time interval t_i to t_{i+1} due to propagated uncertainties from interval t_{i-1} to t_i. During each interval, the control force is continuous; however, at the boundary between each interval, a discontinuity results from the choice of a new optimal control for the next control period.

In order to minimize the cost of regulating the system, we seek to minimize the average cost over time. To achieve this, one must find the time-between-updates that minimizes the expected cost per segment divided by the time-between-updates; $\mathrm{E}[J]/T_u$, where J is the cost incurred and T_u is the time-between-updates. That is, the optimal time-between-updates, T_u^*, is given by

$$T_u^* = \underset{T_u}{\operatorname{argmin}} \frac{\mathrm{E}[J]}{T_u}. \tag{2.1}$$

The time-between-updates is assumed to be a constant parameter over the analysis period of interest. This choice fits with our desire to develop a "steady state" control, and is

particularly appropriate considering our analysis of control in the vicinity of a periodic system, which naturally lends itself to a repetative control strategy.

We split the control problem into two pieces:

1. Determination of a control that targets the nominal periodic trajectory/state in a finite time, T_u.

2. Determination of the effect of state uncertainty on the nominal control, and how we can decrease the overall cost in the presence of uncertainty.

In problem (1) above, the control time, T_u, is a free parameter and, in the absence of noise, cost is reduced by taking $T_u \to \infty$, even for unstable systems.

For problem (2), where we do not know the precise initial state, we find that the error can have a catastrophic penalty if our dynamical system is unstable. Hence, this injects a specific "structure" or "natural time scale" into our control problem. This optimal update time is nominally related to the characteristic time scale of the instability. Although the control update time cannot be solved in closed form, even for simple linear systems, the natural dynamics still provide insight to its value. A simple control law elucidates the practical relevance of the unstable characteristic time when estimating the optimal update time, as will be discussed.

This combined control and measurement strategy is a periodic update procedure where the optimal control problem is solved using a finite-horizon time span equal to the time between control updates. This can be viewed as an extreme case of receding horizon control (RHC, or model predictive control, MPC) where the execution horizon is equal to the planning horizon. In RHC, the execution horizon is typically much shorter than the planning horizon [13, 14]; however, spacecraft state estimates are made using data from ground-based radar tracking stations, which perform measurements infrequently compared to typical RHC applications. This necessitates a relatively long execution horizon. Extending the planning horizon does allow for a lower expected cost; however, this also increases the steady-state

uncertainty, as shown later. For simplicity, we assume that the control update time equals the planning horizon. One could relax this assumption by modifying the cost function to be a weighted combination of fuel-based cost as well as some uncertainty cost, then solving for optimal values of both the update time and the horizon time. To further clarify, the typical application of RHC is to approximate a feedback control law, which is not the goal here. Instead, we are interested in optimizing the time between control law updates, which is the key parameter to our overall optimization process.

2.1 Deterministic Optimal Control Law

The system resulting from the linearization near a desired trajectory is a linear, time-varying system, written as

$$\dot{\vec{x}} = \mathbf{A}(t)\vec{x} + \mathbf{B}\vec{u}.$$

Our control objective is to minimize the energy expended over a finite horizon,

$$J^*(t_0, t_f) = \min_{\vec{u}} \frac{1}{2} \int_{t_0}^{t_f} \vec{u} \cdot \vec{u} \, dt, \tag{2.2}$$

subject to the boundary conditions of a given initial state and a hard terminal constraint;

$$\vec{x}(t_0) = \vec{x}_0, \quad \text{given}$$
$$\vec{x}(t_f) = \vec{0}.$$

Our method of choice to integrate this system numerically is the sweep method [9], which is an efficient and robust method for linear systems with terminal constraints. The sweep method for this optimization problem involves the numerical integration of two linear

matrix differential equations:

$$\dot{\mathbf{R}}(t;t_0,t_f) = -\mathbf{A}^{\mathrm{T}}\mathbf{R}(t;t_0,t_f),$$
$$\dot{\mathbf{Q}}(t;t_0,t_f) = \mathbf{R}^{\mathrm{T}}(t;t_0,t_f)\mathbf{B}\mathbf{B}^{\mathrm{T}}\mathbf{R}(t;t_0,t_f),$$

subject to the terminal constraints

$$\mathbf{R}(t_f;t_0,t_f) = \mathbf{I},$$
$$\mathbf{Q}(t_f;t_0,t_f) = \mathbf{0}.$$

Once these equations are integrated backward in time, the costate vector as a function of the initial state is given by

$$\lambda(t;t_0,t_f) = -\mathbf{R}(t;t_0,t_f)\mathbf{Q}^{-1}(t_0;t_0,t_f)\mathbf{R}^{\mathrm{T}}(t_0;t_0,t_f)\vec{x}(t_0).$$

From this, the deterministic optimal control is defined as

$$\begin{aligned}\vec{u}(t;t_0,t_f) &= -\mathbf{B}^{\mathrm{T}}\lambda(t;t_0,t_f) \\ &= -\mathbf{B}^{\mathrm{T}}\mathbf{R}(t;t_0,t_f)\mathbf{Q}^{-1}(t_0;t_0,t_f)\mathbf{R}^{\mathrm{T}}(t_0;t_0,t_f)\vec{x}(t_0).\end{aligned}$$

If we define the matrix L as

$$\mathbf{L}(t;t_0,t_f) = -\mathbf{B}^{\mathrm{T}}\mathbf{R}(t;t_0,t_f)\mathbf{Q}^{-1}(t_0;t_0,t_f)\mathbf{R}^{\mathrm{T}}(t_0;t_0,t_f),$$

and the Grammian matrix $\mathbf{G}$ as

$$\mathbf{G}(t_0,t_f) = \int_{t_0}^{t_f} \mathbf{L}^{\mathrm{T}}(\tau;t_0,t_f)\mathbf{L}(\tau;t_0,t_f)d\tau,$$

then the form of the deterministic optimal control and the deterministic optimal cost function

are

$$\vec{u}^*(t;t_0,t_f) = \mathbf{L}(t;t_0,t_f)\vec{x}(t_0), \tag{2.3}$$

$$\begin{aligned} J^*(t_0,t_f) &= \frac{1}{2}\vec{x}_0^{\mathrm{T}}\mathbf{G}(t_0,t_f)\vec{x}_0 \\ &= \frac{1}{2}\mathrm{Tr}\left[\mathbf{G}(t_0,t_f)\vec{x}_0\vec{x}_0^{\mathrm{T}}\right]. \end{aligned} \tag{2.4}$$

This form of J^* provides for straightforward computation of the expected value of the cost function because the statistics of $\vec{x}_0$ are assumed to be given. Also, this linear method may be extended to a nonlinear method by using the generating function approach for optimal control [15].

2.2 Control Law Updates

We start by studying three simple linear systems to demonstrate the control and measurement strategy as well as the derivation of the expected cost and optimal time between measurements.

In our analysis of the timing of the control law updates, the state is assumed to be a Gaussian random vector (GRV), with the mean and covariance taken as outputs of an estimation process. Specifically, we assume that these are the mean and covariance conditioned on the past history of observations. In practice, this estimation/filtering process would run on-line with the control determination; however, we assume that the estimation is performed external to this analysis. This greatly simplifies the control computation – only the most current mean and covariance are needed to compute the control law with this method.

The multivariate Gaussian probability distribution function for a vector $\vec{x} \in \mathbb{R}^n$ with mean $\vec{m} \in \mathbb{R}^n$ and covariance matrix $\mathbf{P} \in \mathbb{R}^{n\times n}$ is defined as[16]

$$p(\vec{x}) = \frac{1}{\sqrt{(2\pi)^n \det\mathbf{P}}} \exp\left(-\frac{1}{2}(\vec{x}-\vec{m})^{\mathrm{T}}\mathbf{P}^{-1}(\vec{x}-\vec{m})\right).$$

The expected value of a function of the GRV is

$$\mathrm{E}[f(\vec{x})] = \int_{\infty} f(\xi) p(\xi)\, \mathrm{d}\xi,$$

with mean, $\vec{m}$, and covariance, $\mathbf{P}$,

$$\vec{m} = \mathrm{E}[\vec{x}] = \int_{\infty} \xi\, p(\xi)\, \mathrm{d}\xi$$
$$\mathbf{P} = \mathrm{E}\left[\vec{x}\vec{x}^{\mathrm{T}}\right] - \vec{m}\vec{m}^{\mathrm{T}} = \int_{\infty} \xi\xi^{\mathrm{T}} p(\xi)\, \mathrm{d}\xi - \vec{m}\vec{m}^{\mathrm{T}}.$$

The concepts involved in this analysis will be explained in the context of three illustrative systems. The choice of the three simple systems is motivated by previous results [12] for impulsive control. Consider the following 2-dimensional system with one scalar input,

$$\dot{\vec{x}} = \mathbf{A}\vec{x} + \mathbf{B}u.$$

The three different cases result from three different $\mathbf{A}$ matrices:

1. the oscillatory case: $\mathbf{A} = \begin{bmatrix} 0 & 1 \\ -\beta^2 & 0 \end{bmatrix}$
2. the double-integrator case: $\mathbf{A} = \begin{bmatrix} 0 & 1 \\ 0 & 0 \end{bmatrix}$
3. the hyperbolically unstable case: $\mathbf{A} = \begin{bmatrix} 0 & 1 \\ +\beta^2 & 0 \end{bmatrix}$

For all three systems, $\mathbf{B} = [0 \quad 1]^{\mathrm{T}}$. The cost function for the deterministic optimal control is

$$J = \frac{1}{2} \int_{t_0}^{t_f} u(t)^2\, \mathrm{d}t,$$

and the deterministic optimization problem to be solved is to find $u(t)$ such that $u(t)$

minimizes J subject to given initial and final states.

We can conclude that if the deterministic optimal control is applied from time t_0 to time t_1, with a GRV of initial conditions,

$$\mathrm{E}\left[\vec{x}_0\right] = \vec{0}, \tag{2.5}$$

$$\mathrm{Var}\left[\vec{x}_0\right] = \mathbf{P}_0, \tag{2.6}$$

the expectation and covariance describing the state at time t_1 are given by

$$\mathrm{E}\left[\vec{x}_1\right] = \vec{0}, \tag{2.7}$$

$$\mathrm{Var}\left[\vec{x}_1\right] = \mathbf{P}_1 = \Phi(t_1 - t_0)\mathbf{P}_0\Phi^{\mathrm{T}}(t_1 - t_0). \tag{2.8}$$

For the three systems listed above, the state transition matrices and covariance matrices are as follows.

1. oscillatory case:

$$\Phi(t,0) = \begin{bmatrix} \cos(\beta t) & \frac{1}{\beta}\sin(\beta t) \\ -\beta\sin(\beta t) & \cos(\beta t) \end{bmatrix}$$

,

$$\begin{aligned} P_{11}(t) &= \frac{\beta^2(1+\cos(2\beta t))P_{11} + 2\beta\sin(2\beta t)P_{12} + (1-\cos(2\beta t))P_{22}}{2\beta^2}, \\ P_{12}(t) = P_{21}(t) &= \frac{-\beta^2\sin(2\beta t)P_{11} + 2\beta\cos(2\beta t)P_{12} + \sin(2\beta t)P_{22}}{2\beta}, \\ P_{22}(t) &= -\frac{\beta^2(1+\cos(2\beta t))P_{11} + 2\beta\sin(2\beta t)P_{12} + (1-\cos(2\beta t))P_{22}}{2}. \end{aligned}$$

2. double-integrator case:

$$\Phi(t,0) = \begin{bmatrix} 1 & t \\ 0 & 1 \end{bmatrix}$$

,

$$P_{11}(t) = P_{11} + 2P_{12}t + P_{22}t^2,$$
$$P_{12}(t) = P_{21}(t) = P_{12} + P_{22}t,$$
$$P_{22}(t) = P_{22}.$$

3. hyperbolically unstable case:

$$\Phi(t,0) = \begin{bmatrix} \cosh(\beta t) & \frac{1}{\beta}\sinh(\beta t) \\ \beta \sinh(\beta t) & \cosh(\beta t) \end{bmatrix}$$

,

$$P_{11}(t) = \frac{\beta^2(1+\cosh(2\beta t))P_{11} + 2\beta\sinh(2\beta t)P_{12} + (\cosh(2\beta t)-1)P_{22}}{2\beta^2},$$
$$P_{12}(t) = P_{21}(t) = \frac{-\beta^2\sinh(2\beta t)P_{11} + 2\beta\cosh(2\beta t)P_{12} + \sinh(2\beta t)P_{22}}{2\beta},$$
$$P_{22}(t) = \frac{\beta^2(\cosh(2\beta t)-1)P_{11} + 2\beta\sinh(2\beta t)P_{12} + (1+\cosh(2\beta t))P_{22}}{2}.$$

2.3 Statistical Cost of Control

Let the state be denoted by the GRV $\vec{X}(t)$. At time t, $t_0 < t < t_f$, the state is given by

$$\vec{X}(t) = \Phi(t,t_0)\vec{X}(t_0) + \mathbf{F}(t;t_0,t_f)\vec{X}(t_0),$$

where

$$\mathbf{F}(t;t_0,t_f) = \int_{t_0}^{t} \Phi(t,\tau)\mathbf{BL}(\tau;t_0,t_f)d\tau.$$

Suppose that after a long period of time, we are at the end of an update period just before we take a measurement. The GRV has a statistical distribution with zero mean and

covariance

$$\mathbf{P}_{ss} = \mathrm{E}\left[\vec{X}(T_u)\vec{X}^{\mathrm{T}}(T_u)\right].$$

After taking a new measurement, the GRV is

$$\vec{X}(t_{0_+}) = \vec{M} + \vec{V},$$

where $\vec{M} \sim \mathscr{N}(\vec{0}, \mathbf{P}_{ss})$, $\vec{V} \sim \mathscr{N}(\vec{0}, \mathbf{P}_m)$, and $\vec{M}$ and $\vec{V}$ are independent; the $+$ subscript on t_0 indicates an instant just after a measurement. At the update time,

$$\begin{aligned}\vec{X}(T_u) &= \Phi(T_u, t_0)\vec{X}(t_{0_+}) + \mathbf{F}(T_u; t_0, t_f)\vec{M} \\ &= \left(\Phi(T_u, t_0) + \mathbf{F}(T_u; t_0, t_f)\right)\vec{M} + \Phi(T_u, t_0)\vec{V}.\end{aligned}$$

For convenience, let $\Phi = \Phi(T_u, t_0)$ and $\mathbf{F} = \mathbf{F}(T_u; t_0, t_f)$. The covariance is

$$\begin{aligned}\mathrm{E}\left[\vec{X}(T_u)\vec{X}^{\mathrm{T}}(T_u)\right] &= (\Phi + \mathbf{F})\,\mathrm{E}\left[\vec{M}\vec{M}^{\mathrm{T}}\right](\Phi + \mathbf{F})^{\mathrm{T}} + \Phi\mathrm{E}\left[\vec{V}\vec{V}^{\mathrm{T}}\right]\Phi^{\mathrm{T}} \\ \mathbf{P}_{ss} &= (\Phi + \mathbf{F})\,\mathbf{P}_{ss}\,(\Phi + \mathbf{F})^{\mathrm{T}} + \Phi\mathbf{P}_m\Phi^{\mathrm{T}}.\end{aligned}$$

This is in the form of the discrete-time Lyapunov equation. The solution may be computed efficiently in many software packages, for example, the command 'dlyap' in MATLAB. Alternatively, a direct solution for $\mathbf{P}_{ss}$ maybe be written with the vectorization (or stacking) operator and the Kronecker product:

$$\begin{aligned}\mathrm{vec}\,(\mathbf{P}_{ss}) &= \mathrm{vec}\left((\Phi + \mathbf{F})\,\mathbf{P}_{ss}\,(\Phi + \mathbf{F})^{\mathrm{T}}\right) + \mathrm{vec}\left(\Phi\mathbf{P}_m\Phi^{\mathrm{T}}\right) \\ &= \left[(\Phi + \mathbf{F}) \otimes (\Phi + \mathbf{F})\right]\mathrm{vec}\,(\mathbf{P}_{ss}) + \mathrm{vec}\left(\Phi\mathbf{P}_m\Phi^{\mathrm{T}}\right) \\ &= \left[\mathbf{I} - (\Phi + \mathbf{F}) \otimes (\Phi + \mathbf{F})\right]^{-1}\mathrm{vec}\left(\Phi\mathbf{P}_m\Phi^{\mathrm{T}}\right).\end{aligned}$$

$\mathbf{P}_{ss}$ is obtained by unstacking $\mathrm{vec}\,(\mathbf{P}_{ss})$. If $T_u = t_f$, then $\mathbf{F} = -\Phi$ and the above equation

simplifies to

$$\mathbf{P}_{ss} = \Phi \mathbf{P}_m \Phi^{\mathrm{T}}.$$

The relevant covariance matrix for calculating the expected cost is the covariance just after taking a measurement, $\mathbf{P}_+$;

$$\begin{aligned}\mathbf{P}_+ &= \mathrm{E}\left[\vec{X}(t_{0_+})\vec{X}^{\mathrm{T}}(t_{0_+})\right] \\ &= \mathbf{P}_{ss} + \mathbf{P}_m.\end{aligned}$$

Continuing with the prior examples, we may partition the initial state for convenience. Let r_0 be the initial position and v_0 be the initial velocity. Then $\vec{x}_0 = [r_0 \quad v_0]^{\mathrm{T}}$. Similarly, partition $\mathbf{G}$ from Equation (2.4) as

$$\mathbf{G} = 2J_\Delta \begin{bmatrix} J_r & J_{rv} \\ J_{rv} & J_v \end{bmatrix},$$

where the factor J_Δ is pulled out for convenience. This yields the following expression for the deterministic cost:

$$J = J_\Delta (J_r r_0^2 + 2J_{rv} r_0 v_0 + J_v v_0^2), \tag{2.9}$$

where J_Δ, J_r, J_{rv}, and J_v are functions of the linear dynamics and the update time, given in Table 2.1.

	Double-integrator	Oscillatory	Hyperbolically Unstable
J_Δ	$1/T$	$\frac{\beta^2}{\cos(2\beta T)+2\beta^2T^2-1}$	$\frac{\beta^2}{\cosh(2\beta T)-2\beta^2T^2-1}$
J_{rr}	$6/T^2$	$\beta\sin(2\beta T)+2\beta^2 T$	$\beta\sinh(2\beta T)+2\beta^2 T$
J_{rv}	$3/T$	$1-\cos(2\beta T)$	$\cosh(2\beta T)-1$
J_{vv}	2	$2T-\frac{1}{\beta}\sin(2\beta T)$	$\frac{1}{\beta}\sinh(2\beta T)-2T$

Table 2.1 Summary of Cost Coefficients

Once the deterministic cost is known, the expected value and variance of the cost can be

computed. Taking the expectation, $\mathrm{E}[\cdot]$, of Equation (2.4) yields

$$\mathrm{E}[J] = \frac{1}{2}\mathrm{Tr}\left\{\mathbf{G}\left(\mathbf{P}_+ + \mathrm{E}[\vec{x}_0]\,\mathrm{E}\left[\vec{x}_0^{\mathrm{T}}\right]\right)\right\}, \tag{2.10}$$

or in the form of Equation (2.9),

$$\begin{aligned}\mathrm{E}[J] =& J_\Delta\left(J_r\mathrm{E}\left[r_0^2\right] + 2J_{rv}\mathrm{E}[r_0 v_0] + J_v\mathrm{E}\left[v_0^2\right]\right) && (2.11)\\ =& J_\Delta\Big(J_r\left(\sigma_r^2(t_0) + \mathrm{E}[r_0]^2\right)\\ &+ 2J_{rv}\left(\sigma_{rv}^2(t_0) + \mathrm{E}[r_0]^{\mathrm{T}}\,\mathrm{E}[v_0]\right)\\ &+ J_v\left(\sigma_v^2(t_0) + \mathrm{E}[v_0]^2\right)\Big), && (2.12)\end{aligned}$$

where σ denotes the (co)variance of the subscripted quantities at the beginning of the update interval, just after a measurement.

Now, since the control law was chosen so that the expected values of the state is the zero vector $\left(\mathrm{E}[\vec{r}_0] = \mathrm{E}[\vec{v}_0] = \vec{0}\right)$, Equations (2.10) and (2.12) simplify to

$$\begin{aligned}\mathrm{E}[J] &= \frac{1}{2}\mathrm{Tr}\{\mathbf{G}\mathbf{P}_+\} && (2.13)\\ &= J_\Delta\left(J_r\sigma_r^2(t_0) + 2J_{rv}\sigma_{rv}^2(t_0) + J_v\sigma_v^2(t_0)\right). && (2.14)\end{aligned}$$

It is worthwhile to note that this expected cost is only a function of the time-between-updates, T_u, and the initial covariances, $\mathbf{P}_m$, because for a given system, $\mathbf{G}$ is determined completely by T_u and $\mathbf{P}_+$ is determined by $\mathbf{P}_m$.

The variance of J, $\mathrm{Var}[J]$, is given by

$$\mathrm{Var}[J] = \mathrm{E}\left[J^2\right] - (\mathrm{E}[J])^2. \tag{2.15}$$

Computing $\mathrm{E}\left[J^2\right]$ using the Gaussian joint characteristic function yields

$$\begin{aligned}\mathrm{E}\left[J^2\right] =& \frac{1}{2}\mathrm{Tr}\left\{(\mathbf{GP}_+)^2\right\} + \frac{1}{4}\mathrm{Tr}^2(\mathbf{GP}_+) && (2.16)\\ =& J_\Delta^2\Big\{3J_r^2(\sigma_r^2)^2 + 4J_{rv}^2\left(2(\sigma_{rv}^2)^2 + \sigma_r^2\sigma_v^2\right)\\ &+ 3J_v^2(\sigma_v^2)^2 + 8J_rJ_{rv}\sigma_r^2\sigma_{rv}^2\\ &+ 2J_rJ_v(\sigma_r^2\sigma_v^2 + 2(\sigma_{rv}^2)^2) + 12J_{rv}J_v\sigma_{rv}^2\sigma_v^2\Big\}. && (2.17)\end{aligned}$$

Substituting Equation (2.14) and Equation (2.17) into Equation (2.15) yields the variance of J:

$$\begin{aligned}\mathrm{Var}\left[J\right] =& \frac{1}{2}\mathrm{Tr}\left\{(\mathbf{GP}_+)^2\right\} && (2.18)\\ =& 2J_\Delta^2\Big\{J_r^2(\sigma_r^2)^2 + 2J_{rv}^2\left((\sigma_{rv}^2)^2 + \sigma_v^2\sigma_v^2\right)\\ &+ J_v^2(\sigma_v^2)^2 + 4J_rJ_{rv}\sigma_r^2\sigma_{rv}^2\\ &+ 2J_rJ_v(\sigma_{rv}^2)^2 + 4J_{rv}J_v\sigma_{rv}^2\sigma_v^2\Big\}. && (2.19)\end{aligned}$$

As with the expected value of J, the variance of J is only a function of T_u and $\mathbf{P}_m$.

2.4 Steady-State Minimum Expected Cost

Due to the complicated form of the expression for $\mathrm{E}\left[J\right]/T_u$, even for simple time-invariant systems, Equation (2.1) cannot typically be solved for T_u^* in closed-form. Some statements can be made, however, about the behavior of T_u^*, depending on the dynamics of the linear systems under study. For any double-integrator and oscillatory type dynamics, it can be shown that $\mathrm{E}\left[J\right]/T_u$ achieves its minimum by letting $T_u \to \infty$ and that the actual value of $\mathrm{E}\left[J\right]/T_u$ approaches zero. This is analogous to the impulsive control result previously obtained [12] and implies that maneuver execution errors dominate the uncertainty. The behavior is different for a hyperbolically unstable system. As T_u increases, the hyperbolic

instability of the system causes $\mathrm{E}[J]$ to grow exponentially and drives $\mathrm{E}[J]/T_u$ toward ∞. For all three cases, $\mathrm{E}[J]/T_u$ goes toward ∞ as T_u approaches zero. Thus, for the oscillatory and double-integrator cases it is optimal to let the time between measurements go to infinity, however, for hyperbolically unstable dynamics, there exists an optimal time between measurements.

This can be shown more formally with the limits of $\mathrm{E}[J]/T_u$ as $T_u \to 0$ and as $T_u \to \infty$. For all three example systems $\lim_{T_u \to 0} \mathrm{E}[J]/T_u$ is undefined, i.e., $\mathrm{E}[J]/T_u$ grows without bound as T_u approaches zero. For the oscillatory and double-integrator dynamics, $\lim_{T_u \to \infty} \frac{\mathrm{E}[J]}{T_u} = 0$, but for the hyperbolically unstable case, $\lim_{T_u \to \infty} \mathrm{E}[J]/T_u$ is undefined ($\mathrm{E}[J]/T_u$ also grows without bound as T_u tends toward infinity in this case). Since $\mathrm{E}[J]/T_u$ is still finite for any finite value of T_u, this implies the existence of a minimum by continuity. Numerical studies of a wide range of systems show that the value of T_u^* is closely tied to the characteristic time of the unstable mode ($1/\alpha$), although it also depends on the initial values of the covariance matrix. This is also analogous to previously obtained results for impulsive control [1]. For an ideal one degree of freedom unstable system, it can be shown that the optimal update time for impulsive control equals the characteristic time [12]. For our continuous control, time-varying systems, the relationship is not exact, but numerical simulations support the extension as a "rule of thumb." This relationship breaks down when applied to periodic trajectories that are too far from their initial origin, as shown in the example implementation. An example of the cost as a function of T_u for the three linear cases described above is shown in Figure 2.1. For all three cases, $P_{0_{11}} = P_{0_{22}} = 1$ and $P_{0_{12}} = 0$. For the hyperbolically unstable and oscillatory cases, $\beta = .1$.

The overall trends of the cost are very predictable as β changes. Figure 2.2 shows the expected cost per unit time in the unstable system with three different values of β, normalized on each axis so that the update time is scaled by β and the cost is scaled such that the minimum value equals unity. Although β varies by two orders of magnitude, the normalized optimal values of T_u only change by about 10%. Since $\mathrm{E}[J]$ scales linearly with

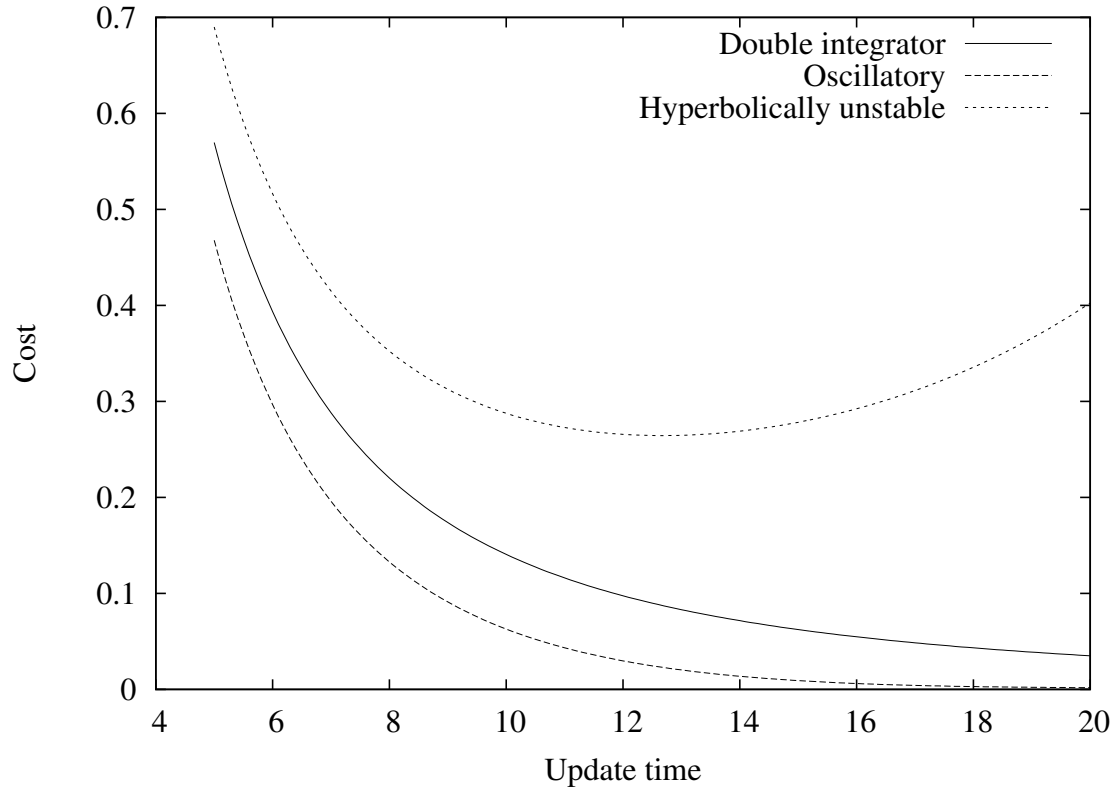

Figure 2.1 Example cost as a function of update time for three example systems – double integrator, oscillatory, and unstable

$\mathbf{P}_m$, scaling $\mathbf{P}_m$ does not change the location of the optimal update time.

The effect of t_f on $\mathrm{E}[J]/T_u$ in the unstable example is shown in Figure 2.3. As the horizon is extended, a cost reduction can be obtained. However, as a practical matter, the reduction in cost must be weighed against the growth in $\|\mathbf{P}_{ss}\|$ as shown in Figure 2.4. For the examples in this paper, we assume $T_u = t_f$, as this is common for spacecraft control due to the limited ability for communication of new control laws.

2.5 Estimates for Control Costs

In spacecraft control, one is often concerned with minimizing ΔV – the total velocity change required by the propulsion system to follow a given trajectory. For our continuous control

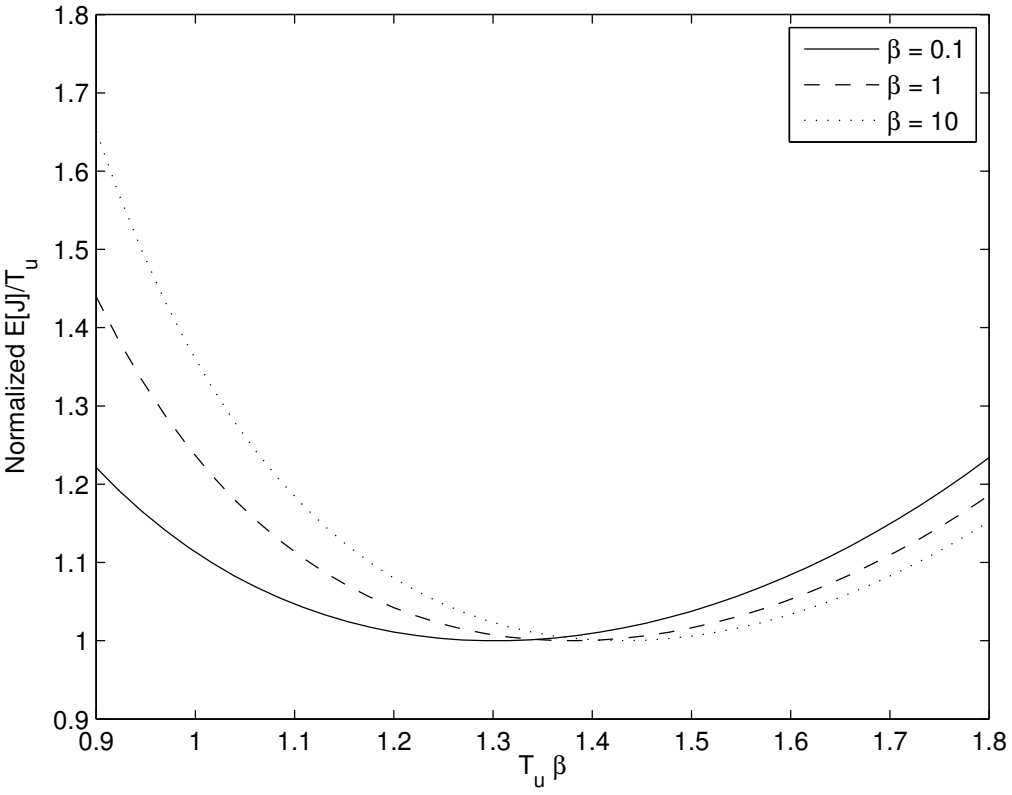

Figure 2.2 Example cost as a function of update time for three unstable example systems

case, the ΔV between two time periods, t_0 and $t_0 + T_u$, is given by

$$\Delta V = \int_{t_0}^{t_0+T_u} \|\vec{u}(t)\| dt \tag{2.20}$$

$$= \int_{t_0}^{t_0+T_u} \sqrt{\vec{u}(t) \cdot \vec{u}(t)} dt. \tag{2.21}$$

The analysis methods in this paper use an energy cost function as in Equation (2.2), although we may obtain an upper bound on the ΔV spent per unit time from our energy cost

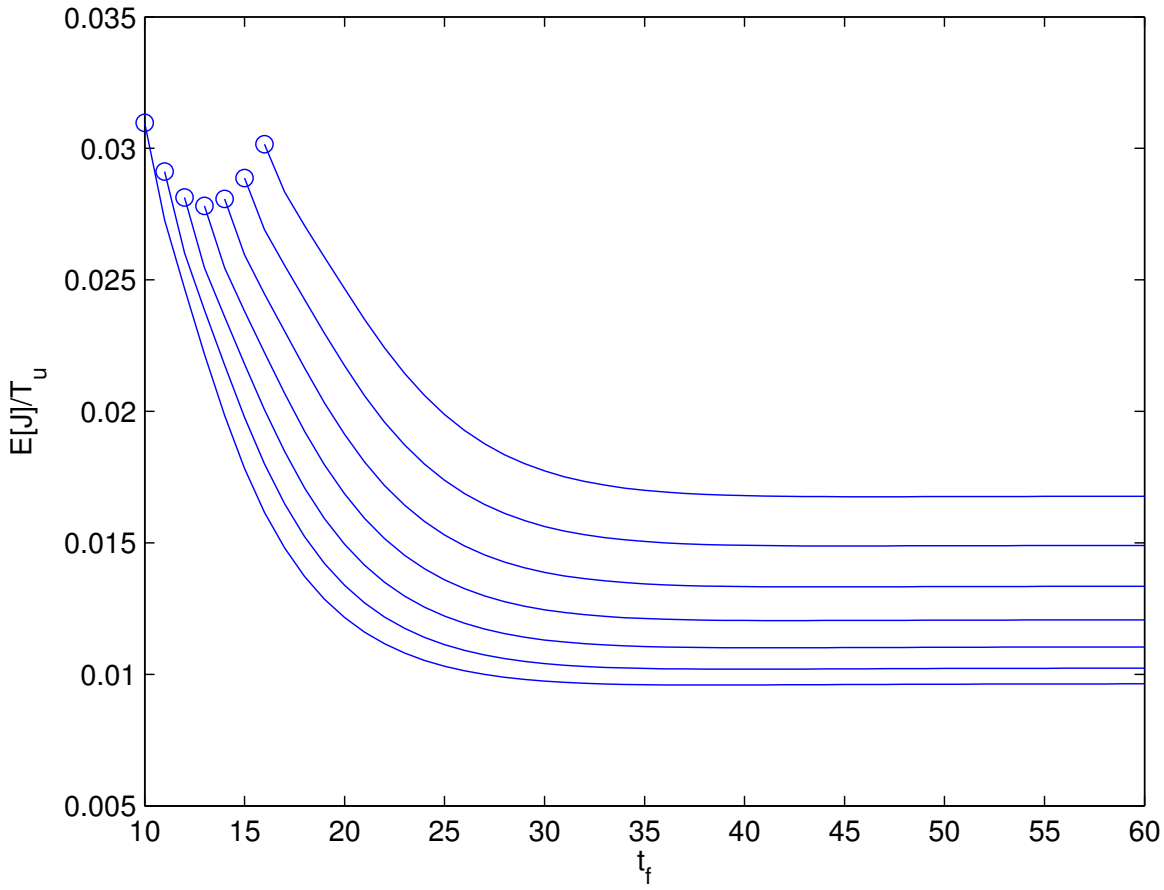

Figure 2.3 $\mathrm{E}[J]/T_u$ as t_f increases for a family of T_u values in the unstable example with $\beta = 1$. The circled points are where $T_u = t_f$ (t_f must be greater than T_u)

per unit time. Using the Cauchy-Schwarz inequality,

$$\int_{t_0}^{t_0+T_u} \sqrt{\vec{u}(t)\cdot\vec{u}(t)}dt \leq \sqrt{\int_{t_0}^{t_0+T_u} \left(\sqrt{\vec{u}(t)\cdot\vec{u}(t)}\right)^2 dt \cdot \int_{t_0}^{t_0+T_u} dt} \tag{2.22}$$

$$= \sqrt{\int_{t_0}^{t_0+T_u} \vec{u}(t)\cdot\vec{u}(t)dt \cdot T_u}. \tag{2.23}$$

Therefore, a bound on the ΔV used in each control segment is

$$\Delta V \leq \sqrt{2T_u}\sqrt{J}. \tag{2.24}$$

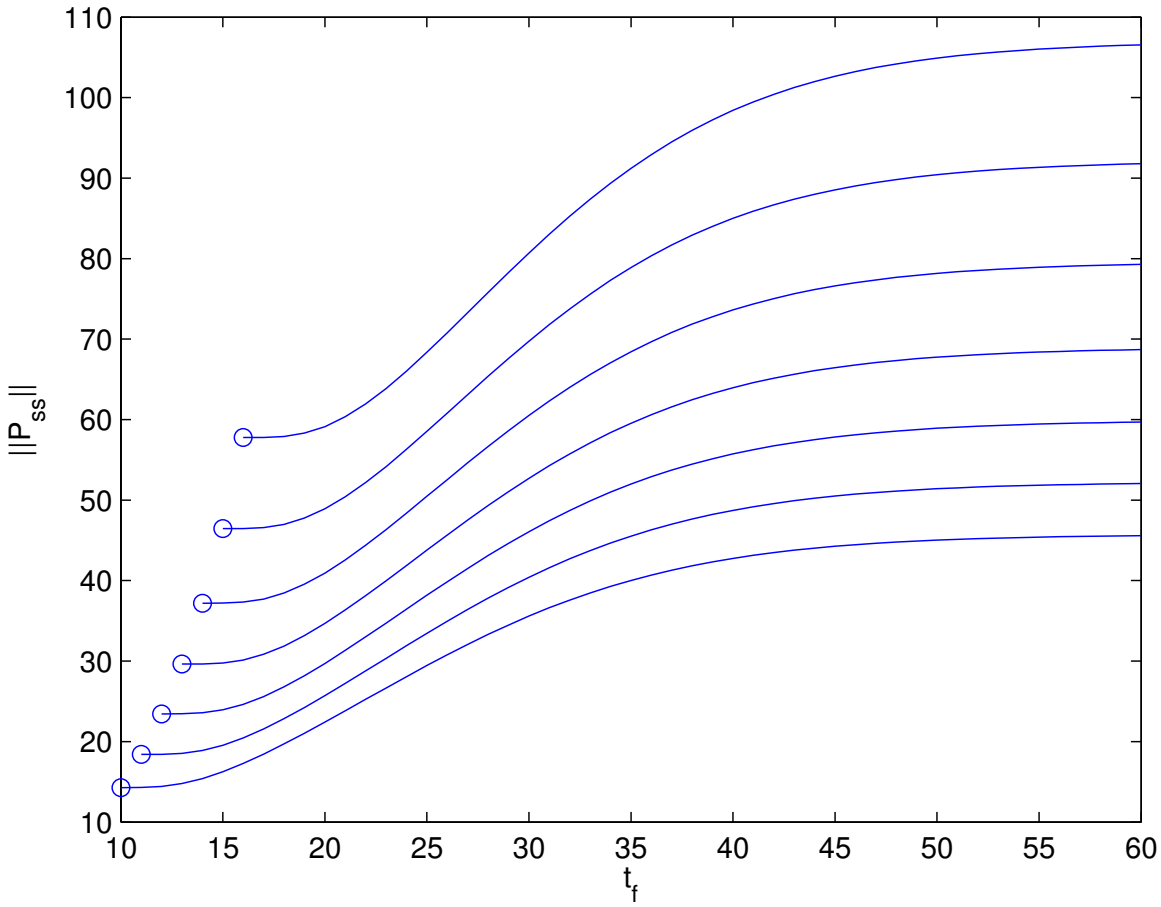

Figure 2.4 $\|\mathbf{P}_{ss}\|$ as t_f increases for a family of T_u values in the unstable example with $\beta = 1$. The circled points are where $T_u = t_f$.

Taking the expectation of this yields

$$\mathrm{E}[\Delta V] \leq \sqrt{2T_u}\mathrm{E}\left[\sqrt{J}\right] \tag{2.25}$$

$$\leq \sqrt{2T_u}\sqrt{\mathrm{E}[J]}, \tag{2.26}$$

where the last inequality comes again from the Cauchy-Schwarz inequality. The expected ΔV spent per unit time is then bounded by

$$\frac{\mathrm{E}[\Delta V]}{T_u} \leq \sqrt{2\frac{\mathrm{E}[J]}{T_u}}. \tag{2.27}$$

2.6 Example Implementation

In this section we will study two cases of spacecraft control in the Hill Three-Body Problem (H3BP) using continuous thrust. In the first case, we limit ourselves to the planar motion of a spacecraft in the vicinity of one of the relative equilibrium points, and in the second, we study a spacecraft perturbed from a nominal halo orbit. A previous study of the equilibrium point control problem [1] considered control using impulsive maneuvers. In addition, we show that the results obtained for the linear time-invariant case can be extended to linear time-varying systems.

The equations of motion for a spacecraft's position in the H3BP are [1]

$$\ddot{x} - 2\omega\dot{y} = -\frac{\mu}{r^3}x + 3\omega^2 x + a_x \tag{2.28}$$

$$\ddot{y} + 2\omega\dot{x} = -\frac{\mu}{r^3}y + a_y \tag{2.29}$$

$$\ddot{z} = -\frac{\mu}{r^3}z - \omega^2 z + a_z, \tag{2.30}$$

where x, y, and z are the positions of the spacecraft in the rotating frame relative to the secondary body, a_x, a_y, and a_z are the spacecraft control accelerations, ω is the angular velocity of the secondary body about the primary, $\mu = GM$, M is the mass of the secondary body, and r is the radius ($r = \sqrt{x^2+y^2+z^2}$). These equations may be nondimensionalized using the length scale $l = (\mu/\omega^2)^{1/3}$ and time scale $\tau = 1/\omega$. For the Earth-Sun system, $\mu = 3.986 \times 10^5$ km^3/s^2, $\omega = 1.991 \times 10^{-7}$ rad/s, $l = 2.158 \times 10^6$ km, and $\tau = 5.023 \times 10^6$ s.

The dimensional covariance matrix associated with the state estimates is assumed to be a 6×6 diagonal matrix with entries P_r and P_v,

$$\mathbf{P_d} = \begin{bmatrix} P_r \cdot I_3 & 0_{3\times 3} \\ 0_{3\times 3} & P_v \cdot I_3 \end{bmatrix}.$$

The covariance from an actual on-line filter would likely have off-diagonal terms, but for the examples shown here, the qualitative results are the same. This covariance matrix may be nondimensionalized to obtain

$$\begin{aligned}\mathbf{P} &= \begin{bmatrix} P_r/l^2 \cdot I_3 & 0_{3\times 3} \\ 0_{3\times 3} & P_v/(\omega l)^2 \cdot I_3 \end{bmatrix} \\ &= P_r/l^2 \begin{bmatrix} I_3 & 0_{3\times 3} \\ 0_{3\times 3} & P_v/(P_r\omega^2) \cdot I_3 \end{bmatrix}.\end{aligned}$$

This may be parameterized to yield further insight into how the uncertainties affect the optimal update time and cost using the parameters $\sigma_r = \sqrt{P_r}/l$ and $\lambda = \omega\sqrt{P_r/P_v}$. This nondimensionalization and parameterization yields the following form for $\mathbf{P}_m$:

$$\mathbf{P}_m = \sigma_r^2 \begin{bmatrix} I_3 & 0_{3\times 3} \\ 0_{3\times 3} & 1/\lambda^2 \cdot I_3 \end{bmatrix}. \tag{2.31}$$

Typical values of $P_r = (10 \text{ km})^2$ and $P_v = (10^{-6} \text{ km/s})^2$ relating to typical spacecraft uncertainties are used for the simulations, resulting in the nondimensional parameters $\sigma_r = 4.633 \times 10^{-6}$ and $\lambda = 1.991$ in the Sun-Earth system and $\sigma_r = 1.13 \times 10^{-4}$ and $\lambda = 26.6$ in the Earth-Moon system.

Given a nondimensional expected cost per unit time, $\mathrm{E}[J]/T_u$, the dimensional cost per unit time is given as

$$\left(\frac{\mathrm{E}[J]}{T_u}\right)\frac{l^2}{\tau^4}.$$

To convert nondimensional $\Delta V/T_u$ values to their dimensional values, scale by l/τ^2 instead of l^2/τ^4. The results may also be reported as a cost per period of the secondary body, $2\pi/\omega$. The dimensional cost per secondary body period is $(\mathrm{E}[J]/T_u)\,2\pi l^2/\tau^3$ and the dimensional ΔV per secondary body period is $(\mathrm{E}[\Delta V]/T_u)\,2\pi l/\tau$.

For reference, a nondimensional expected value of J/T_u equal to 1×10^{-7} corresponds

to an upper bound on the dimensional ΔV per period of 1.21×10^{-3} km/(s $\cdot$ period) in the Sun-Earth system or 6.62×10^{-4} km/(s $\cdot$ period) in the Earth-Moon system.

2.6.1 Planar Equilibrium Point Control

When the system is nondimensionalized by setting $\mu = \omega = 1$ in Equations (2.28) and (2.29), the system has two equilibrium points using no control at $x = \pm 3^{-1/3}$, $y = 0$. Linearizing about either of these points and defining the perturbed state $\delta\vec{x} = [\delta x \quad \delta y \quad \delta\dot{x} \quad \delta\dot{y}]^{\mathrm{T}}$ yields the linear system

$$\delta\dot{\vec{x}} = \begin{bmatrix} 0 & 0 & 1 & 0 \\ 0 & 0 & 0 & 1 \\ 9 & 0 & 0 & 2 \\ 0 & -3 & -2 & 0 \end{bmatrix} \delta\vec{x} + \begin{bmatrix} 0 & 0 \\ 0 & 0 \\ 1 & 0 \\ 0 & 1 \end{bmatrix} \begin{bmatrix} a_x \\ a_y \end{bmatrix}.$$

This system has an unstable mode, a stable mode, and an oscillatory mode, associated with the eigenvalues $+\sqrt{1+2\sqrt{7}} \approx 2.5$, $-\sqrt{1+2\sqrt{7}} \approx -2.5$, and $\pm j\sqrt{2\sqrt{7}-1} \approx \pm 2.1j$, respectively. The unstable mode's characteristic time is then $1/\sqrt{1+2\sqrt{7}} \approx 0.4$, leading us to expect the optimal update time to be approximately 0.4 time units.

In this example, the cost function, J, being minimized during each update interval is the "energy" used,

$$J = \frac{1}{2}\int_{t_0}^{t_0+T_u} \left(a_x^2 + a_y^2\right)\, dt.$$

The deterministic optimal control law, and hence the trajectories themselves, depend on the final time and are plotted in Figure 2.5 for three different final times and various initial conditions. We will show that using an update time of 0.5 time units, corresponding to Figure 2.5b, is optimal. Note this optimal update time of 0.5 is near the characteristic time of the unstable mode, 0.4.

A plot of the expected cost as a function of update time is shown in Figure 2.6, using the uncertainty parameters given above. Due to the hyperbolically unstable dynamics, an

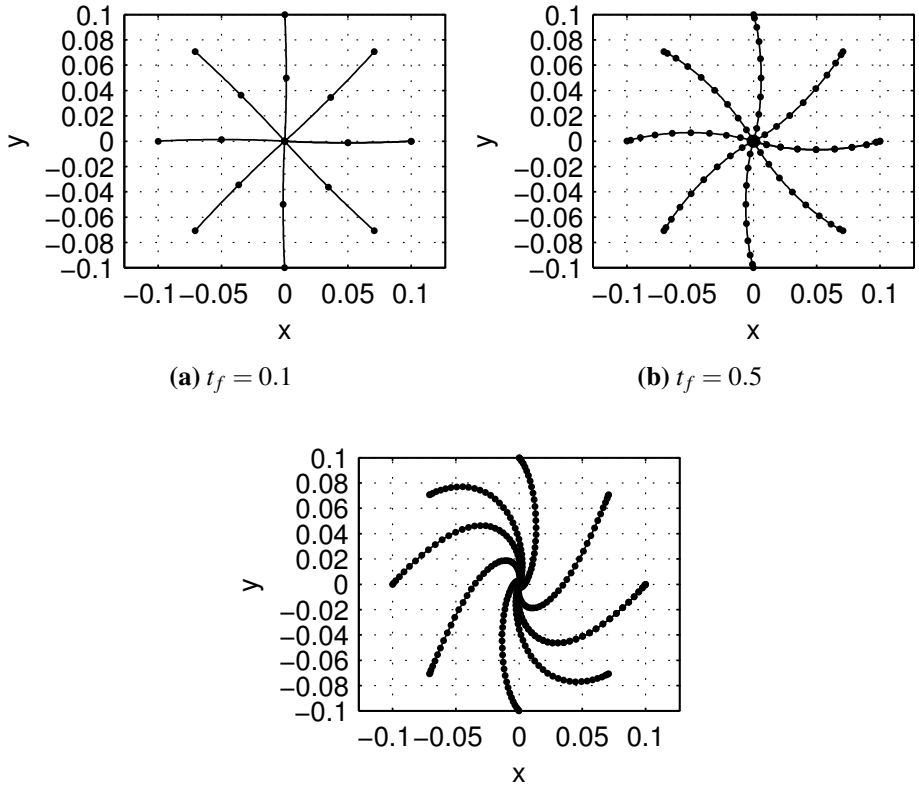

(a) $t_f = 0.1$ **(b)** $t_f = 0.5$

(c) $t_f = 2.0$

Figure 2.5 Example trajectories in the planar H3BP with varying transfer times. Dots are placed every 0.05 time units.

optimal value of T_u clearly exists which minimizes the expected cost.

These cost values may also be compared to similar studies. For the impulsive control strategy in Renault and Scheeres [1], the estimate for ΔV per period is 4.70×10^{-4} km/(s $\cdot$ period) in the Sun-Earth system, although that assumes slightly larger uncertainties than those used in this study. When using their uncertainties, we obtain a ΔV per period of 6.21×10^{-4} km/(s $\cdot$ period) with our continuous thrust method.

Figure 2.7 shows the effect of the nondimensional parameter λ on the optimal update time for the H3BP using the parameters described above. The variation in the optimal update time over the range of λ shown is about 1.75 days for the Earth-Sun system. It is important to note that the optimal update time does not depend on σ_r itself, only the ratio λ. For reference, a nondimensional time value of 0.5 corresponds to about 29 days in the

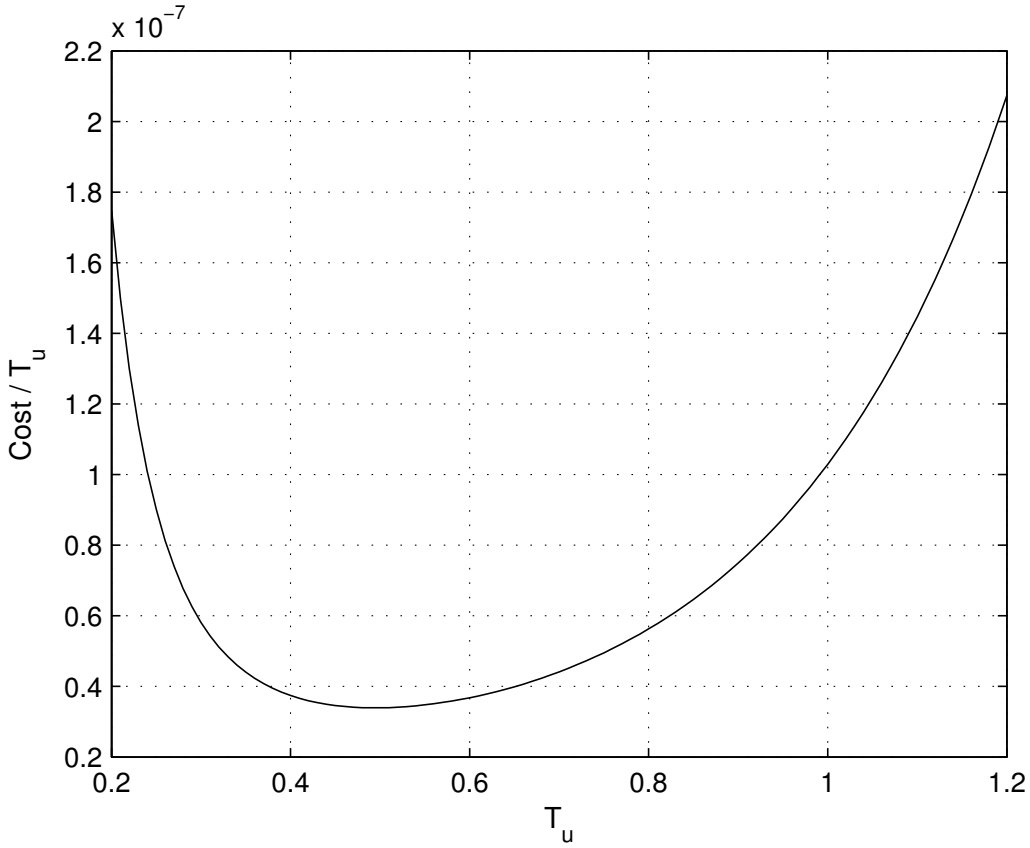

Figure 2.6 Expected cost divided by T_u as a function of T_u in the planar H3BP

Earth-Sun H3BP and 2.2 days in the Earth-Moon HR3BP. Interestingly, even though the formulations for the previous impulsive studies[1] are quite different from this continuous control derivation, the results are consistent in that the ΔV computed from the continuous thrust method is reasonably close to the impulsive ΔV and that the optimal update times for each method are close to the characteristic time of the unstable mode.

Figures 2.8 and 2.9 show the effect of λ on the value of the cost incurred over an update interval divided by the optimal update time, i.e.

$$\min_{\vec{u},T_u} \mathrm{E}\left[J(\vec{u},T_u)\right]/T_u.$$

As can be seen in Figure 2.8, if σ_r is fixed, it is optimal to let λ go to infinity, which is equivalent to letting P_v approach zero, i.e., low uncertainty in the velocity components.

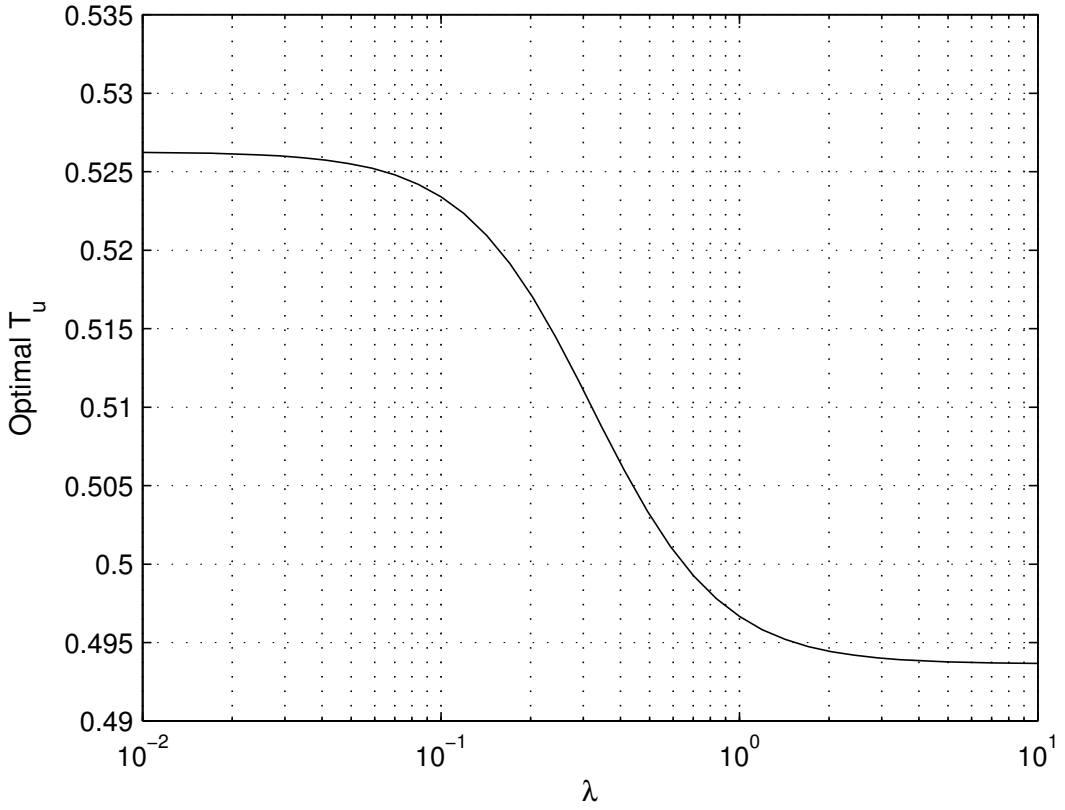

Figure 2.7 Optimal nondimensional update time as a function of λ, for fixed σ_r in the planar H3BP

However, if $|\mathbf{P}|$ is held constant as λ varies, note the presence of an optimal value of λ in Figure 2.9, $\lambda \approx 0.34$, indicating that given a certain amount of uncertainty (measured by a constant $|\mathbf{P}|$), there is an optimal way to distribute the position and velocity uncertainties. For the Earth-Sun system, $\lambda = 0.34$ corresponds to a ratio between 1-σ uncertainties $\sqrt{P_r/P_v} \approx 1.7 \times 10^6$, which is close to our assumed ratio between these measurement uncertainties. For the Earth-Moon system, the optimal ratio of uncertainties is approximately 1.3×10^5. For a position uncertainty of 1 km, the "optimal" velocity uncertainty is about 0.75 cm/s.

The curve in Figure 2.9 scales with $|\mathbf{P}|$, so that the value of λ yielding the minimum value does not change with $|\mathbf{P}|$. From Equation (2.13), the expected value of the cost divided by the optimal update time scales linearly as the entries in $\mathbf{P}$ are scaled.

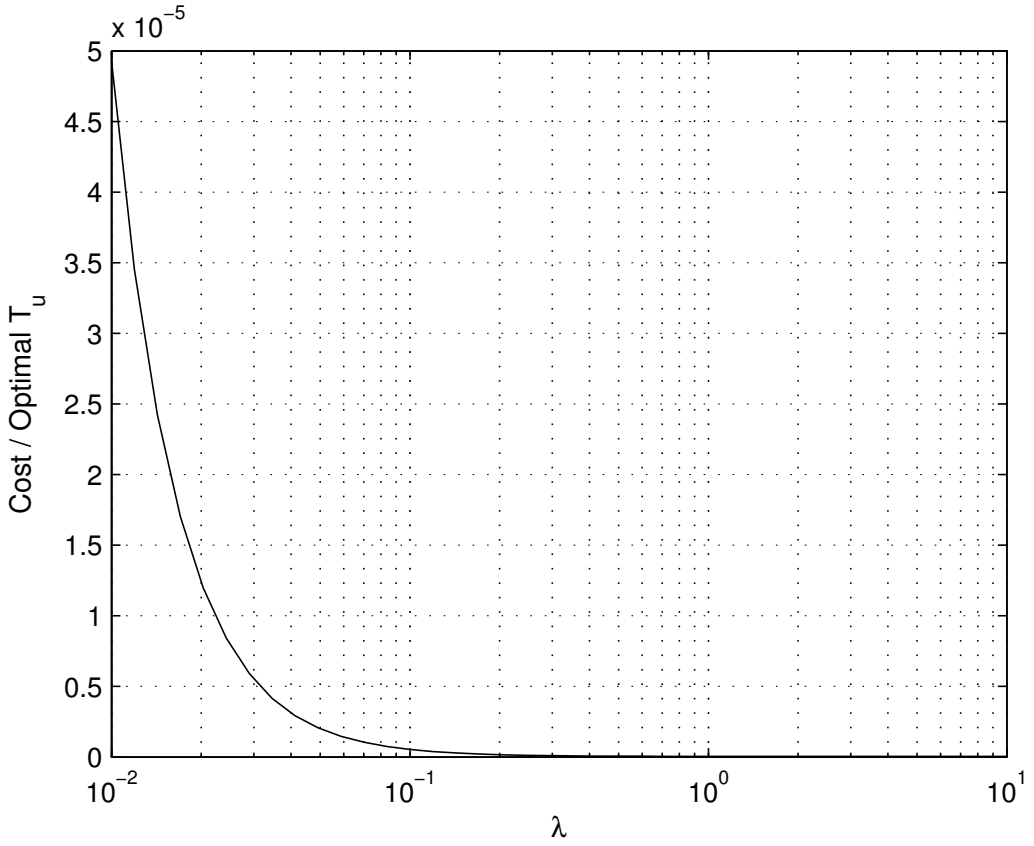

Figure 2.8 Optimal nondimensional cost as a function of λ, σ_r fixed in the planar H3BP

Since $|c\mathbf{P}|$ scales in proportion to $c^n|\mathbf{P}|$, where c is a scalar and $\mathbf{P} \in \mathbb{R}^{n\times n}$, we have that $\left(\min_{\vec{u},T_u} \mathrm{E}\left[J(\vec{u},T_u)\right]/T_u\right) \sim |\mathbf{P}|^{1/n}$. In this planar case, $n = 4$, so the cost scales with $|\mathbf{P}|^{0.25}$.

	$\mathrm{E}[J]/T_u$ (non-dimensional)	ΔV/period (km/s/period)	Optimal Update Time (seconds)
Sun-Earth	1.79×10^{-7}	6.21×10^{-4}	2.71×10^{6}
Earth-Moon	2.88×10^{-5}	4.22×10^{-3}	2.01×10^{5}
Jupiter-Europa	5.72×10^{-4}	3.22×10^{-2}	2.61×10^{4}
Jupiter-Io	9.56×10^{-4}	6.46×10^{-2}	1.30×10^{4}
Saturn-Titan	3.90×10^{-5}	7.19×10^{-3}	1.17×10^{5}
Saturn-Enceladus	1.18×10^{-1}	8.34×10^{-2}	1.01×10^{4}

Table 2.2 Summary of results for control about the H3BP equilibrium point for various systems.

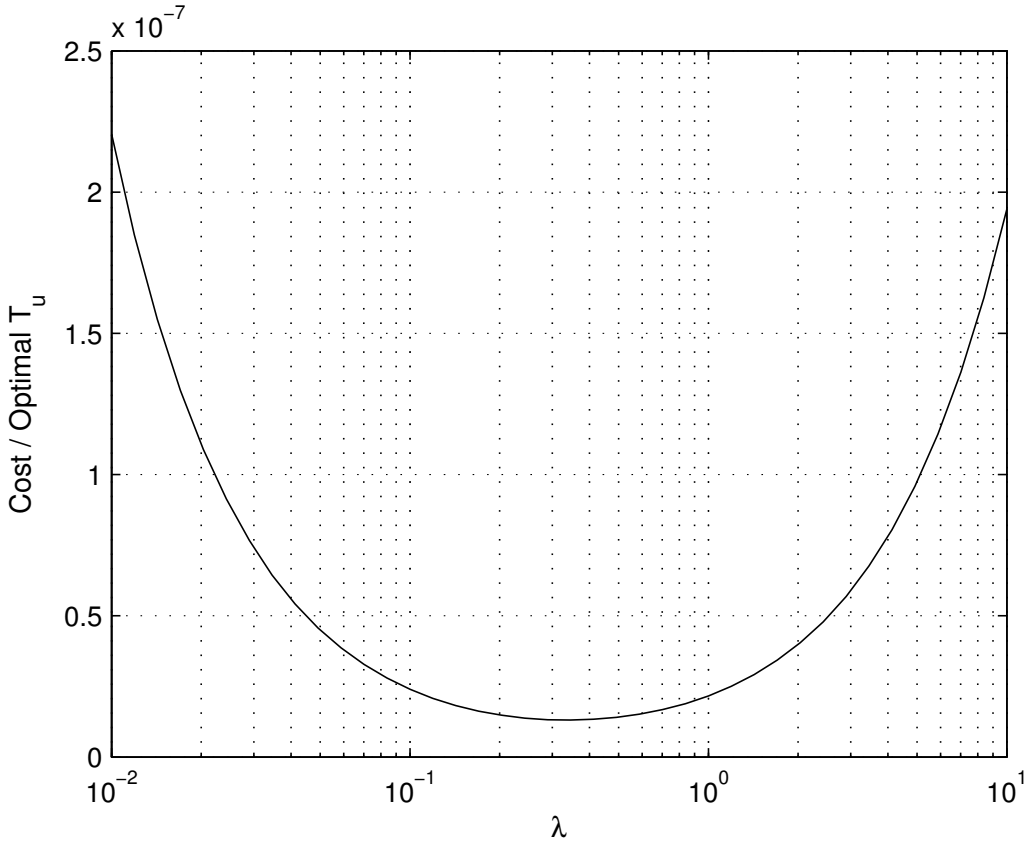

Figure 2.9 Optimal nondimensional cost as a function of λ, $|\mathbf{P}|$ fixed in the planar H3BP

2.6.2 Halo Orbit Control

From the two oscillatory modes mentioned in the previous section, we see that near the equilibrium point, the linearized system is capable of producing planar periodic orbits. These orbits can also be found in the full nonlinear dynamics by examining the monodromy matrix, $\Phi(T,0)$. The monodromy matrix locally captures the dynamics in a discrete-time, linear, time-invariant mapping, and thus allows the system to be analyzed by eigenvalue methods. As the amplitude of these periodic orbits is increased, the eigenvalues of the monodromy matrix bifurcate and a new family of periodic orbits is produced. This new family is called the family of "halo orbits", which are no longer in the plane and cannot be predicted using the equilibrium point linearization. The halo orbits used in this paper, denoted as orbits A though E in Figure 2.10, may be parameterized by their initial x-coordinate, x_0. The values

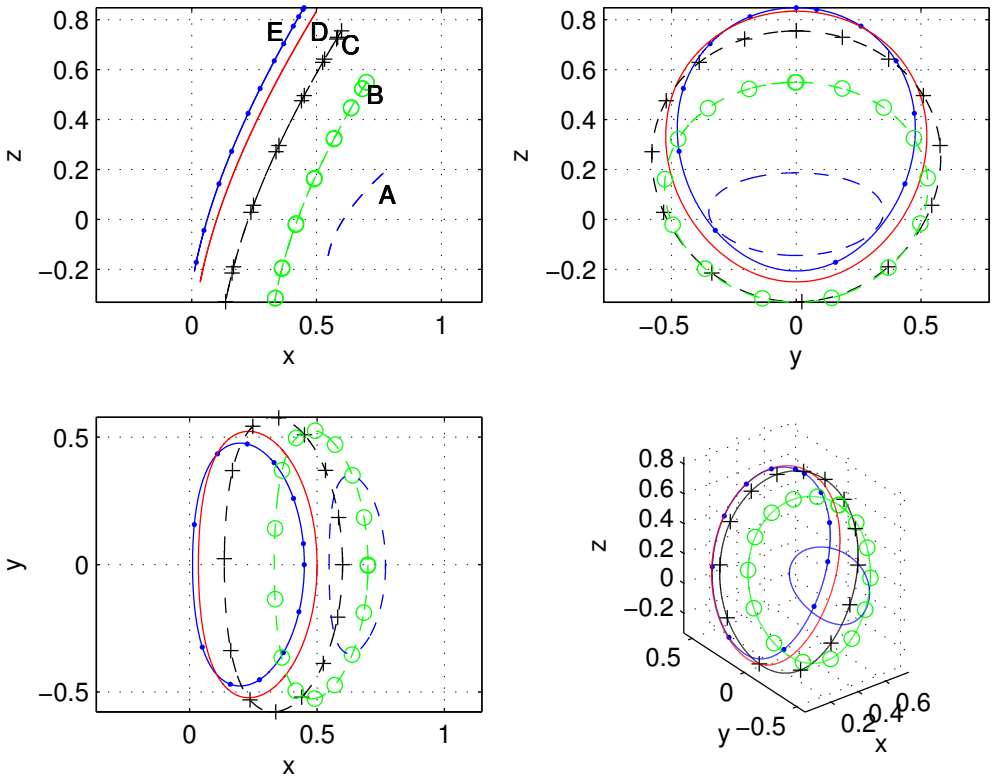

Figure 2.10 Nominal halo orbit trajectories

of x_0 for orbits A through E are 0.769, 0.7, 0.6, 0.5, 0.45, respectively. The other initial conditions for the halo orbits were obtained using a method developed by Howell [17] which takes advantage of symmetry in the system. We developed software to numerical integrate the equations of motion using an 8^{th}-order arbitrary-precision symplectic Runge-Kutta method [18] with 256 bits of precision [19].

In the previous time-invariant example, each segment of control had the same statistical cost. Therefore, we only needed to consider the cost of one segment of control in order to draw conclusions about the long-term average cost. However, in this time-varying case, each segment will generally have a different cost. We may still determine the long-term average cost by considering only a finite length of time, due to the periodic nature of our system. We simply need to consider a period of time long enough such that the cost associated with all

segments of the nominal trajectory are included. A natural choice for this is to choose two positive integers, n and m, such that the update time is approximated by $T_u \approx \frac{n}{m}T$, where T is the period of the system. We then only need to include the cost of segments up to time nT because any segments after that will have already been included in the average long-term cost. An additional complication is that for each update time, the average cost per unit time will vary with the starting point of the algorithm along the orbit. Therefore, in order to obtain a statistical result that is independent of an arbitrary starting time, an average is performed with respect to the starting time. The unaveraged expected cost per update time for a halo orbit that is highly sensitive to the starting time is shown in Figure 2.11, along with the average value for comparison. Another view of the same data is show in Figure 2.12, which displays the data in a similar manner to Figure 2.6.

Significant computational effort can be saved when computing the cost associated with multiple update times by choosing n and m wisely. By setting m to be the number of starting times we wish to average over, the expected cost of control for each segment can be stored for each starting time, and each n of interest. An illustration of this is shown in Figure 2.13 for $m = 6$, with $n = 1$ and $n = 2$. In this analysis, we used $m = 100$ with n ranging from 5 to 95 for orbits A through D, and $m = 200$ with n ranging from 10 to 190 for orbit E. This gives a worst case resolution of T_u equal to 0.031 nondimensional time units, corresponding to orbit A. Once the expected cost for each segment has been calculated, an arithmetic average is taken with respect to each starting time.

To determine whether a given periodic orbit is stable or not, we define the Lyapunov characteristic exponent using the associated monodromy matrix, similar to the definition in [12]:

$$\alpha = \frac{\ln \max_i |\lambda_i|}{T},$$

where λ_i are the eigenvalues of $\Phi(T,0)$. The characteristic exponent gives an idea of how quickly the state of the system will grow in time (on the order of $e^{\alpha t}$). If $\alpha > 0$, the system is unstable. The characteristic time is then $1/\alpha$, which gives a time scale on which the

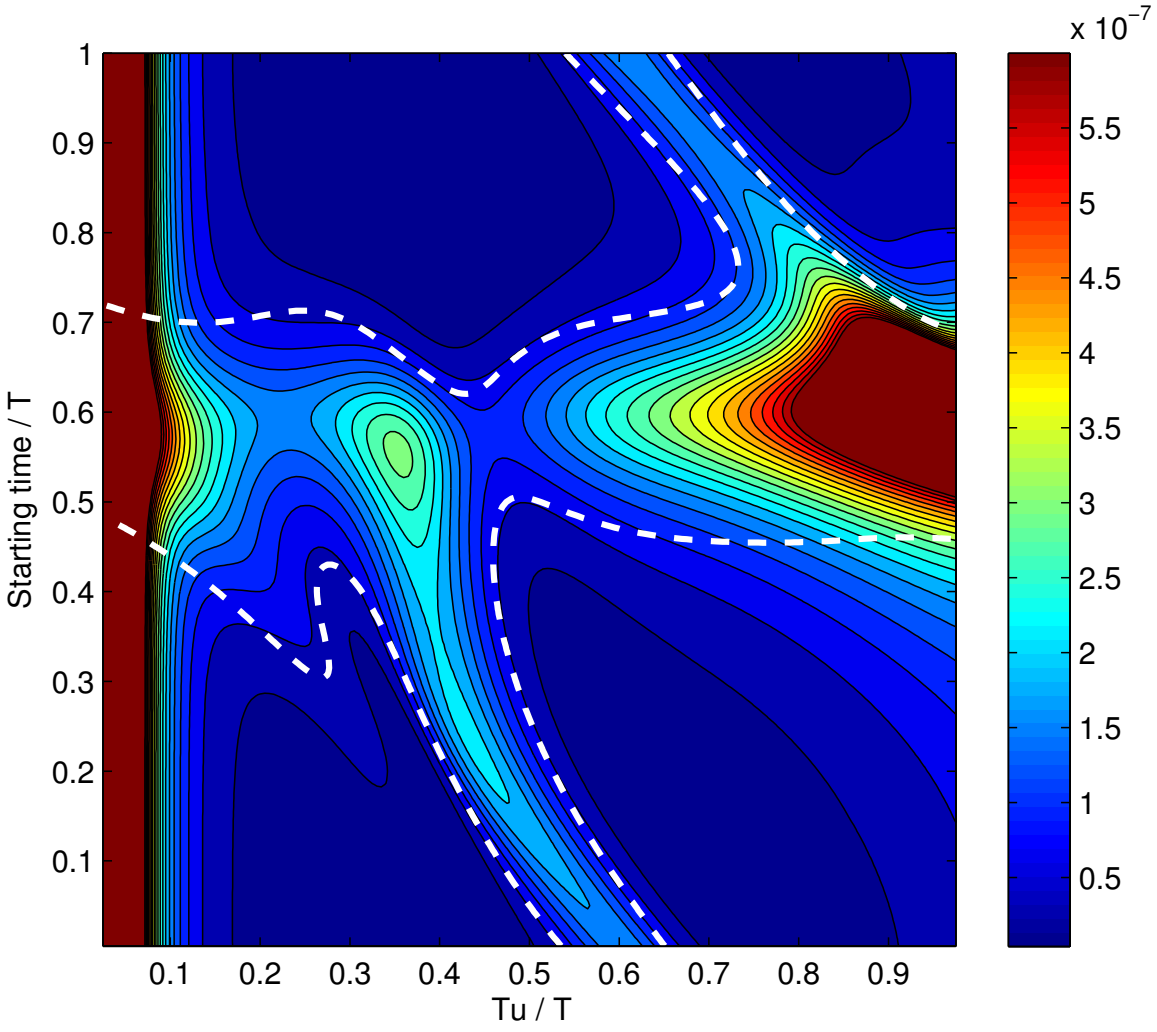

Figure 2.11 Contours of the unaveraged expected cost per update time as a function of the update time and starting time for halo orbit E. Each axis is scaled by the orbit period and the average value for a given update time is shown as the dashed white line.

exponential effects develop. For linear time-invariant systems, this simplifies to the usual condition on the eigenvalues of the dynamics matrix, i.e., the system is unstable if any of the eigenvalues have a real part greater than zero. For Hamiltonian systems, the existence of a stable manifold implies the existence of an unstable manifold.

The primary result of this analysis is that an optimal control law update time exists for unstable time-varying systems, just as in the time-invariant case, as shown in Figure 2.14. For halo orbit A using the same levels of uncertainty, the characteristic time of the instability was 0.42 time units, with the actual value occurring at about 0.61 time units (about 35

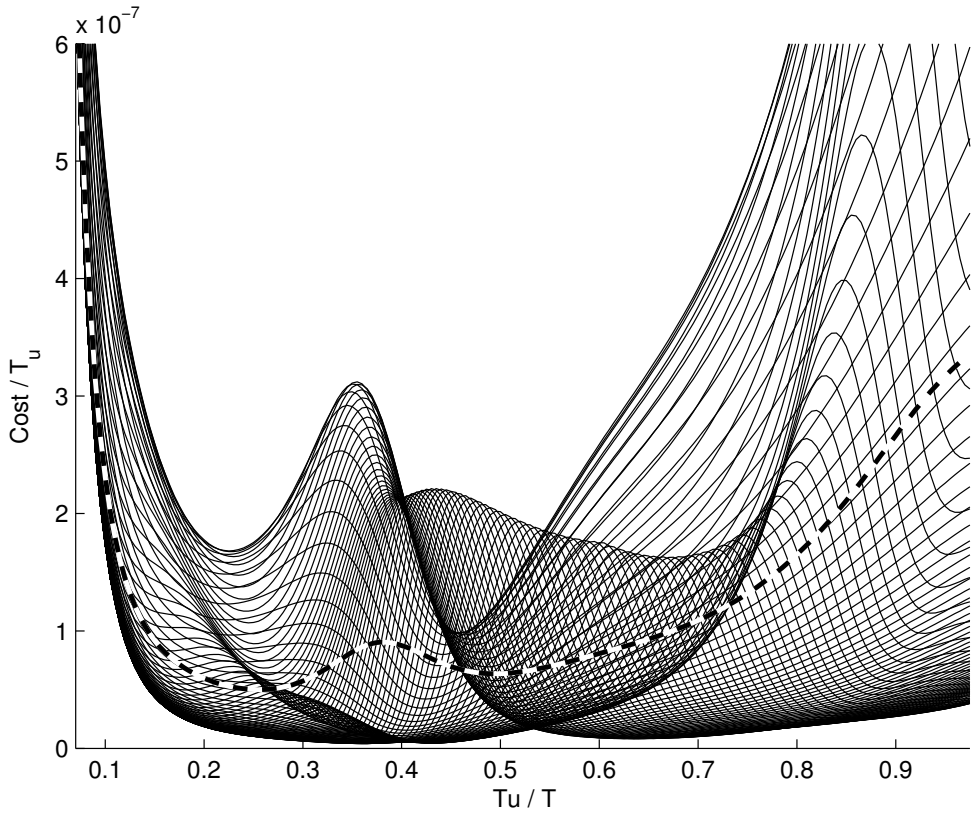

Figure 2.12 Unaveraged expected cost per update time as a function of the update time for halo orbit E. Each solid line corresponds to a different starting time and the thick dashed line is the average over all starting times.

days for the Earth-Sun system and about 2.7 days for the Earth-Moon system). The cost associated with using the characteristic time as the update time is only 10% higher than the true minimum cost for this orbit, supporting a correlation between the characteristic time of the instability and the actual optimal update time. Note that the minimum cost per unit of time occurs very near to $T_u = 1/\alpha$ for orbits A, B, and C.

As seen in Figure 2.14, the structure of the cost for orbits D and E bifurcates into a double minimum case. This is due to the interesting dynamics of the halo orbits; as the orbits move farther out of plane, they make a closer approach to the secondary body, resulting in dynamics that are very strong compared to the rest of the orbit. Combining (2.28) through (2.30) into standard first-order form with state $\vec{x} = [x \quad y \quad z \quad \dot{x} \quad \dot{y} \quad \dot{z}]^{\mathrm{T}}$ and linearizing

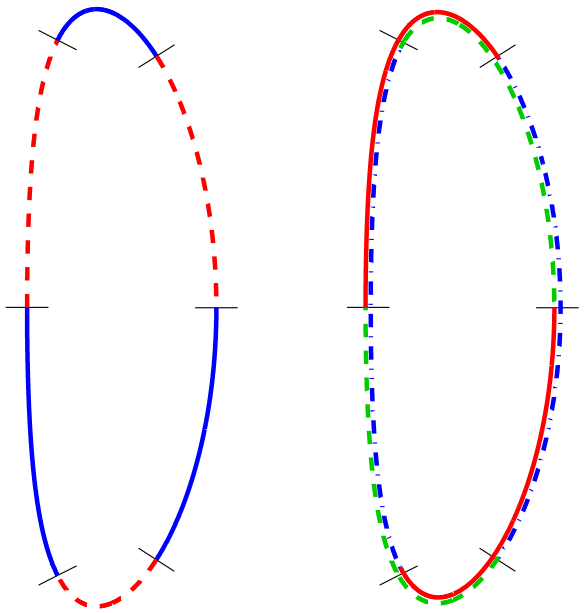

Figure 2.13 An example halo orbit and control segments divided into $m = 6$ equal-time segments, with $n = 1$ on the left and $n = 2$ on the right.

about the periodic orbit, we find $\delta\dot{\vec{x}} = \mathbf{A}(t)\delta\vec{x}$. The induced norm of $\mathbf{A}(t)$ gives an indication of how the eigenvalues of $\mathbf{A}(t)$ vary along the orbit, which in turn make the trajectory sensitive to uncertainties. The larger the norm, the stronger the sensitivity. Figure 2.15 shows a plot of $\log\|\mathbf{A}(t)\|$ and $\log\|\Phi(t,0)\|$ for two halo orbits; one highly out-of-plane, the other more in-plane. Note that for the highly out-of-plane orbit, the sensitivity varies by up to 1.5 orders of magnitude throughout the orbit, whereas in the more in-plane orbit, it varies by less than 0.3. Due to this variation, the cost of control along a halo orbit varies depending on where measurements are taken. For example, consider a control segment where $\|A\|$ is large initially, then decreases quickly. In this, the unstable effect on the probability distribution is greatly enhanced, resulting in a higher control cost for the next segment. For a given update time, if the segments are structured such that $\|A\|$ is large when measurements are made, the cost is much higher than if $\|A\|$ were only large between measurements. This behavior is strong enough to hold even through the orbit average, and is clearly visible in Figure 2.14, particularly in orbits D and E. Each local maxima occurs just before the halfway point of the corresponding orbit, where $\|A\|$ is large, as in Figure 2.15. In practice, orbit determination

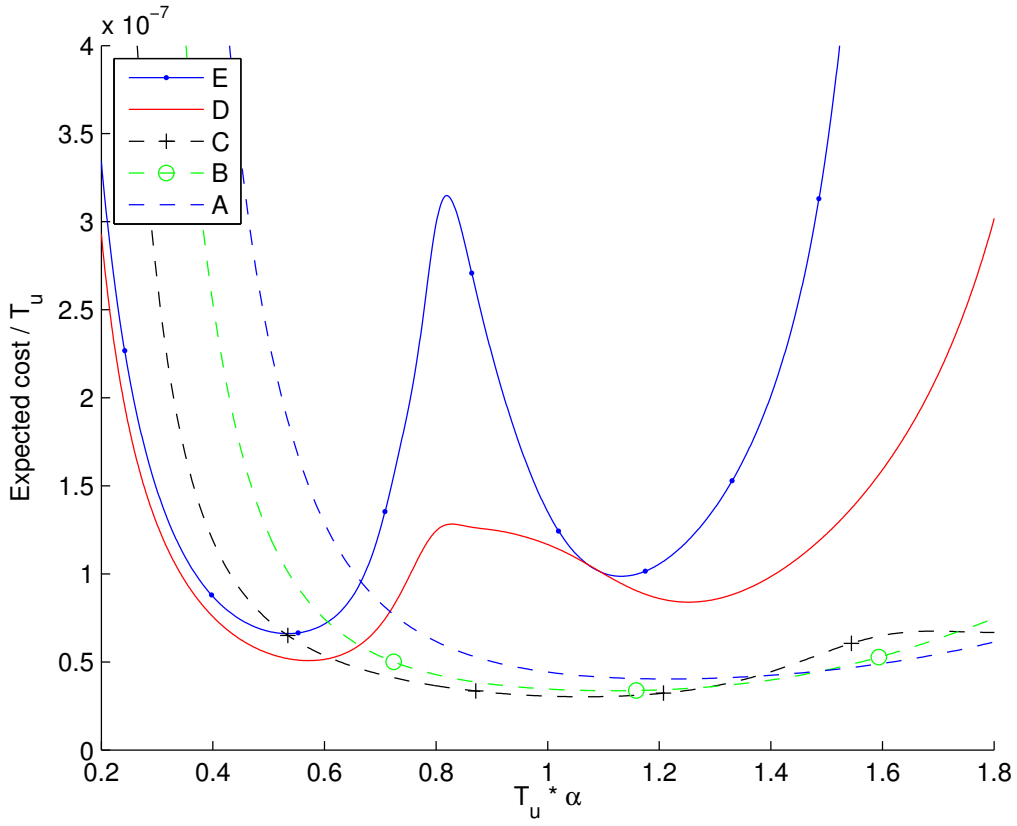

Figure 2.14 Expected cost divided by T_u as a function of T_u (scaled by the characteristic time of the unstable mode) near several halo orbits.

may be more accurate near periapsis, which could potentially be weighed against the higher statistical control cost.

The optimal update time for this time-varying system has a dependence on λ that is very similar to the equilibrium point example. Figure 2.16 shows the effect of λ on the optimal update time for orbit A, using the same parameters as in the equilibrium point analysis. The variation in the optimal update time over the range of λ shown is about 3.74 days for the Earth-Sun system.

We find a strong correlation between the characteristic time of an unstable trajectory and the optimal update time for the control of this trajectory. For strongly varying trajectories we also find additional structure in the optimal time update due to interactions between the trajectory and the gravitating bodies. These interactions raise interesting questions

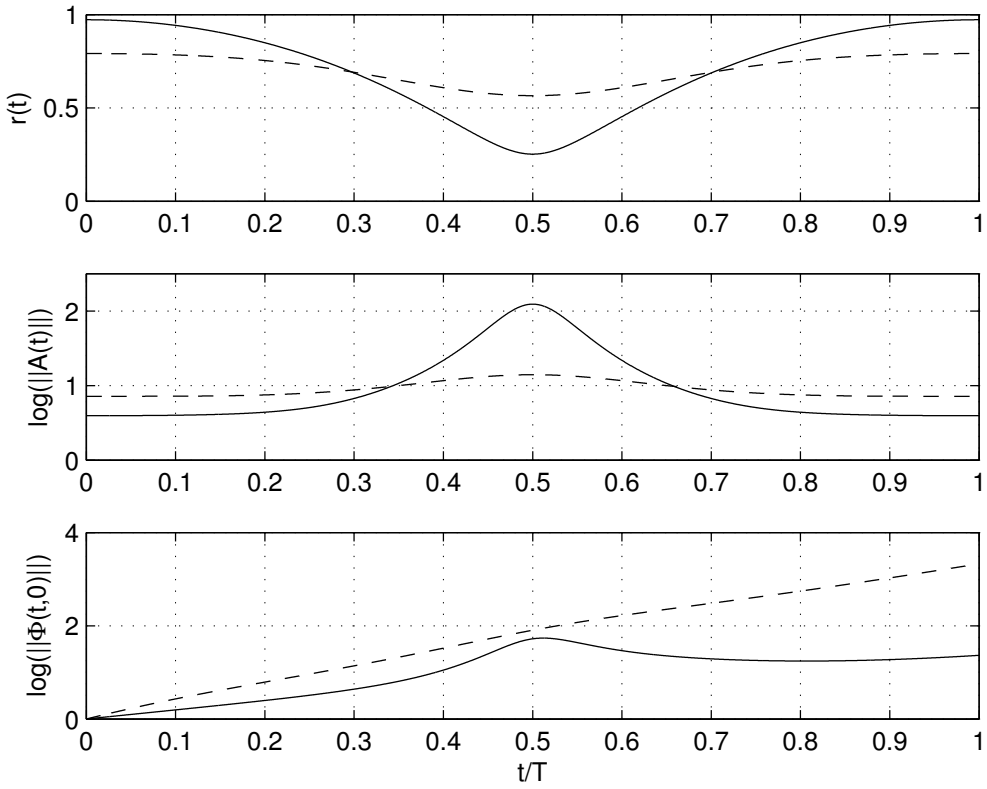

Figure 2.15 Plots of $r(t)$ (the distance from the secondary body), $\log \|\mathbf{A}(t)\|$, and $\log \|\Phi(t,0)\|$ for halo orbits D (solid) and A (dashed), plotted against a fraction of their respective orbit periods, T.

about how the interplay of measurement uncertainty, instability, and statistical costs are interrelated. We plan to further study these issues in the future, and to consider the effect of stochastic accelerations on the system.

The actual nondimensional minimum expected value of J/T_u for orbit A in the Sun-Earth system is 4.55×10^{-8}, corresponding with $T_u = 0.55$ nondimensional time units. Therefore, the upper bound on the expected ΔV per period from Equation (2.27) is 8.15×10^{-4}, whereas the actual value is 5.97×10^{-4}, or 73.2% of the upper bound. As dimensional value, this equates to $\mathrm{E}[\Delta V]/\text{period} = 5.97 \times 10^{-4}$ km/(s $\cdot$ period). The expected value of ΔV was calculated by a Monte Carlo simulation with 10,000 trials for each of the 100 starting points along the orbit. Confidence interval analysis shows that $\mathrm{E}[\Delta V]/T_u$ is within 1.7% of the reported value with 99% confidence. More accurate performance estimates could be

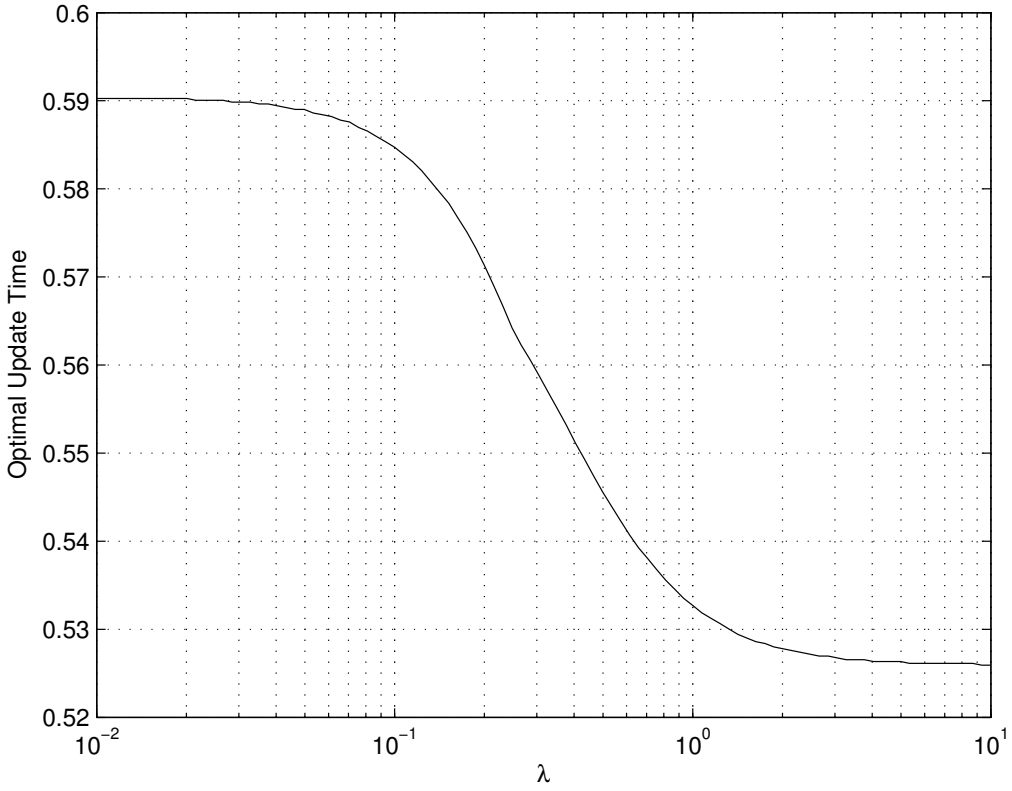

Figure 2.16 Halo orbit A optimal nondimensional update time as a function of λ, σ_r fixed

performed with more information about detailed spacecraft specifications such as engine efficiencies.

Also, Hill et al., [20] conducted a study of a Lunar L_2 orbiter with measurement uncertainties of $P_r = 1$ km^2 and $P_v = 0$ km^2/s^2 and obtained a ΔV estimate of approximately 16 cm/s per year, although they budget 1 m/s per year. Using a similar halo orbit and those uncertainties, we obtain an upper bound of 12.3 cm/s per year, an actual value of 11.2 cm/s per year, and an optimal update time of 3.00 days. If we instead use a velocity uncertainty of $P_v = (10^{-5})^2$ km^2/s^2, we obtain an upper bound of 20.5 cm/s per year, an actual value of 19.7 cm/s per year, and an optimal update time of 3.13 days. It should be noted that the dynamics of the Earth-Moon system are not well represented by the H3BP; however, the approximation is adequate for relative cost comparison. [1]

Chapter 3

Spectral Method for Stochastic Optimal Control

This chapter discusses computation of the optimal feedback control law for stochastic systems with control-dependent noise. Solutions are obtained by numerical integration of the stochastic Riccati equation for linear systems, and by numerical solution of the stochastic Hamilton-Jacobi-Bellman (SHJB) equation for nonlinear systems. The spectral method for partial differential equations (PDEs) is summarized, along with two useful transformations on the domain and range of the HJB equation. The primary contribution here is an analysis showing that noise levels present in current electric propulsion technology are large enough to significantly impact the optimal feedback control laws.

Experiments performed by Reid et al. [2] characterized the variations in thrust level for a Hall thruster. The experiments show that significant discharge current fluctuations of about 10%-20% about the mean occur in the discharge chamber up to high frequencies (greater than 10^5 Hz). These current fluctuations are directly proportional to thrust variations. This suggests that analyzing the control force as stochastic, rather than deterministic, is the more appropriate modelling approach. We assume the resulting system may be defined by an Itô stochastic differential equation. Additionally, we assume the system is driven by just one Brownian motion process, which is equivalent to assuming that there is only a single thruster on the spacecraft. For most missions, this is the case; however, the Japanese Space Agency's Hayabusa mission used four independent thrusters [21]. NASA's Dawn mission has three ion thrusters; however, only one operates at a time. Dealing with multiple Brownian motions

is much more difficult than the single case because one must compute multiple stochastic integrals [22, p. 167], which cannot be expressed simply in terms of Brownian motion increments. Technical intricacies such as this are common when dealing with stochastic differential equations. The following section describes the details one must consider when modeling stochastic systems.

3.1 Technical Background

Stochastic systems have many interesting differences from their deterministic counterparts. For mathematical rigor, stochastic systems are not described by ordinary differential equations (ODEs) like deterministic systems, but by stochastic differential equations (SDEs). Unlike ODEs, SDEs allow for different interpretations as to which form of calculus is appropriate. Additionally, the notion of a solution to an SDE is also up to interpretation; one may choose between "strong" or "weak" solutions as discussed Section 3.1.2. It is also worth noting that within the realm of SDEs, there is a qualitative difference between noise that is purely additive and noise that is multiplied by a function of the state.

3.1.1 Modeling: Itô, Stratonovich, and Langevin Forms

Starting with a deterministic ODE such as

$$\frac{dX_t}{dt} = f(t, X_t), \tag{3.1}$$

where $X_t = X(t)$, we may heuristically add noise to obtain the Langevin form of a stochastic differential equation (SDE);

$$\frac{dX_t}{dt} = f(t, X_t) + b(t, X_t)\xi_t. \tag{3.2}$$

Here, $b(t,X_t)$ is a time and state-dependent scaling term multiplying a standard Gaussian random process, ξ_t. The white noise in the Langevin form may be thought of informally as the derivative of Brownian motion (which does not mathematically exist). To be mathematically precise, we must write Equation (3.2) as a SDE, which may be interpreted as either an Itô SDE or a Stratonovich SDE. For physical systems, the Gaussian white nose in Equation (3.2) is often only an idealization of the physical noise, which is usually smooth to some extent. In this case, the Stratonovich approach is the correct one [22]. However, both forms are mathematically valid and useful in their own ways. For example, Stratonovich calculus mirrors most of the deterministic calculus results such as the chain rule, but Itô coefficients must be used in the Fokker-Planck equation and moment equations.

An Itô SDE, is written as

$$dX_t = f(t,X_t)dt + b(t,X_t)dW_t, \tag{3.3}$$

where W_t is a Brownian motion process. In the stochastic integral form, Equation 3.3 is equivalent to

$$X_t = X_{t_0} + \int_{t_0}^{t} f(s,X_s)ds + \int_{t_0}^{t} b(s,X_s)dW_s, \tag{3.4}$$

where the second integral is an Itô integral. The following notation is used to describe Stratonovich SDEs:

$$dX_t = f(t,X_t)dt + b(t,X_t) \circ dW_t, \tag{3.5}$$

or in integral form,

$$X_t = X_{t_0} + \int_{t_0}^{t} f(s,X_s)ds + \int_{t_0}^{t} b(s,X_s) \circ dW_s, \tag{3.6}$$

When noise is additive $\left(\frac{\partial b}{\partial X} = 0\right)$, the Itô and Stratonovich solutions are equivalent. In the general case, each form can be converted to the other by transforming the coeffiecents in the SDE. If X_t is a solution to the Itô equation (3.3), then it is also a solution to the

Stratonovich equation

$$dX_t = \tilde{f}(t,X_t)dt + b(t,X_t) \circ dW_t, \tag{3.7}$$

where the ith component of $\tilde{f}(t,X_t)$ is

$$\tilde{f}_i(t,X) = f_i(t,X) - \frac{1}{2}\sum_{j=1}^{n}\sum_{k=1}^{m} b_{j,k}(t,X)\frac{\partial b_{i,k}}{\partial X_j}(t,X). \tag{3.8}$$

The dimensions are $f, \tilde{f}, X \in \mathbb{R}^n$, $b \in \mathbb{R}^{n\times m}$, $W \in \mathbb{R}^m$.

The interpretation of the Langevin equation (3.2), is somewhat tricky. If the noise process, ξ_t, is taken to be a piecewise linear approximation of Brownian motion, then it approaches a Brownian motion process as samples are taken close together. However, the approximate solution, X_t, does *not* approach the solution of the Itô SDE (3.3). Instead, the approximation approaches the solution of the corresponding Stratonovich SDE, which can be converted to the Itô SDE:

$$dX_t = \overline{f}(t,X_t)dt + b(t,X_t)dW_t, \tag{3.9}$$

$$\overline{f}(t,X_t) = f(t,X_t) + \frac{1}{2}\sum_{j=1}^{n}\sum_{k=1}^{m} b_{j,k}(t,X)\frac{\partial b_{i,k}}{\partial X_j}(t,X). \tag{3.10}$$

3.1.2 Strong vs. Weak Solutions to SDEs

The concept of a solution to a determinstic ODEs is clearly defined, along with properties such as existence and uniqueness [23]. In the stochastic case, however, we have two types of solutions: strong and weak. The strong solution captures actual sample paths for a given realization of the noise process while the weak solution only captures moments.

Following the nomenclature in Kloeden and Platten [22], a strong solution of an SDE is an actual sample path of the system, given a realization of the noise process. In contrast, a weak solution is one which has the same distribution as the strong solution, but does not depend on the particular noise realization. An approximation, Y, converges in the strong

sense with order γ if there exists a finite constant K and positive constant δ_0 such that

$$\mathrm{E}\left[|X_T - Y_N|\right] \leq K\delta^{\gamma}, \tag{3.11}$$

for any time discretization with maximum step size $\delta \in (0, \delta_0)$. In the limit as the noise goes to zero, this becomes the traditional convergence criterion.

Weak solutions don't necessarily capture sample paths, but still preserve functions of the process at some time. For example, a weak solution would still give the correct mean, covariance, and expectation of a general function of the solution. An approximation, Y, converges in the weak sense with order β if for any polynomial g there exists a finite constant K and positive constant δ_0 such that

$$\left|\mathrm{E}\left[g(X_T)\right] - \mathrm{E}\left[g(Y_N)\right]\right| \leq K\delta^{\beta}, \tag{3.12}$$

for any time discretization with maximum step size $\delta \in (0, \delta_0)$.

3.1.3 Scalar Linear System with Multiplicative Noise Example

In this section, we begin with an example physical system; then we discuss the explicit form of the strong solution and the statistics of the solution. The statistics can be somewhat misleading when compared to the actual sample paths. The choice of Itô vs. Stratonovich calculus can make a large difference in system stability and long-term behavior.

We begin with the simple scalar, time-invariant, linear system with multiplicative noise, given in the Langevin form:

$$\frac{dX_t}{dt} = aX_t + DX_t\xi_t. \tag{3.13}$$

To properly analyze this, we may either interpret this using Itô or Stratonovich stochastic

calculus. The Itô form is given by

$$dX_t = aX_t dt + DX_t dW_t, \tag{3.14}$$

and the Stratonovich form is

$$d\tilde{X}_t = a\tilde{X}_t dt + D\tilde{X}_t \circ dW_t. \tag{3.15}$$

Strong Solutions The solution to Equation (3.14) is

$$X_t = X_0 \exp\left[\left(a - \frac{1}{2}D^2\right)t + DW_t\right], \tag{3.16}$$

and the solution to Equation (3.15) is

$$\tilde{X}_t = \tilde{X}_0 \exp\left[at + DW_t\right]. \tag{3.17}$$

From the properties of Brownian motion, we may make some statements about the asymptotic behavior of sample paths [24]. For the Itô solution, as $t \to \infty$, $X_t \to 0$ almost surely (a.s.) if $a < \frac{1}{2}D^2$, and $X_t \to \infty$ a.s. if $a > \frac{1}{2}D^2$. This is notably different than the deterministic case. For the Stratonovich solution, we recover the deterministic criteria: as $t \to \infty$, $\tilde{X}_t \to 0$ a.s. if $a < 0$, and $\tilde{X}_t \to \infty$ a.s. if $a > 0$.

Statistics Intuition might suggest that if the solution to an SDE approaches zero asymptotically a.s., then the expected value of the solution should tend towards zero as well. Unfortunately, this is not the case in systems with multiplicative noise, and illustrates that the statistics of a solution do not give good insight into the actual sample paths.

Taking the expectation of the Itô solution, Equation (3.16) gives

$$\begin{aligned}
\mathrm{E}[X_t] &= X_0 \exp\left[\left(a - \frac{1}{2}D^2\right)t\right] \mathrm{E}[\exp(DW_t)] \\
&= X_0 \exp\left[\left(a - \frac{1}{2}D^2\right)t\right] \exp\left(\frac{1}{2}D^2 t\right) \\
&= X_0 e^{at}.
\end{aligned}$$

So, for a satisfying $0 < a < \frac{1}{2}D^2$, the expectation of the Itô solution grows exponentially even though the solution converges to zero with probability one.

The expectation of the Stratonovich solution is

$$\begin{aligned}
\mathrm{E}\left[\tilde{X}_t\right] &= \tilde{X}_0 e^{at} \mathrm{E}\left[e^{DW_t}\right] \\
&= \tilde{X}_0 e^{at} e^{\frac{1}{2}D^2 t} \\
&= \tilde{X}_0 e^{\left(a + \frac{1}{2}D^2\right)t}.
\end{aligned}$$

If a satisfies $-\frac{1}{2}D^2 < a < 0$, then the expectation of the Stratonovich solution grows exponentially even though the solution converges to zero with probability one.

In summary, within the Itô framework, the addition of multiplicative noise can cause samples paths to converge to zero even when the system's deterministic counterpart is unstable. On the other hand, addition of such noise in the Stratonovich framework does not change the sample path behavior, but it can cause the mean to diverge.

The probability distribution function (PDF) of X_t is not Gaussian as it would be with only additive noise; however, if the noise is small, then the PDF may be close to Gaussian. The PDF may be extremely skewed so that the peak is near zero, but with a significant tail.

3.1.4 Numerical Solution of SDEs

In light of Section 3.1.1, it is not surprising that deterministic numerical integration schemes cannot generally be used to simulate stochastic systems. Even when a deterministic algorithm can be modified for stochastic systems, the order of convergence may be lower. For example, the Euler scheme is valid for stochastic systems, but the strong order of convergence is only 1/2 (the weak order is 1).

Another interesting facet of stochastic simulation is that when approximating weak solutions, the noise doesn't necessarily have to correspond to the underlying physical model. For example, in an inegrator driven by standard Gaussian white noise, dW_t, the mean and variance are

$$\mathrm{E}\left[dW_t\right] = 0 \tag{3.18}$$

$$\mathrm{E}\left[(dW_t)^2\right] = \Delta, \tag{3.19}$$

where Δ is the time step. Instead of simulating a Gaussian random process, we may use an approximating process with similar moments. For the Euler scheme, we may use a two-point random process, $\Delta\hat{W}$ such that $P(\Delta\hat{W} = \pm\sqrt{\Delta}) = 1/2$. As the convergence order of the scheme is increased, more points may be added to the distribution. For a 2nd order weak scheme, we can choose a three-point random process such that $P(\Delta\hat{W} = \pm\sqrt{3\Delta}) = 1/6$, $P(\Delta\hat{W} = 0) = 2/3$.

Scalar Milstein Scheme The Milstein scheme is the correct generalization of the Euler scheme for stochastic systems. It is strong order 1.0 accurate. When computing a numerical approximation, Y_t of the true solution X_t of Equation (3.3), the Milstein scheme is

$$Y_{n+1} = Y_n + f(t_n, Y_n)\Delta + b(t_n, Y_n)\Delta W_n + \frac{1}{2} b(t_n, Y_n) \left.\frac{\partial b(t,X)}{\partial X}\right|_{X=Y_n} \left((\Delta W_n)^2 - \Delta\right), \tag{3.20}$$

where Δ is the time step and ΔW_n is a random process of Brownian motion increments.

Multi-Dimensional Milstein Scheme Numerical integration of multi-dimensional systems is much more complicated than the scalar counterpart with the exception of a few special cases. For the general case of multi-dimensional noise (state dimension d, noise dimension m), we have

$$Y_{n+1}^k = Y_n^k + f^k\Delta + \sum_{j=1}^{m} b^{k,j}\Delta W_n^j + \sum_{j_1,j_2=1}^{m}\sum_{\ell=1}^{d} b^{\ell,j_1}\frac{\partial b^{k,j_2}}{\partial x^\ell} I_{(j_1,j_2)}, \tag{3.21}$$

where $I_{(j_1,j_2)}$ is a multiple stochastic integral that cannot generally be expressed in terms of ΔW. In general, it must be approximate by a sum.

In the case where the noise is scalar ($m = 1$), Equation (3.21) reduces to

$$Y_{n+1}^k = Y_n^k + f^k\Delta + \sum_{j=1}^{m} b^k\Delta W_n + \frac{1}{2}\left(\sum_{\ell=1}^{d} b^\ell\frac{\partial b^k}{\partial x^\ell}\right)\left((\Delta W_n)^2 - \Delta\right). \tag{3.22}$$

Another simplifying case is diagonal noise, in which case Equation (3.21) reduces to

$$Y_{n+1}^k = Y_n^k + f^k\Delta + b^{k,k}\Delta W_n^k + \frac{1}{2}b^{k,k}\frac{\partial b^{k,k}}{\partial x^k}\left((\Delta W_n^k)^2 - \Delta\right). \tag{3.23}$$

Scalar noise and diagonal noise are special cases of commutative noise, which satisfies

$$\sum_{\ell=1}^{d} b^{\ell,j_1}\frac{\partial b^{k,j_2}}{\partial x^\ell} = \sum_{\ell=1}^{d} b^{\ell,j_2}\frac{\partial b^{k,j_1}}{\partial x^\ell} \tag{3.24}$$

for all j_1, j_2, and k. The Milstein scheme for commutative noise simplifies to

$$Y_{n+1}^k = Y_n^k + f^k\Delta + \sum_{j=1}^{m} b^{k,j}\Delta W_n^j + \frac{1}{2}\sum_{j_1,j_2=1}^{m}\sum_{\ell=1}^{d} b^{\ell,j_1}\frac{\partial b^{k,j_2}}{\partial x^\ell}\Delta W^{j_1}\Delta W^{j_2}. \tag{3.25}$$

3.2 Dynamic Programming: the Stochastic Hamilton Bellman Jacobi Equation

In the general case, the dynamics are given by

$$dx(t) = b(t,x(t),u(t))dt + \sigma(t,x(t),u(t))dW(t), \tag{3.26}$$

with cost function

$$J = \mathrm{E}\left[\int_{t_0}^{t_f} f(t,x(t),u(t))dt + h(x(t_f))\right]. \tag{3.27}$$

The stochastic HJB equation describing the evolution of the value function V is

$$V_t = \sup_{u\in U}\left[-V_x^{\mathrm{T}} b(t,x,u) - f(t,x,u) - \frac{1}{2}\mathrm{Tr}\left\{V_{xx}\sigma(t,x,u)\sigma(t,x,u)^{\mathrm{T}}\right\}\right], \tag{3.28}$$

with boundary condition that $V(t_f,x(t_f)) = h(x(t_f))$.

If we restrict the system in Equation (3.26) to be linear in the control and the cost function to be quadratic in the control, we have $b(t,x,u) = a(t,x) + Bu$, $\sigma(t,x,u) = C(t,x) + Du$, and $f(t,x,u) = d(t,x) + \frac{1}{2}u^{\mathrm{T}}Ru$:

$$dx(t) = (a(t,x) + Bu)dt + (C(t,x) + Du)dW(t), \tag{3.29}$$

$$J = \mathrm{E}\left[\int_{t_0}^{t_f}\left(d(t,x) + \frac{1}{2}u^{\mathrm{T}}Ru\right)dt + h(x(t_f))\right]. \tag{3.30}$$

We may solve for the control that achieves the supremum in Equation (3.28) as

$$u = -(R + D^{\mathrm{T}}V_{xx}D)^{-1}(B^{\mathrm{T}}V_x + D^{\mathrm{T}}V_{xx}C). \tag{3.31}$$

When this control is substituted into the HJB equation, it becomes

$$V_t = -V_x^{\mathrm{T}}a - d - \frac{1}{2}C^{\mathrm{T}}V_{xx}C + \frac{1}{2}(C^{\mathrm{T}}V_{xx}D + V_x^{\mathrm{T}}B)(R + D^{\mathrm{T}}V_{xx}D)^{-1}(B^{\mathrm{T}}V_x + D^{\mathrm{T}}V_{xx}C). \tag{3.32}$$

In our case we're only interested in control-dependent noise (no state-dependent noise, so $C = 0$) because in typical spacecraft environments, the thruster noise is orders of magnitude larger than other stochastic effects. When $C = 0$, the control is

$$u = -(R + D^{\mathrm{T}} V_{xx} D)^{-1} B^{\mathrm{T}} V_x, \tag{3.33}$$

with corresponding HJB equation

$$V_t = -V_x^{\mathrm{T}} a - d + \frac{1}{2} V_x^{\mathrm{T}} B (R + D^{\mathrm{T}} V_{xx} D)^{-1} B^{\mathrm{T}} V_x. \tag{3.34}$$

This is the form of the equation we consider subsequently.

3.3 The Spectral Method for Numerical Solutions of the Stochastic HJB Equation

When solving partial differential equations numerically, one needs a means of approximating spatial derivatives of the solution. Most numerical methods such as finite differencing take a local approach where the derivatives are approximated by a function of nearby grid points. The idea behind spectral methods is to take a global approach by fitting a set of basis functions to the solution over a given domain. The numerical derivatives are then functions of the bases. A thorough introduction to the spectral method is given in the book by Boyd [25].

Common choices for the basis functions are elements in a Fourier series, Chebyshev series, Hermite polynomials, sinc functions, and more. We use Chebyshev polynomials because they can exactly fit common solutions, and are very computationally efficient. Large computational savings can be obtained if knowledge of symmetry is included. For example, an even function only needs to include even terms of Chebyshev polynomials. This cuts the required number of coefficients in half.

3.3.1 Chebyshev Polynomials

Chebyshev polynomials are a set of orthogonal polynomials over the interval $[-1,1]$. The standard definition for the Chebyshev polynomials is the recurrence relation

$$T_0(x) = 1$$
$$T_1(x) = x$$
$$T_{n+1}(x) = 2xT_n(x) - T_{n-1}(x).$$

They also satisfy the trigonometric identities

$$T_n(x) = \cos(n \arccos x) = \cosh(n \operatorname{arccosh} x).$$

The roots of Chebyshev polynomials, known as Chebyshev nodes, are very useful as interpolation points. The values of the $N+1$ nodes for the N-th order Chebyshev polynomial are given by

$$x_k = \cos\left(\pi \frac{2k+1}{2(N+1)}\right), \quad k = 0, 1, \ldots, N$$

The approximation to a scalar function $f(x)$, where x is a scalar, over the interval $[-1,1]$ by Chebyshev polynomials is given as

$$f(x) \approx \frac{1}{2} c_0 T_0(x) + \sum_{n=1}^{N} c_n T_n(x),$$

where

$$c_n = \frac{2}{N+1} \sum_{k=0}^{N} f(x_k) T_n(x_k).$$

These two equations may be used to compute the value of the approximating function and the coefficients. However, since they are really just discrete cosine transforms, it is easier and more efficient to compute them using a fast Fourier transform library[26].

It is important to note that the information contained in the coefficients of the expansion is equivalent to the information in the values of the function evaluated at the Chebyshev nodes – this is key for nonlinear PDEs. Given a sequence of coefficients approximating $f(x)$, c_n, it is easy to obtain the coefficients, c'_n, that approximate $df(x)/dx$:

$$c'_{i-1} = c'_{i+1} + 2ic_i, \quad (i = N-1, N-2, \ldots, 1).$$

This allows us to compute the spatial derivatives easily.

3.3.2 Spectral Method for Nonlinear Time-Varying PDEs

Suppose we have a PDE describing the solution V that has the form

$$\frac{\partial V(t,x)}{\partial t} = F\left(t, x, V, \frac{\partial V}{\partial x}, \frac{\partial^2 V}{\partial x^2}\right),$$

where F is some function of time, state, the function $V(t,x)$, and its derivatives. The basic spectral method is as follows:

1. Calculate and store the initial values of the $V(t,x)$ at the Chebyshev nodes, x_k.
2. Convert the node values to coefficients of the Chebyshev series, c_n.
3. From these coefficients, find the coefficients for the first and second spatial derivatives, c'_n and c''_n.
4. Evaluate the approximations for $\frac{\partial V}{\partial x}$, and $\frac{\partial^2 V}{\partial x^2}$ at the Chebyshev nodes, x_k.
5. Evaluate $F\left(t, x, V, \frac{\partial V}{\partial x}, \frac{\partial^2 V}{\partial x^2}\right)$ at the Chebyshev nodes and propagate the node values by an ODE method:

$$\frac{dV(t,x_k)}{dt} = F\left(t, x_k, V(t,x_k), \left.\frac{\partial V}{\partial x}\right|_{x_k}, \left.\frac{\partial^2 V}{\partial x^2}\right|_{x_k}\right).$$

6. Return to step 2.

3.3.3 Transformations

The HJB equation has both an infinite domain and range. The domain of the independent variable, x (the state variable), can take any real value. Also, the value function, V, may take any positive real value. Therefore, both the domain and range are unbounded, and this can cause computational complications.

To handle the range, we use a transformation that maps the infinite range to a bounded range. For the domain we either apply a similar mapping, or simply scale the domain to a region of interest. The transformations used here are not the only ones that accomplish this, and other transformations could have other nice properties or better accuracy.

If using a domain transformation that compresses an infinite domain to a finite domain, the range transformation should ensure that the transformed function decreases rapidly enough near the edges of the transformed domain boundary. The transformations used here certainly aren't the only ones that accomplish this, and other transformations could have useful properties or better accuracy. For example, the nice quadratic property of these two transformations doesn't hold in multiple dimensions. On the other hand, an exponential mapping would be able to be split the value function into factors easily.

For a general range transformation $V = f(W)$, we have

$$\frac{\partial V}{\partial t} = \frac{\partial f}{\partial W}\frac{\partial W}{\partial t}, \tag{3.35}$$

$$\frac{\partial V}{\partial \vec{x}} = \frac{\partial f}{\partial W}\frac{\partial W}{\partial \vec{x}}, \tag{3.36}$$

$$\frac{\partial^2 V}{\partial \vec{x}^2} = \frac{\partial^2 f}{\partial W^2}\left(\frac{\partial W}{\partial \vec{x}}\right)\left(\frac{\partial W}{\partial \vec{x}}\right)^{\mathrm{T}} + \frac{\partial f}{\partial W}\frac{\partial^2 W}{\partial \vec{x}^2}. \tag{3.37}$$

Using subscript notation for partial derivatives, the range-transformed HJB equation is

$$W_t = -W_{\vec{x}}a - \frac{1}{f_W}d + \frac{1}{2}f_W W_{\vec{x}}^{\mathrm{T}} B \left[R + D^{\mathrm{T}}\left(f_{WW}W_{\vec{x}}W_{\vec{x}}^{\mathrm{T}} + f_W W_{\vec{x}\vec{x}}\right)D\right]^{-1} B^{\mathrm{T}} W_{\vec{x}},$$

with the optimal control given by

$$u = -\left[R + D^{\mathrm{T}}\left(f_{WW}W_{\vec{x}}W_{\vec{x}}^{\mathrm{T}} + f_W W_{\vec{x}\vec{x}}\right)D\right]^{-1} B^{\mathrm{T}} f_W W_{\vec{x}}.$$

It is often the case that f_{WW} can be written as $g(W)f_W$ for some function g, in which case, the HJB equation and control may be written as

$$W_t = -W_{\vec{x}}a - \frac{1}{f_W}d + \frac{1}{2}W_{\vec{x}}^{\mathrm{T}} B \left[\frac{1}{f_W}R + D^{\mathrm{T}}\left(g(W)W_{\vec{x}}W_{\vec{x}}^{\mathrm{T}} + W_{\vec{x}\vec{x}}\right)D\right]^{-1} B^{\mathrm{T}} W_{\vec{x}}, \tag{3.38}$$

$$u = -\left[\frac{1}{f_W}R + D^{\mathrm{T}}\left(g(W)W_{\vec{x}}W_{\vec{x}}^{\mathrm{T}} + W_{\vec{x}\vec{x}}\right)D\right]^{-1} B^{\mathrm{T}} W_{\vec{x}}. \tag{3.39}$$

Table 3.1 lists some feasible range transformations. In subsequent simulations, we used the third choice in the table:

$$W = \exp(-(V+\delta)^{\gamma})/\beta) \Longleftrightarrow V = (-\beta \ln W)^{1/\gamma} - \delta,$$

with $\beta = 1$, $\gamma = \delta = 1/2$.

Transformation	f_W	$g(W)$
$W = \frac{1}{(\gamma+V)^n}$	$-\frac{1}{n}W^{(-1/n-1)}$	$-\left(\frac{1}{n}+1\right)W^{-1}$
$W = \exp(-V/L^2)$	$-L^2 W^{-1}$	$-W^{-1}$
$W = \exp(-(V+\delta)^{\gamma})/\beta)$	$(-\beta \ln W)^{(1/\gamma)}/(\gamma W \ln W)$	$-(\gamma(1+\ln W)-1)/(\gamma W \ln W)$

Table 3.1 Common range transformations

For the domain transformation, we used linear scaling from the Chebyshev nodes, y_i, to the domain values, x_i, as $x_i = L_i y_i$, for each dimension i. The spatial derivatives are needed

as well for use in Equations (3.38) and (3.39):

$$\frac{dy_i}{dx_i} = \frac{1}{L} \tag{3.40}$$

$$\frac{d^2y_i}{dx_i^2} = 0 \tag{3.41}$$

$$\left[\frac{\partial W}{\partial \vec{x}}\right]_i = \frac{\partial W}{\partial y_i}\frac{dy_i}{dx_i} \tag{3.42}$$

$$\left[\frac{\partial^2 W}{\partial \vec{x}^2}\right]_{ij} = \begin{cases} \frac{\partial^2 W}{\partial y_i^2}\left(\frac{dy_i}{dx_i}\right)^2 + \frac{\partial W}{\partial y_i}\frac{d^2y_i}{dx_i^2}, & i = j \\ \frac{\partial^2 W}{\partial y_i \partial y_j}\frac{dy_i}{dx_i}\frac{dy_j}{dx_j}, & i \neq j \end{cases} \tag{3.43}$$

3.4 Spectral Method Verification and Error Analysis

In this section, we present three different 1-D linear systems to verify this method. Time-stepping was performed with the 2nd order accurate implicit Crank-Nicolson scheme. Errors are computed in both the value function V and the resulting optimal control, u. The truth values are obtained from solutions to the Riccati equation. The system for each case is defined to be

$$dx(t) = (ax+u)dt + udW(t),$$
$$J = \mathrm{E}\left[\int_0^1 \frac{1}{2}u^2 dt + x(1)^2\right],$$

with $a = 1$ for the unstable system, $a = -1$ for the stable system, and $a = 1/3$ for stationary system.

When the $V \rightarrow W$ transformation is applied to the HJB equation (3.34), we obtain

$$W_t = -W_x a - \frac{1}{2}\frac{W_x^2}{\frac{W^2}{\alpha L^2} + (2/W)W_x^2 - W_{xx}}. \tag{3.44}$$

The control is calculated by substituting the transformation into Equation (3.33) to obtain

$$u = \frac{W_x}{W^2/(\alpha L^2) + (2/W)W_x^2 - W_{xx}}. \tag{3.45}$$

The derivatives W_x and W_{xx} are computed by calculating W_y and W_{yy} from the Chebyshev series, and then using Equations (3.42) and (3.43).

We also apply another transformation, this time to the domain. For each spatial dimension, i, define the new independent variable y_i as

$$x_i = \frac{Ly_i}{\sqrt{1-y_i^2}} \Longleftrightarrow y_i = \frac{x_i}{\sqrt{L^2+x_i^2}}.$$

Since each x_i ranges from $-\infty$ to ∞, y_i is bounded between -1 and 1, as shown in Figure 3.1.

When the nodes of y are chosen to be Chebyshev nodes,

$$y_k = \cos\left(\pi \frac{2k+1}{2(N+1)}\right), \quad k = 0,1,\ldots,N,$$

then the corresponding values of x are given by

$$x_k = \frac{L}{\tan\left(\pi \frac{2k+1}{2(N+1)}\right)}.$$

It is useful to know the range of x based on our choice of L and N. The maximum value of y_k is given when $k = 0$:

$$y_{max} = y_0 = \cos\left(\frac{\pi}{2(N+1)}\right)$$

giving the maximum x value of

$$x_{max} = x_0 = \frac{L}{\tan\left(\frac{\pi}{2(N+1)}\right)} \approx \frac{2L(N+1)}{\pi},$$

where the approximation holds for large N (really when $\pi/(2(N+1))$ is small). Therefore,

the maximum value of x scales linearly in both L and N.

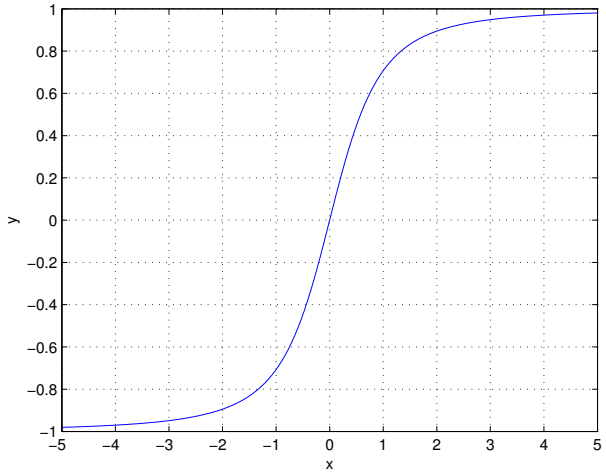

Figure 3.1 x to y transformation for $L = 1$

It is worth noting that for the scalar case, when $V = \alpha x^2$ and we apply the two transformations, $x = \frac{Ly}{\sqrt{1-y^2}}$, and $W = \frac{1}{1+V/(\alpha L^2)}$, we have that $W = 1 - y^2$ for all α and L, plotted in Figure 3.2.

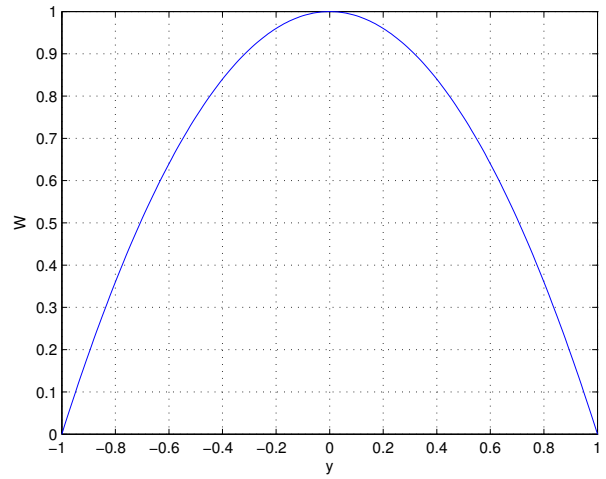

Figure 3.2 W vs. y for all α and L

The global behavior seems to be very promising. Between the collocation points in the x domain, the percent error was independent of L. At large values of x, the percent error for both V and u appears to grow like $O(\ln \ln x)$, which is very slow.

The following are 15 cases for the stable and unstable system – combinations of N and

L, where $N \in \{20,30,40,50,60\}$ and $L \in \{0.5,1,2\}$. The extent of the collocation points is given in Table 3.2. It's interesting that although the maximum value of x is only 77.65 over all cases, the transformations still include information from the entire domain, so the error does not grow quickly outside of those bounds.

	L		
N	0.5	1	2
20	6.67	13.34	26.69
30	9.86	19.72	39.44
40	13.04	26.09	52.18
50	16.23	32.46	64.91
60	19.41	38.83	77.65

Table 3.2 Maximum x value

3.4.1 Stationary Solution

With the parameters chosen in this problem, the solution for V is time-invariant when $a = 1/3$ ($V_t(t,x) = 0$ for all t,x. Since the initial condition can be expressed as a quadratic function, we only need to expand the solution to order $N = 2$ to obtain the exact solution. The maximum percent error for u was $2.19 \times 10^{-13}\%$ and the maximum percent error for V was $4.03 \times 10^{-12}\%$ over the collocation range. Over the x range of $[-1000,1000]$, the maximum percent errors are summarized in Table 3.3 and Table 3.4. These errors are entirely due to numerical roundoff.

L	Max. % error in u
0.5	2.13×10^{-7}
1	6.39×10^{-8}
2	1.86×10^{-8}

Table 3.3 Maximum percent error in u over x range $[-1000,1000]$ for stationary system

L	Max. % error in V
0.5	1.06×10^{-7}
1	3.19×10^{-8}
2	9.30×10^{-9}

Table 3.4 Maximum percent error in V over x range $[-1000,1000]$ for stationary system

3.4.2 Unstable System

The unstable system shows very good accuracy over the collocation range as listed in Table 3.5 and Table 3.6. Over the large x range $[-1000, 1000]$, the algorithm still gives very good results, summarized in Table 3.7 and Table 3.8. Figure 3.3 shows the percent error over the collocation range – the curve with higher error is the solution at the initial time (the end of the PDE integration). The collocation nodes are clearly visible by the low error at those points. Figure 3.4 shows the percent error over a very large range – again, the higher error is at $t = 0$. Each axis is a log scale, and the error is linear, indicating a growth proportional to $\ln\ln x$. Even though the collocation points range from $x \approx -78$ to $x \approx 78$, the error is less than 1% all the way up to $x \approx 5 \times 10^5$. Towards very large values of x ($x > 10^7$), rounding errors dominate as opposed to truncation error in the approximation.

N	Max. % error in u
20	2.85×10^{0}
30	1.08×10^{-2}
40	3.68×10^{-5}
50	1.08×10^{-7}
60	1.74×10^{-8}

Table 3.5 Maximum percent error in u over collocation range for unstable system

N	Max. % error in V
20	2.72×10^{-1}
30	7.79×10^{-4}
40	2.10×10^{-5}
50	2.10×10^{-5}
60	2.10×10^{-5}

Table 3.6 Maximum percent error in V over collocation range for unstable system

	L		
N	0.5	1	2
20	3.92×10^{5}	3.92×10^{5}	3.92×10^{5}
30	6.30×10^{1}	2.31×10^{1}	6.52×10^{0}
40	2.11×10^{-1}	5.27×10^{-2}	1.32×10^{-2}
50	3.99×10^{-4}	9.97×10^{-5}	2.50×10^{-5}
60	4.67×10^{-5}	1.18×10^{-5}	2.96×10^{-6}

Table 3.7 Maximum percent error in u over x range $[-1000, 1000]$ for unstable system

	L		
N	0.5	1	2
20	9.95×10^{1}	9.99×10^{1}	9.22×10^{1}
30	5.09×10^{1}	9.21×10^{0}	2.15×10^{0}
40	6.535×10^{-2}	1.63×10^{-2}	4.08×10^{-3}
50	1.21×10^{-4}	2.84×10^{-5}	2.11×10^{-5}
60	2.19×10^{-5}	2.12×10^{-5}	2.11×10^{-5}

Table 3.8 Maximum percent error in V over x range $[-1000, 1000]$ for unstable system

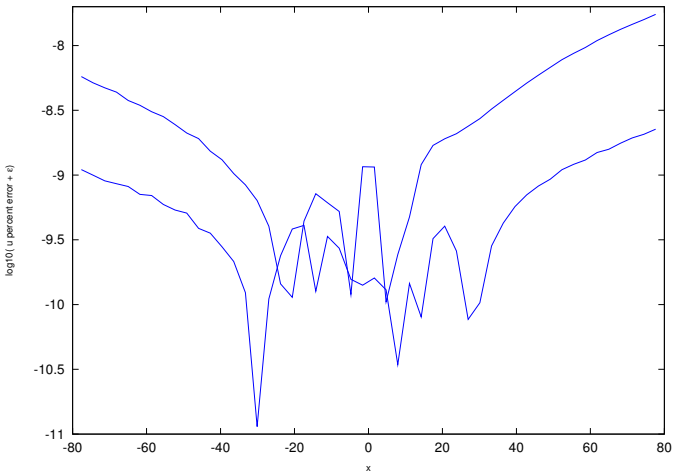

Figure 3.3 Percent error in u for unstable system over collocation range with $N = 60$, $L = 2$

Another nice feature of the spectral method is ease of convergence analysis. In finite differencing approaches, you typically have to perform a grid-refinement study to ensure that the solution has converged appropriately. In a spectral method, you can get a good idea of the convergence just by looking at the coefficients. As n increases, the sequence of coefficients, a_n, typically decreases exponentially. Figure 3.5 is a plot of the coefficient, a_n, for the unstable expansion – both at the initial and final times. At all odd values of n, a_n should be zero because V is an even function. Moreover, the exponential decay of the coefficients is clearly visible. At $n = 60$, the coefficients are on the order of machine precision, indicating good convergence.

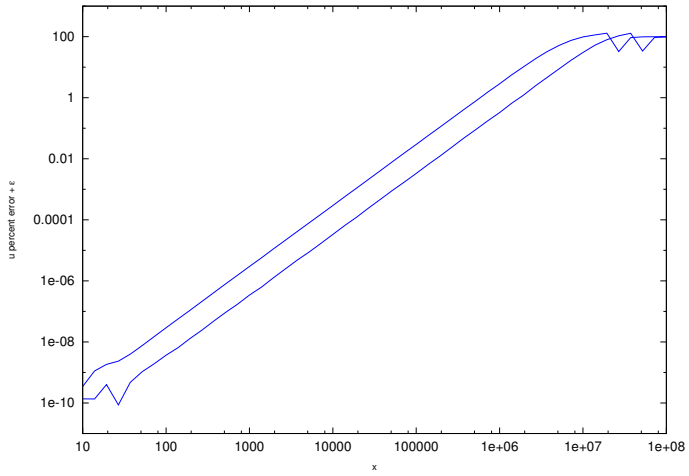

Figure 3.4 Percent error in u for unstable system over wide range with $N = 60$, $L = 2$

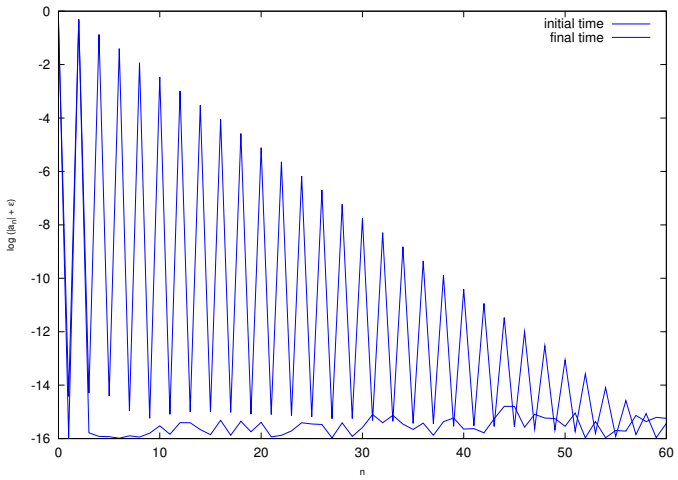

Figure 3.5 Chebyshev coefficients for unstable system with $N = 60$, $L = 2$

3.4.3 Stable System

The unstable system also shows good accuracy, although not quite as good as the unstable case. Over the collocation range, the maximum percent errors are listed in Table 3.9 and Table 3.10. Over the large x range $[-1000, 1000]$, the results are summarized in Table 3.11 and Table 3.12.

N	Max. % error in u
20	8.89×10^{0}
30	8.78×10^{-1}
40	4.83×10^{-2}
50	3.55×10^{-3}
60	1.25×10^{-4}

Table 3.9 Maximum percent error in u over collocation range for stable system

N	Max. % error in V
20	4.24×10^{0}
30	1.09×10^{-1}
40	7.07×10^{-3}
50	5.09×10^{-4}
60	2.39×10^{-4}

Table 3.10 Maximum percent error in V over collocation range for stable system

3.5 Spectral Method Applied to the Hill Three-Body Problem

These methods can now be applied to the Hill Three-Body Problem (H3BP).

For illustrative purposes, we will focus on the planar system where $z = 0$. When the system is nondimensionalized by setting $\mu = \omega = 1$ in Equations (2.28) and (2.29), the system has two equilibrium points using no control at $x = \pm 3^{-1/3} \approx 0.69336$, $y = 0$. Linearizing about either of these points and defining the perturbed state $\delta\vec{x} = [\delta x \quad \delta y \quad \delta\dot{x} \quad \delta\dot{y}]^{\mathrm{T}}$ yields the linear system

$$\delta\dot{\vec{x}} = \begin{bmatrix} 0 & 0 & 1 & 0 \\ 0 & 0 & 0 & 1 \\ 9 & 0 & 0 & 2 \\ 0 & -3 & -2 & 0 \end{bmatrix} \delta\vec{x} + \begin{bmatrix} 0 & 0 \\ 0 & 0 \\ 1 & 0 \\ 0 & 1 \end{bmatrix} \begin{bmatrix} a_x \\ a_y \end{bmatrix}.$$

This system has an unstable mode, a stable mode, and an oscillatory mode, associated with the eigenvalues $+\sqrt{1+2\sqrt{7}} \approx 2.5$, $-\sqrt{1+2\sqrt{7}} \approx -2.5$, and $\pm j\sqrt{2\sqrt{7}-1} \approx \pm 2.1j$, respectively. The unstable mode's characteristic time is then $1/\sqrt{1+2\sqrt{7}} \approx 0.4$.

The domain of analysis is a four-dimensional hypercube centered at the equilibrium point associated with $x = +3^{-1/3}$. Unless specifically noted, the parameters of each run are

	L		
N	0.5	1	2
20	1.00×10^{2}	1.00×10^{2}	9.99×10^{1}
30	9.98×10^{1}	9.78×10^{1}	8.17×10^{1}
40	7.21×10^{1}	2.85×10^{1}	7.45×10^{0}
50	5.19×10^{0}	1.29×10^{0}	3.20×10^{-1}
60	2.24×10^{-1}	5.58×10^{-2}	1.39×10^{-2}

Table 3.11 Maximum percent error in u over x range $[-1000, 1000]$ for stable system

	L		
N	0.5	1	2
20	9.98×10^{1}	9.93×10^{1}	9.74×10^{1}
30	9.62×10^{1}	8.65×10^{1}	6.14×10^{1}
40	5.26×10^{1}	2.17×10^{1}	6.47×10^{0}
50	4.61×10^{0}	1.19×10^{0}	3.00×10^{-1}
60	2.10×10^{-1}	5.26×10^{-2}	1.32×10^{-2}

Table 3.12 Maximum percent error in V over x range $[-1000, 1000]$ for stable system

the same, except for the value of noise. All common parameters are as follows:

- Number of gridpoints: 9 along each dimension (6561 points total)
- Terminal time: 0.4 non-dimension time units
- Scaling parameters, L_i: 0.1 along the position dimensions and 0.2 along the velocity dimensions
- Time-stepping algorithm: Crank-Nicolson
- Crank-Nicolson iteration limit: 3
- Iteration tolerances: absolute and relative tolerances of 1×10^{-14}

The Crank-Nicolson scheme is implicit, numerically stable, and second-order accurate in time, [27]. The implicit nature necessitates iterations to solve for the updates, and we use the number of required iterations to guide our time step choice. At each timestep, we begin by computing an initial guess with a forward Euler step. If this initial guess cannot converge to the required tolerances within 3 iterations, then we reduce the timestep and try again.

3.5.1 Verification

To verify the accuracy of the spectral solution, we begin by comparing the solution obtained using the stochastic Riccati equation [28] with the solution obtained by the spectral method with linear dynamics. We computed the control magnitude at a corner of the domain grid

and compared this to the Riccati result. This gives us a worst-case error over the domain. Figure 3.6 show the control-magnitude percent errors of three spectral cases (taking the Riccati solution as truth). The first two cases are low-accuracy runs with zero noise and 10% noise. The noise does not appear to impact accuracy. The third case is with zero noise, but tighter integration tolerance which results in a decrease in error of about an order of magnitude for the optimal control. The worst error under tight integration tolerances is about 0.3%.

The matrices defining the dynamics are cost function for the verification runs are as follows:

- $R = I_2$
- $B = \begin{bmatrix} 0_{2\times 2} \\ I_2 \end{bmatrix}$
- $D = \varepsilon \begin{bmatrix} 0_{2\times 2} \\ I_2 \end{bmatrix}$, where ε is the noise level
- The terminal cost is $h(\vec{x}(T)) = \frac{1}{2}\vec{x}^{\mathrm{T}}\vec{x}$.

A benefit of the spectral method is that it gives a self-contained measure of accuracy through the spectral coefficients. For a well-converged solution, the high-order coefficients should be near machine precision. Since the computation of the basis functions are done by Cartesian product along the grid, these coefficients may be grouped by their index's Manhattan distance from the index. For example, the coefficient corresponding to index (1, 2, 2, 3) is computed using the first order basis function along the first dimension, second order basis functions along the second and third dimension, and third order basis function along the fourth dimension. The "index distance" for this coefficient would be $1+2+2+3=8$. Enough gridpoints should be used such that, for all time during the simulation, the coefficients with the largest index distances should be as close to zero as possible. Figure 3.7 shows a poorly-converged nonlinear solution with 10% noise, 5 gridpoints in each dimension, and iteration tolerances of 1×10^{-10}. The coefficients with large index distances are significantly above machine precision by the end of the simulation. On the other hand, Figure 3.8 shows a well-converged solution with 10% noise, 9 gridpoints in each dimension, and iteration tolerances of 1×10^{-14}.

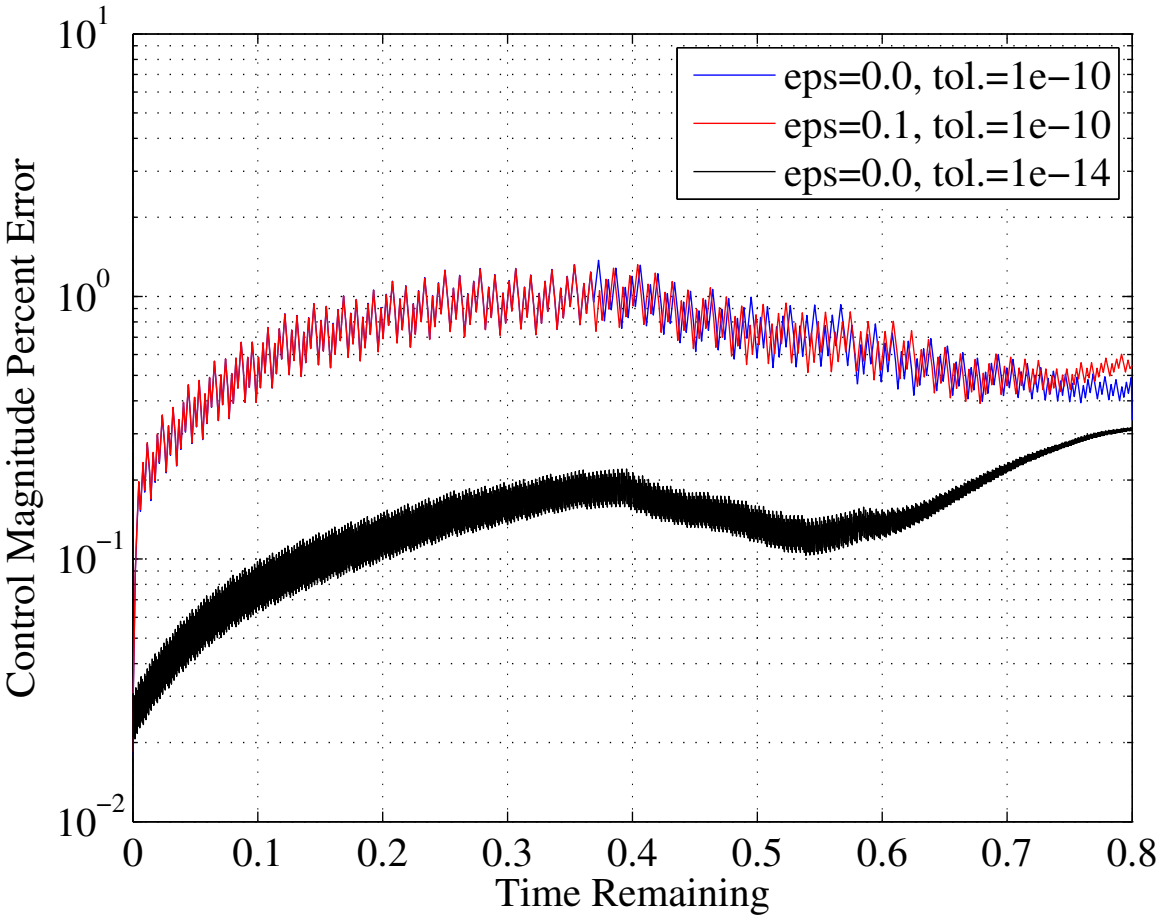

Figure 3.6 Control magnitude error between spectral and Riccati solutions

3.5.2 Results

For these runs, the following parameters were used to give higher preference towards achieving a smaller terminal state by using more control. The weights and control horizon were chosen such that when the control value is re-dimensionalized, the thrust level corresponds to the thrusters on NASA's Dawn mission [29].

- $R = 0.1 I_2$
- $B = \begin{bmatrix} 0_{2\times 2} \\ I_2 \end{bmatrix}$
- $D = \varepsilon \begin{bmatrix} 0_{2\times 2} \\ I_2 \end{bmatrix}$, where ε is the noise level
- The terminal cost is $h(\vec{x}(T)) = \frac{1}{2}\vec{x}^{\mathrm{T}}\mathrm{diag}(4,4,2,2)\vec{x}$.

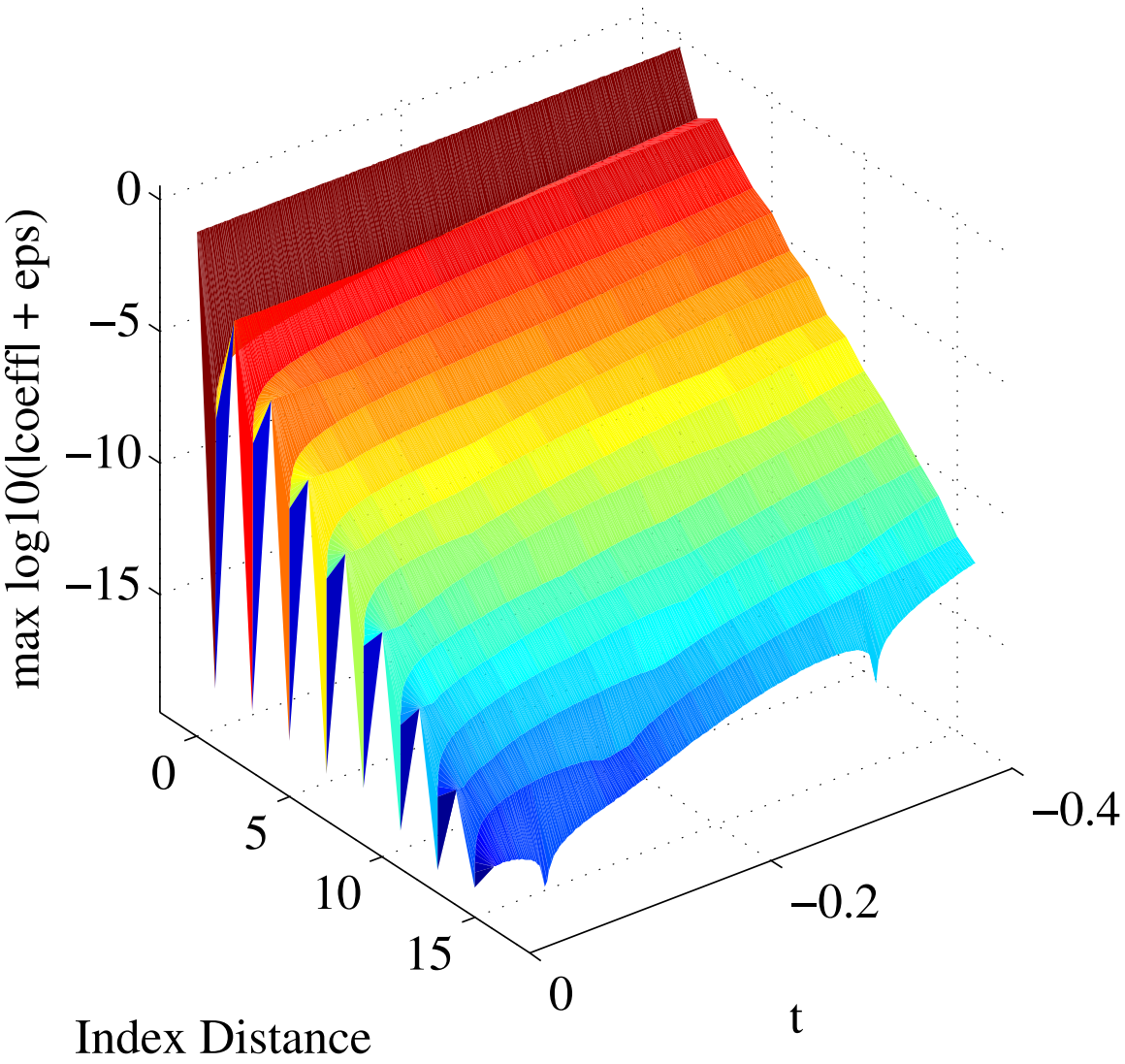

Figure 3.7 Spectral coefficients for poorly-converged run

To compare how the transformed value function changes with noise level, we compute the root-mean-square (RMS) difference between the deterministic and stochastic cases across all nodes. This RMS difference is shown in Figure 3.9 for 1%, 5% and 10% noise. Note that the transformed value function itself does not change dramatically as noise increases. However, since the control is a function of the first and second derivatives of the value function, the change in optimal control is much more pronounced. The RMS percent difference in control across all nodes is reaches a peak of about 10-20% for the case with 10% noise as shown in Figure 3.10. However, the *maximum* percent difference in noise

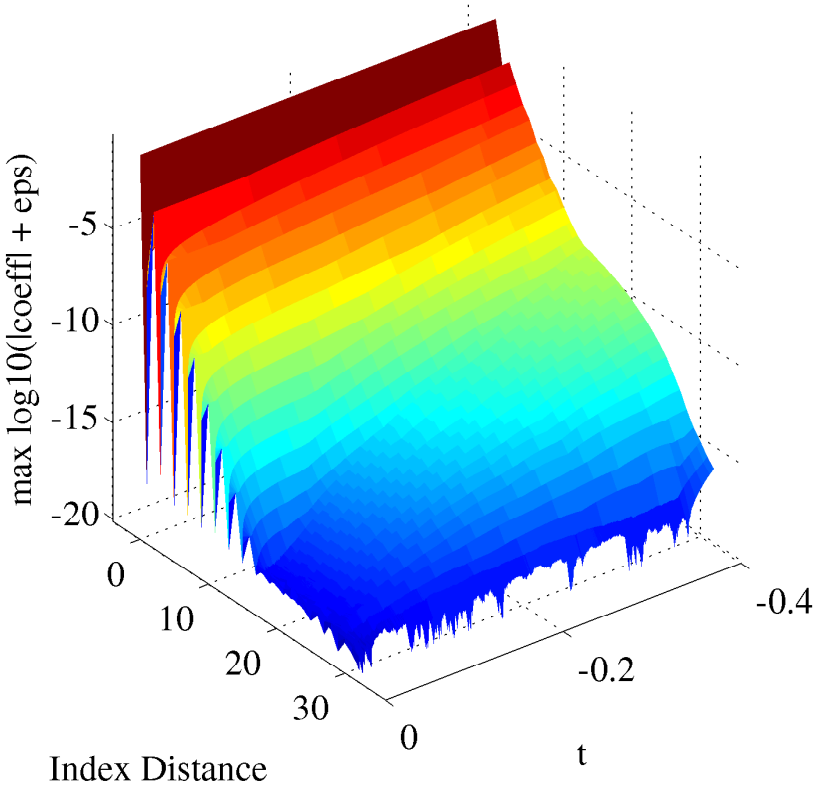

Figure 3.8 Spectral coefficients for well-converged run

ranges from 100% to 1,000% as shown in Figure 3.11.

3.5.3 Monte Carlo Analysis

Once the spectral method has solved the dynamic programming problem, we may perform a Monte Carlo analysis. Four runs were simulated with varying dynamics noise level and control laws.

1. Stochastic dynamics with $\varepsilon = 0.01$, corresponding stochastic control law
2. Stochastic dynamics with $\varepsilon = 0.05$, corresponding stochastic control law
3. Stochastic dynamics with $\varepsilon = 0.1$, corresponding stochastic control law
4. Stochastic dynamics with $\varepsilon = 0.1$, deterministic control law

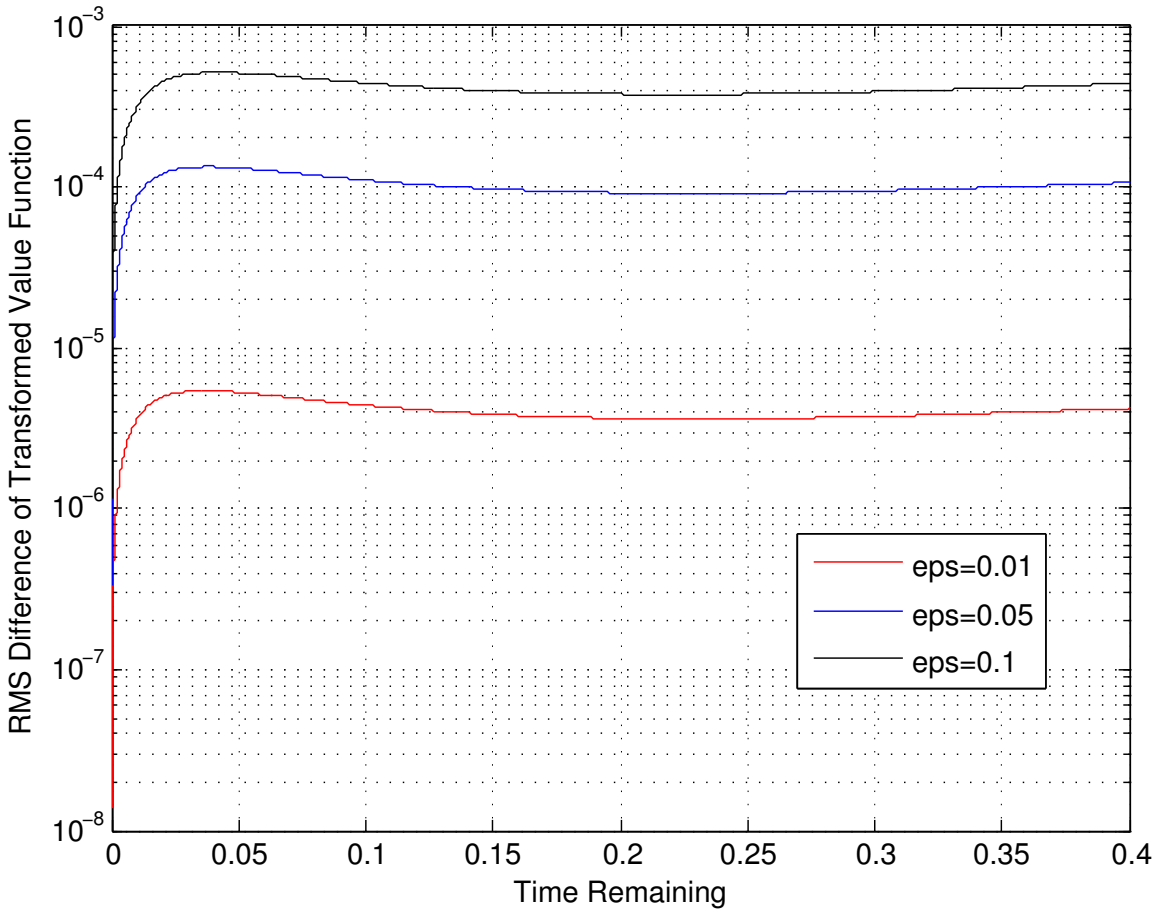

Figure 3.9 RMS difference between deterministic and stochastic transformed value functions

A benefit of having solved the SHJB equation is that we already know the expected cost. The cost obtained via Monte Carlo simulation should be in good agreement with the cost from the dynamic programming approach. (If not, then either more Monte Carlo samples must be taken, or the accuracy of the SHJB equation must be verified.) Table 3.13 shows the difference between the expected cost computed via the spectral method vs. the Monte Carlo method. As a preliminary check, the deterministic control law was simulated in one trial with the Monte Carlo code under deterministic dynamics to verify accuracy. All other cases use 10,000 samples. The worst case deviation was for the 10% noise case, where the SHJB cost differed from the Monte Carlo cost by about 4.3%. This difference could be reduced by taking more sample paths, nonetheless, the results are still quite useful.

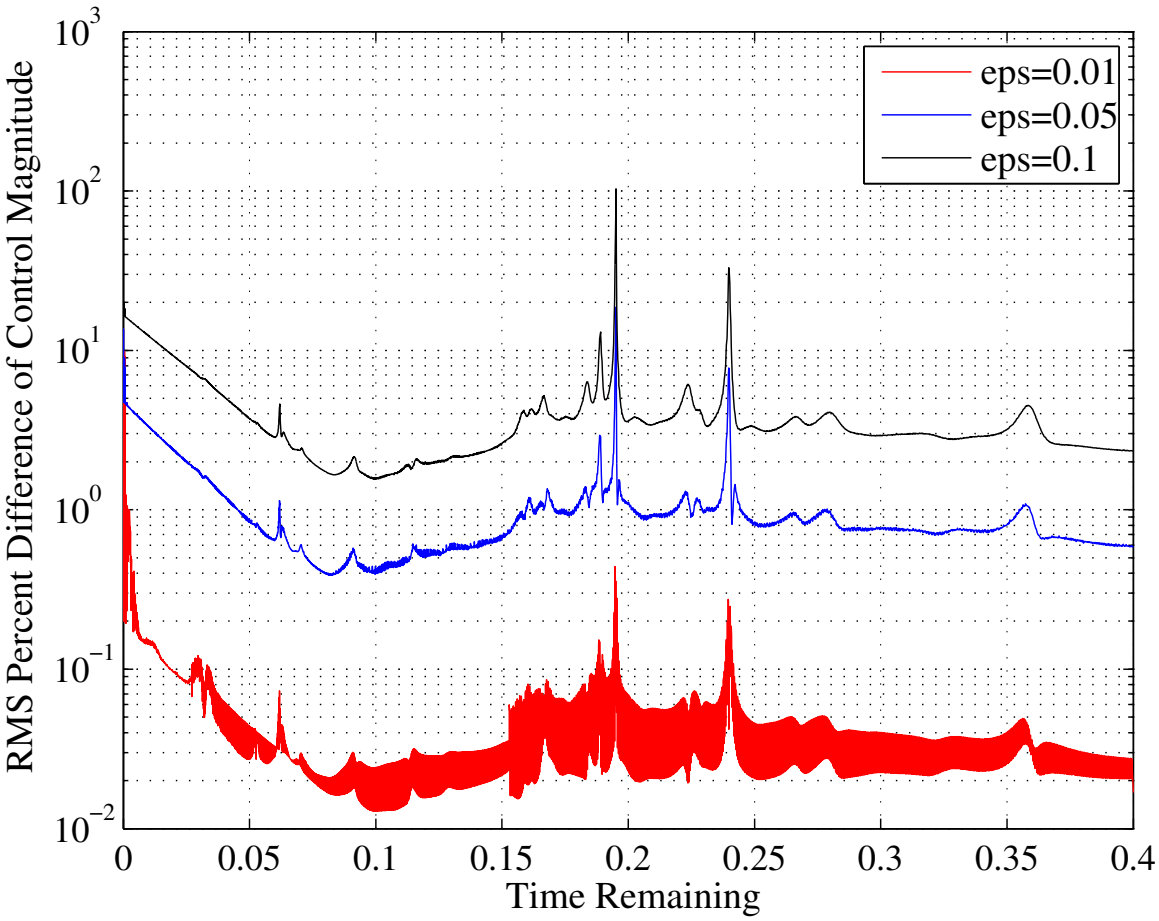

Figure 3.10 RMS difference between deterministic and stochastic optimal control values

Dynamics	SHJB Cost	MC Cost	Percent Difference
deterministic	0.0098277110	0.0098256024	0.021
stochastic, $\varepsilon = 0.01$	0.0098308309	0.0098271528	0.037
stochastic, $\varepsilon = 0.05$	0.0099055748	0.0099285040	0.231
stochastic, $\varepsilon = 0.1$	0.0101374922	0.0105716199	4.282

Table 3.13 Expected costs for SHJB vs. Monte Carlo methods.

Although the dynamic programming approach gives the expectation of the overall cost, it doesn't give any information on how much of the cost is due to the terminal penalty and how much is due to the control cost (the integral term in the cost function). On the other hand, this information is easily obtained from the Monte Carlo method. Figure 3.12 shows the distribution of the control costs. An interested point of note is that the stochastic controllers results in a distribution that is much more Gaussian than the deterministic controls in the

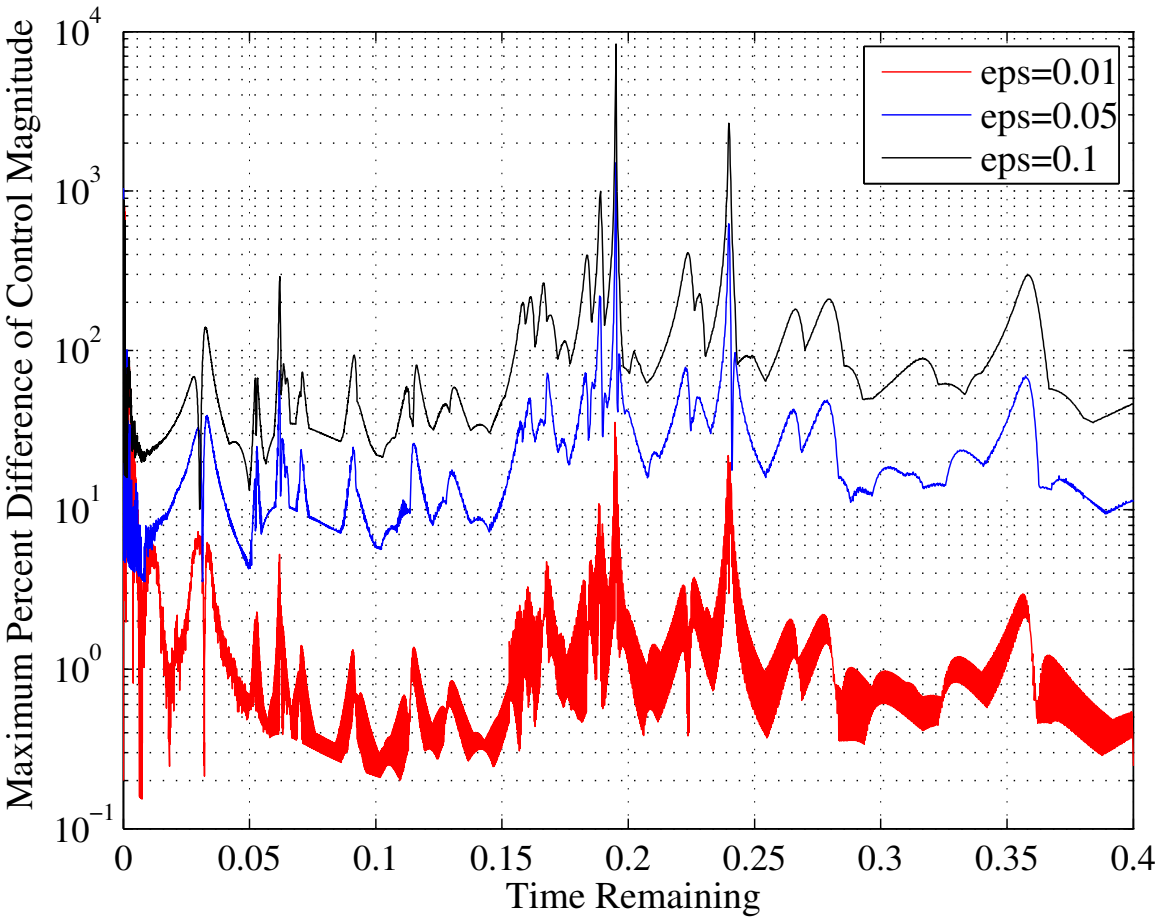

Figure 3.11 Maximum difference between deterministic and stochastic optimal control values

presence of noise. The top row of Figure 3.12 use the same level of noise in the dynamics, but different controllers. Also worth noting is that the overall expected cost increases as the noise level increases, however, the cost of control decreases because the optimal controller trades terminal penalty for reduced control. This is a manifestation of the balance between achieving control objectives and minimizing the effects of random perturbations. Figure 3.13 shows the histogram of the overall cost.

The time-histories of the Monte Carlo runs are also very interesting. Figure 3.14 shows the vector norm of the expected value of the control – the stochastic controllers clearly reduce their effort near the terminal time to avoid introducing any late uncertainty. With 10% noise, the value differs from the deterministic case by up to 35%. The differences of the angle at which the control is applied is much less drastic. As shown in Figure 3.15, the

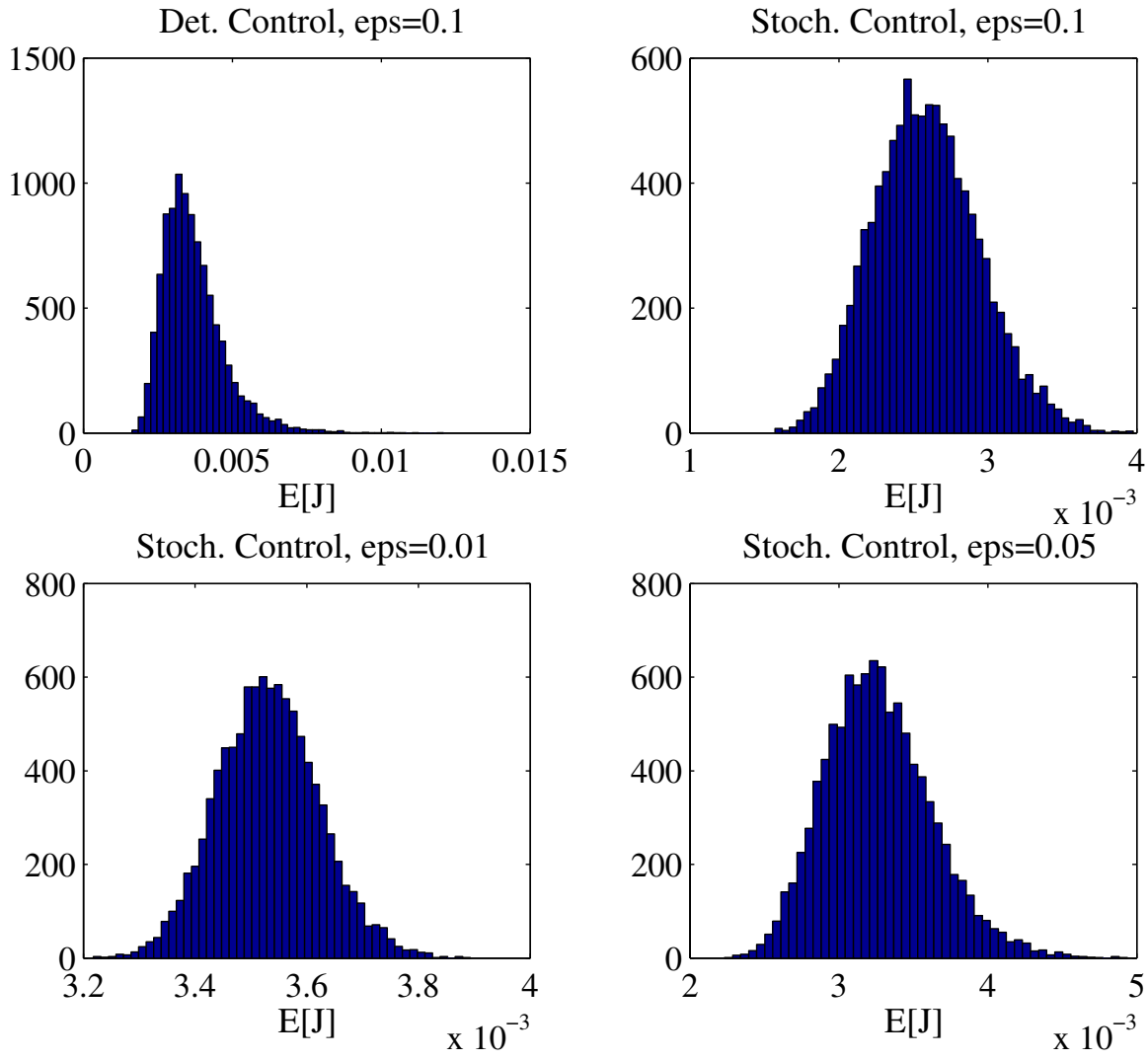

Figure 3.12 Histogram of control cost for Monte Carlo runs

control angle varies by less than 8%.

A clear advantage of using a stochastic control law can be seen in Figure 3.16. The standard deviation of uncertainty in the control when using a deterministic control law for a stochastic system was always higher than when using a stochastic controller. In the case of 10% noise, the terminal standard deviation in the deterministic controller was over 3 times that of the stochastic controller. This indicates that the stochastic controller is acting to reduce uncertainty.

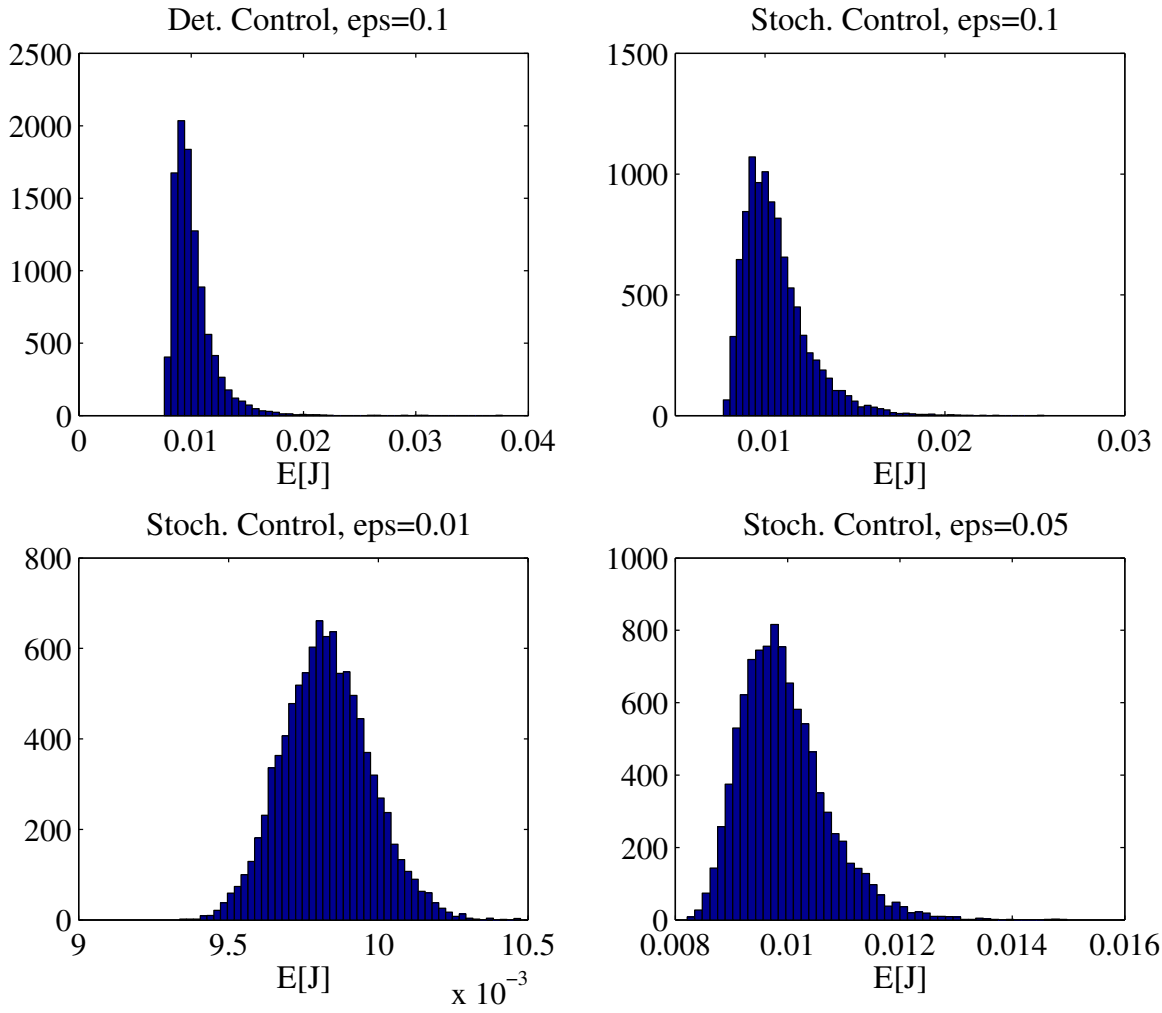

Figure 3.13 Histogram of overall cost for Monte Carlo runs

The deviation of the state is also of concern for spacecraft navigation. Figure 3.17 shows the vector norm of the expected value of the state. The terminal difference in the 10% noise case is about 18%, as compared to about 35% difference in control. Also, the deviation in the state is less than for the control. Figure 3.18 shows a state deviation of about 20% for both deterministic and stochastic controllers.

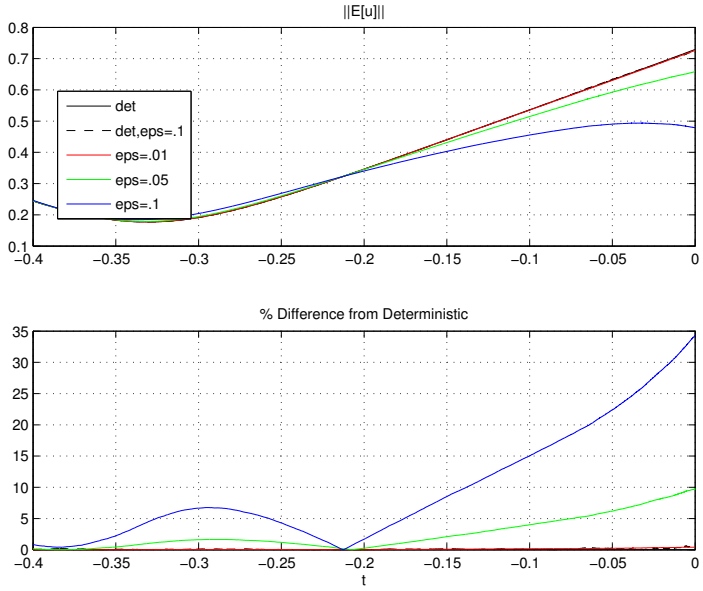

Figure 3.14 Vector norm of control for Monte Carlo runs

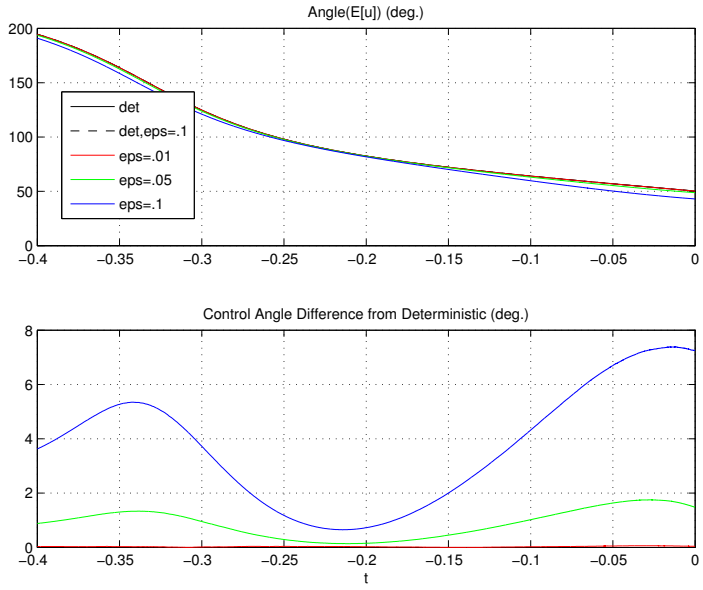

Figure 3.15 Angle of control for Monte Carlo runs

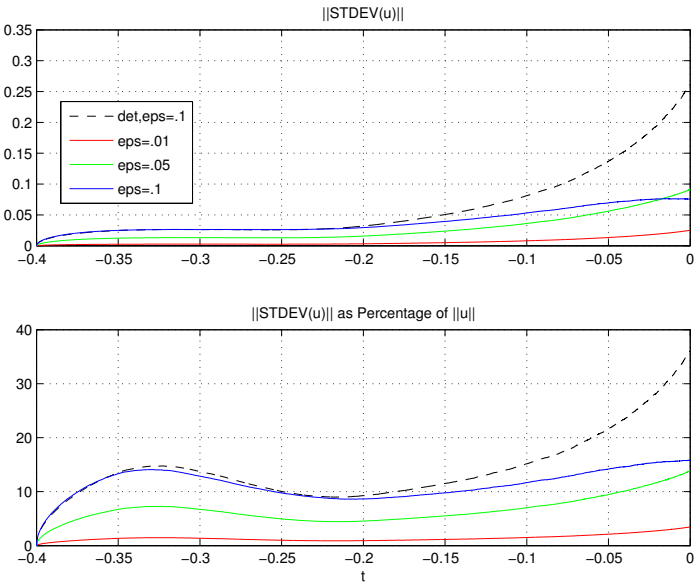

Figure 3.16 Standard deviation of control for Monte Carlo runs

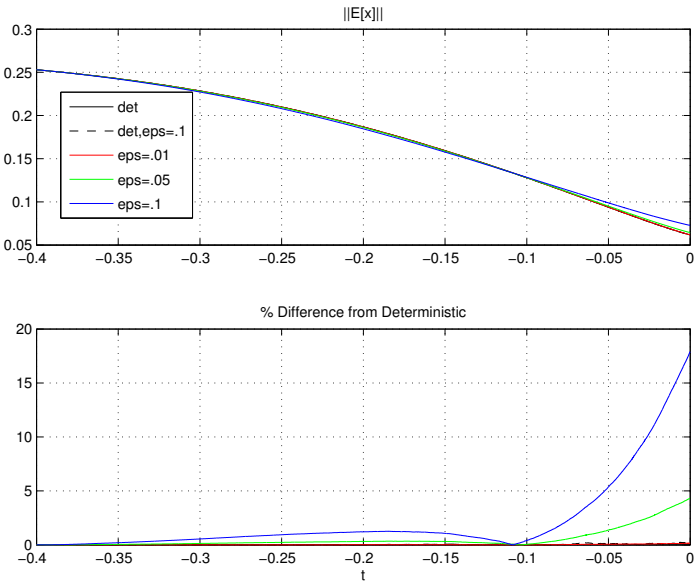

Figure 3.17 Vector norm of the state for Monte Carlo runs

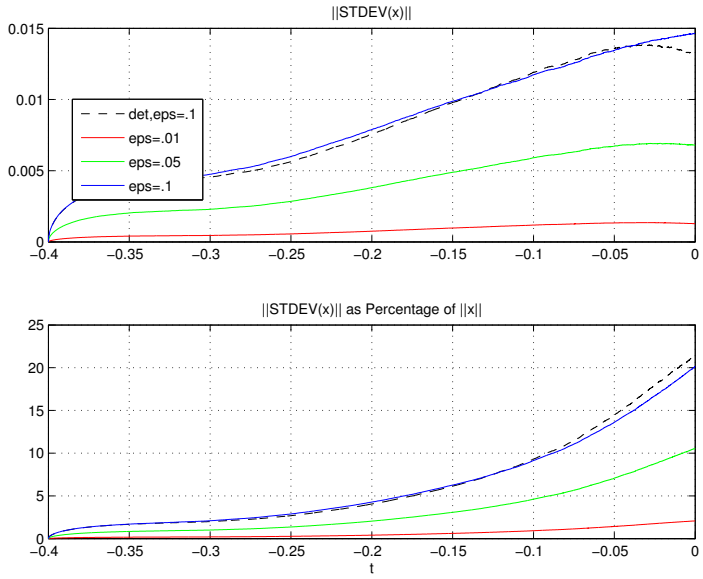

Figure 3.18 Standard deviation of the state for Monte Carlo runs

Chapter 4

Taylor Series Solution for Stochastic Optimal Control

This chapter discusses the series solution of the Stochastic Hamilton-Jacobi-Bellman (SHJB) equation. A straightforward expansion of the SHJB equation using Taylor series would appear at first to be an ineffective solution method. However, under common assumptions discussed later, a Taylor series expansion provides a suitable local approach for solution of the HJB equation. This allows for the construction of a system of ODEs describing the time-evolution of the expansion coefficients.

Another interesting outcome of this series approach is the study of stationary solutions to the HJB equation. This steady-state analysis is applicable to systems with a long control horizon. Proper analysis of the steady-state solution requires the use of a Frobenius series approach. This yields insight into the properties of the Taylor series coefficients. Also, we describe some numerical considerations for accurate computation of the Frobenius solution.

4.1 Local Approach for the Stochastic Hamilton-Jacobi-Bellman Equation

Consider the scalar SDE

$$dx(t) = (a(t,x) + Bu)dt + DudW(t), \tag{4.1}$$

with cost function

$$J = \mathrm{E}\left[\frac{1}{2}\int_0^T Ru^2 dt + h(x(T))\right]. \tag{4.2}$$

The stochastic Hamilton-Jacobi-Bellman (SHJB) equation for this system is

$$V_t = -V_x a + \frac{1}{2}B^2 V_x^2 (R + D^2 V_{xx})^{-1}, \tag{4.3}$$

with terminal condition $V(T,x) = h(x)$.

Expanding the cost function and dynamics in an infinite power series about the origin, we obtain

$$V(t,x) = \sum_{i=0}^{\infty} \tilde{V}_i(t)x^i \quad \text{and} \quad a(t,x) = \sum_{i=0}^{\infty} \tilde{a}_i(t)x^i. \tag{4.4}$$

Note that the first and second derivatives of V are

$$V_x(t,x) = \sum_{i=0}^{\infty}(i+1)\tilde{V}_{i+1}(t)x^i \quad \text{and} \quad V_{xx}(t,x) = \sum_{i=0}^{\infty}(i+2)(i+1)\tilde{V}_{i+2}(t)x^i. \tag{4.5}$$

If we substitute these expansions into the SHJB equation (4.3), we obtain ordinary differential equations (ODEs) for the coefficients $\tilde{V}_i$. The expansion can be truncated at a given order to obtain a finite dimensional system of ODEs which can be numerically solved backwards in time using the terminal conditions given. The apparent limitation in this approach is that the ODE describing $\dot{\tilde{V}}_n$ will depend on $\tilde{V}_{n+1}$ and $\tilde{V}_{n+2}$, due to the second derivative of V in the SHJB equation. Therefore, the system of ODEs resulting from truncating an expansion of $\tilde{V}$ results in a system that is not closed. The n-th order coefficient cannot be computed directly with this approach; it can only be approximated by solving for the coefficients up to an order much higher than n. We now show that under a common assumption on the system dynamics and terminal cost, this limitation is removed.

4.1.1 Implications of Expansion about an Equilibrium Point and Local Minimum/Maximum of the Cost Function

When the origin of the expansion is an equilibrium point of the system, and the gradient of the value function is zero at the expansion point, then the resulting system of ODEs is closed. (As an aside, all systems whose dynamics are described by an odd function, and whose terminal cost function is even, satisfy these conditions.)

Specifically, in order to compute the expansion coefficients at n-th order, we only need to solve for the 2nd through n-th order coefficients. In other words, increasing the order of the expansion does not change the coefficients at lower orders. Therefore, the expansion is the actual expansion of the solution, not just an approximation that only converges as many terms are added. The 0-th order term, $\tilde{V}_0$ is constant for all time, and all other coefficients are independent of $\tilde{V}_0$.

To begin the proof, first note that expanding about an equilibrium point implies that $\tilde{a}_0 = 0$. Second, expanding about a local minimum or maximum of V implies that $\tilde{V}_1$ is initially 0. Third, the previous results imply that $\tilde{V}_1$ is actually zero for all time. To see this, let us simply write out the complete expression for $\dot{\tilde{V}}_1$:

$$\dot{\tilde{V}}_1 = -\frac{\tilde{V}_1[\tilde{V}_1 B^2 D^2 \tilde{V}_3 + 2(D^2\tilde{V}_2 + R)(\tilde{a}_1 D^2\tilde{V}_2 - B^2\tilde{V}_2 + \tilde{a}_1 R)] + \tilde{a}_0[2\tilde{V}_2(D^2\tilde{V}_2 + R)^2]}{2(D^2\tilde{V}_2 + R)^2}. \quad (4.6)$$

If $\tilde{a}_0$ is zero and $\tilde{V}_1$ is initially zero, then $\dot{\tilde{V}}_1 = 0$, and $\tilde{V}_1$ will stay zero for all time. This is essential to the remainder of the proof.

Next, let the first term in the SHJB equation be expanded as follows;

$$-V_x a \equiv -\sum_{i=0}^{\infty} r_i x^i, \quad (4.7)$$

where

$$r_i = \sum_{j=0}^{i} (j+1)\tilde{V}_{j+1}\tilde{a}_{i-j}. \quad (4.8)$$

Generally, r_i depends on $\tilde{V}_{i+1}$. However, under our assumptions, r_i only depends on $\tilde{V}_2$ through $\tilde{V}_i$. Table 4.1 shows the terms in the summation of Equation (4.8). Since any term in r_i that would generally depend on $\tilde{V}_{i+1}$ is multiplied by $\tilde{V}_1(=0)$, we may conclude that r_i only depends on $\tilde{V}_2$ through $\tilde{V}_i$. Also, $r_0 = \tilde{V}_1\tilde{a}_0 = 0$, so this term has no linear dependence on x.

j	$\tilde{V}_{j+1}\tilde{a}_{i-j}$
0	$\tilde{V}_1\tilde{a}_i = 0$
1	$\tilde{V}_2\tilde{a}_{i-1}$
$\vdots$	$\vdots$
$i-1$	$\tilde{V}_i\tilde{a}_1$
i	$\tilde{V}_{i+1}\tilde{a}_0 = 0$

Table 4.1 Terms in the summation defining r_i.

The behavior of the second term in Equation (4.3) can be studied by analyzing the quantity $V_x^2(R+D^2V_{xx})^{-1}$. First, let V_x^2 be expanded as

$$V_x^2 = \sum_{i=0}^{\infty} s_i x^i, \tag{4.9}$$

where s_i is defined as

$$s_i = \sum_{j=0}^{i} (j+1)(i-j+1)\tilde{V}_{j+1}\tilde{V}_{i-j+1}. \tag{4.10}$$

From this, we see that s_i generally depends on $\tilde{V}_{i+1}$. However, we can limit the dependence to just $\tilde{V}_i$ by the same reasoning as the $V_x a$ term; the terms are listed in Table 4.2. Just like r_i, s_i only depends on $\tilde{V}_2$ through $\tilde{V}_i$. Also, later we will use the fact that $s_0 = s_1 = 0$.

j	$\tilde{V}_{j+1}\tilde{V}_{i-j+1}$
0	$\tilde{V}_1\tilde{V}_{i+1} = 0$
1	$\tilde{V}_2\tilde{V}_i$
$\vdots$	$\vdots$
$i-1$	$\tilde{V}_i\tilde{V}_2$
i	$\tilde{V}_{i+1}\tilde{V}_1 = 0$

Table 4.2 Terms in the summation defining s_i.

Now, let $(R+D^2V_{xx})^{-1}$ be expanded as

$$(R+D^2V_{xx})^{-1} \equiv \sum_{i=0}^{\infty} t_i x^i. \tag{4.11}$$

Generally, t_i is given by the standard Taylor formula

$$t_n = \left[\frac{1}{n!}\frac{d^n}{dx^n}(R+D^2V_{xx})^{-1}\right]_{x=0}. \tag{4.12}$$

Using the fact that

$$\tilde{V}_n = \frac{1}{n!}\left.\frac{\partial^n V}{\partial x^n}\right|_{x=0} \tag{4.13}$$

we see that the coefficient at a given order depends directly on the derivative of V at that order, evaluated at the origin. We wish to show that t_n depends of V of orders $\tilde{V}_2$ through $\tilde{V}_{n+2}$, or equivalently, on $V^{(2)}$ through $V^{(n+2)}$. This proof can be done using induction, as follows. The explicit dependence of t_n on $V^{(2)}$ through $V^{(n+2)}$ can be seen by writing t_n in a specific form:

$$t_n = \left[f_n(V^{(2)},\ldots,V^{(n+1)}) - \frac{D^2}{n!(R+D^2V_{xx})^2}V^{(n+2)}\right]_{x=0}, \quad n \geq 1, \tag{4.14}$$

where f_n is some function of $V^{(2)}$ through $V^{(n+1)}$. For the basis step of the induction process, note that

$$t_1 = \left[-\frac{D^2}{(R+D^2V_{xx})^2}V^{(3)}\right]_{x=0}. \tag{4.15}$$

We see that the form in Equation (4.14) holds for $n=1$ with $f_1(V^{(2)})=0$. Now, for the induction step, assume form (4.14) holds for a general n, and let us compute t_{n+1}, given by

$$t_{n+1} = \left[\frac{1}{n+1}\frac{\partial}{\partial x}\left\{f_n(V^{(2)},\ldots,V^{(n+1)}) - \frac{D^2}{n!(R+D^2V_{xx})^2}V^{(n+2)}\right\}\right]_{x=0} \tag{4.16}$$

$$t_{n+1} = \left[\frac{1}{n+1} \left\{ \sum_{i=2}^{n+1} \frac{\partial f_n(V^{(2)},\ldots,V^{(n+1)})}{\partial V^{(i)}} V^{(i+1)} + \frac{2D^4V^{(3)}}{n!(R+D^2V_{xx})^3} V^{(n+2)} \right\} - \frac{D^2}{(n+1)!(R+D^2V_{xx})^2} V^{(n+3)} \right]_{x=0}. \quad (4.17)$$

Therefore, the form holds for t_{n+1} with

$$f_{n+1}(V^{(2)},\ldots,V^{(n+2)}) = \frac{1}{n+1} \left\{ \sum_{i=2}^{n+1} \frac{\partial f_n(V^{(2)},\ldots,V^{(n+1)})}{\partial V^{(i)}} V^{(i+1)} + \frac{2D^4V^{(3)}}{n!(R+D^2V_{xx})^3} V^{(n+2)} \right\}. \quad (4.18)$$

So, in general, t_i is a function of $\tilde{V}_2$ through $\tilde{V}_{i+2}$.

Also, define the entire term as

$$V_x^2(R+D^2V_{xx})^{-1} \equiv \sum_{i=0}^{\infty} u_i x^i, \quad (4.19)$$

where

$$u_i = \sum_{j=0}^{i} s_j t_{i-j}. \quad (4.20)$$

The terms of u_i are listed in Table 4.3.

j	$s_j t_{i-j}$
0	$s_0 t_i = 0$
1	$s_1 t_{i-1} = 0$
2	$s_2 t_{i-2}$
$\vdots$	$\vdots$
$i-1$	$s_{i-1} t_1$
i	$s_i t_0$

Table 4.3 Terms in the summation defining u_i.

The first two terms of the summation vanish because $s_0 = s_1 = 0$, as mentioned previously. Therefore,

$$u_i = \sum_{j=2}^{i} s_j t_{i-j}. \quad (4.21)$$

Now, from this, we see that u_i depends s_2 through s_i and t_0 through t_{i-2}. Therefore, u_i only depends on V_2 through V_i. This allows us to compute the n-th order coefficient without knowledge of any higher order coefficients.

4.2 Steady State Frobenius Solution to the Stochastic Hamilton-Jacobi-Bellman Equation

Expanding the cost function and dynamics as a Taylor series about the origin, we obtain

$$V(t,x) = \sum_{i=0}^{N} \frac{V_i(t)}{n!} x^i \quad \text{and} \quad a(t,x) = \sum_{i=0}^{N} \frac{a_i(t)}{n!} x^i. \tag{4.22}$$

When these series expansions are substituted into the SHJB, we obtain ordinary differential equations (ODEs) describing the time-evolution of the coefficients, V_i. Assuming that the dynamics are odd and the terminal cost function is even, V_i does not depend on higher orders. The ODEs for the first few coefficients are:

$$\begin{aligned}
\dot{V}_0 &= 0 \\
\dot{V}_1 &= 0 \\
\dot{V}_2 &= -V_2 \frac{(2a_1 D^2 - B^2)V_2 + 2a_1 R}{2D^2 V_2 + 2R}
\end{aligned}$$

In trying to understand the nature of solution, one could seek a steady state solution by setting the time derivatives equal to zero. The second order term gives

$$V_2 = 0 \quad \text{or} \quad V_2 = \frac{-2a_1 R}{2a_1 D^2 - B^2} \tag{4.23}$$

as possible steady state solutions. If $V_2 = 0$, then all higher order terms are zero as well, indicating the trivial steady state solution. Alternatively, if we choose the nontrivial solution

for V_2 and compute the steady state values for the higher order coefficients, we obtain

$$V_4 = \frac{2a_3B^2R}{(2a_1D^2 - B^2)(6a_1D^2 - B^2)} \tag{4.24}$$

$$V_6 = \frac{2B^2R(6a_1a_5D^2 - 20a_3^2D^2 - a_5B^2)}{(2a_1D^2 - B^2)(6a_1D^2 - B^2)(10a_1D^2 - B^2)}. \tag{4.25}$$

As the order, n, is increased, the final factor in the denominator is $2(n-1)a_1D^2 - B^2$. For a system with no noise ($D = 0$), these factors are all equal to $-B^2$, which causes no problems. However, if D is a finite value, then the steady steady coefficients will be well defined only up to a certain order. That is, the steady state terms are finite only up to order $\lfloor 1 + B^2/(2a_1D^2) \rfloor$. ($\lfloor \cdot \rfloor$ is the floor operator.) Figure 4.1 show the relationship for a system with $B = a_1 = 1$. Figure 4.2 shows the plot of coefficients of order 2, 4, and 6 for a system with dynamics $a(x) = x - (1/6)x^3$, $B = R = 1$. Figure 4.1 tells us that the order 2, 4, and 6 coefficients in Figures 4.2a and 4.2b all converge to a finite steady-state value, but only orders 2 and 4 converge in Figure 4.2c, and only order 2 converges in Figure 4.2d.

4.2.1 Steady State Solution to the SHJB Equation

In order to study this effect rigorously we may set V_t equal to zero in the HJB to obtain a PDE describing any possible steady-state solution:

$$0 = -V_x a + \frac{1}{2}B^2V_x^2(R + D^2V_{xx})^{-1}. \tag{4.26}$$

Factoring out V_x and rearranging gives

$$0 = V_x \left[V_{xx} + \frac{-B}{2D^2a(x)}V_x + \frac{R}{D^2} \right]. \tag{4.27}$$

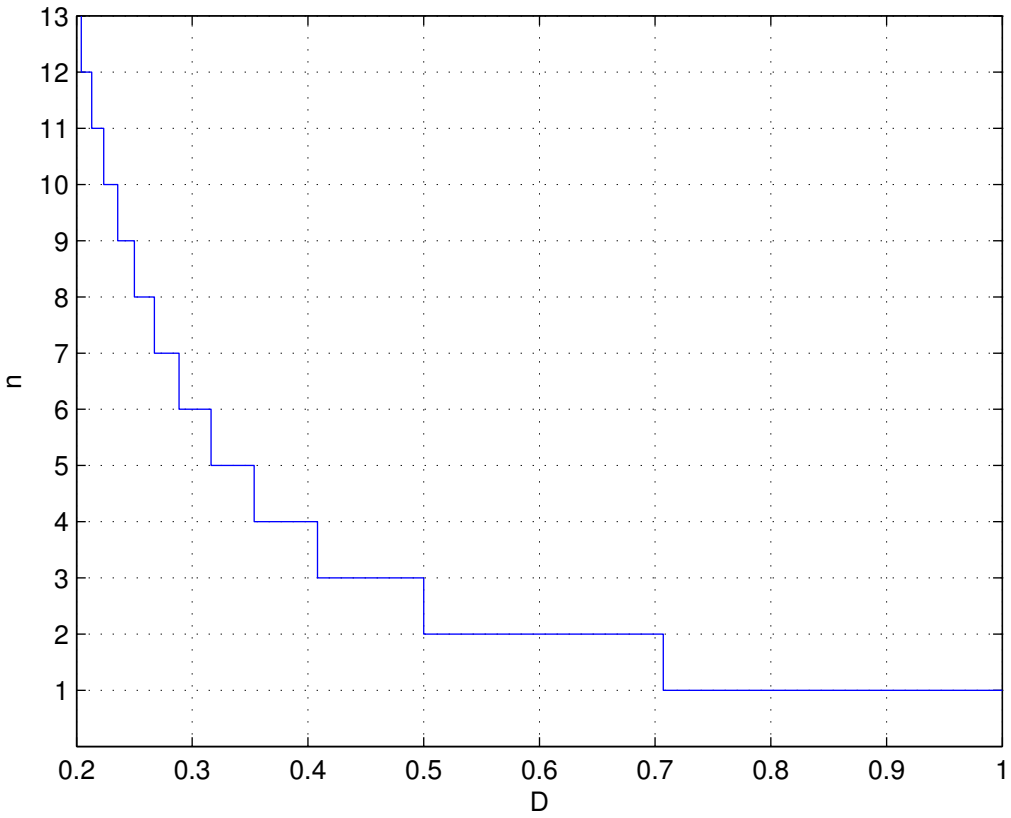

Figure 4.1 Maximum Valid Order of Steady-State Taylor Expansion (n) vs. Noise (D)

For this to hold, we have either

$$V_x = 0 \quad \text{or} \quad V_{xx} + \frac{-B}{2D^2 a(x)} V_x = -\frac{R}{D^2} \tag{4.28}$$

The first case yields the trivial solution $V(x) = 0$. The second is a second order inhomogeneous PDE with initial conditions $V(0) = 0$ and $V'(0) = 0$. Since the dynamics are odd, $a(0) = 0$, and if we assume that $a_1 \neq 0$, then the origin is a "regular singular point". This precludes the possibility of a standard Taylor expansion. Instead, the Frobenius method provides the proper series expansion [30].

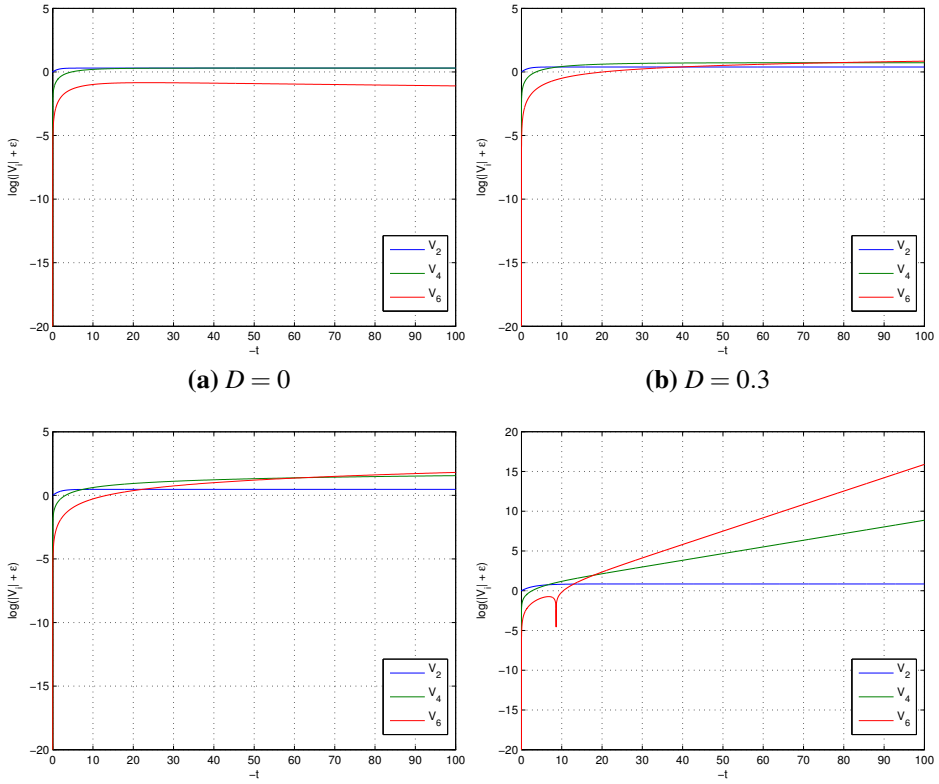

(a) $D = 0$ **(b)** $D = 0.3$

(c) $D = 0.4$ **(d)** $D = 0.6$

Figure 4.2 V coefficients vs. time for different levels of noise, D

Frobenius Method for Series Solution About a Regular Singular Point The Frobenius method finds a solution to the homogeneous equation

$$y'' + p(x)y' + q(x)y = 0, \tag{4.29}$$

of the form

$$y(x) = x^r \sum_{n=0}^{\infty} b_n x^n = \sum_{n=0}^{\infty} b_n x^{r+n}, \tag{4.30}$$

where r is not necessarily a positive integer and $b_0 \neq 0$. We assume that $x > 0$ without loss of generality because V is an even function. For the origin to be a regular singular point, we need the limits

$$p_0 = \lim_{x \to 0} xp(x), \quad \text{and} \quad q_0 = \lim_{x \to 0} x^2 q(x) \tag{4.31}$$

to exist. In general, the roots of the indical equation, $F(r)$, give the possible values of r

$$F(r) = r(r-1) + p_0 r + q_0. \tag{4.32}$$

In our case, q_0 is zero, so the values of r are $r = 0$ and $r = 1 - p_0$. The following recurrence relation gives the values of b_n:

$$F(r+n)b_n + \sum_{k=0}^{n-1} b_k(r+k)p_{n-k} = 0, \quad n \geq 1. \tag{4.33}$$

Letting $r = 1 - p_0$, and the arbitrary $b_0 = 1$, a solution to the general homogeneous equation is then

$$y_1(x) = x^r \sum_{n=0}^{\infty} b_n x^n. \tag{4.34}$$

Since the other possible value of r is zero, then the other possible solution is just the constant solution $y_2(x) = 1$ (assuming that r is not an integer)

For the steady state homogeneous SHJB equation

$$V_{xx} + \frac{-B}{2D^2 a(x)} V_x = 0, \tag{4.35}$$

the first solution is of the form

$$y_1(x) = x^r S(x), \tag{4.36}$$

where

$$S(x) = \sum_{n=0}^{\infty} b_n x^n. \tag{4.37}$$

Variation of Parameters We may now compute the general solution to the actual non-homogeneous SHJB equation by the variation of parameters method. Since finding the analytic form of the antiderivatives in the method would be difficult or impossible, we may

use definite integrals which can be computed numerically. Taking $y_2(x) = 1$, we have

$$V(x) = y_1(x)\left(g\int_\alpha^x \frac{1}{y_1'(s)}ds + c_1(\alpha)\right) - g\int_\alpha^x \frac{y_1(s)}{y_1'(s)}ds + c_2(\alpha), \tag{4.38}$$

where α is some value greater than zero and $c_1(\alpha)$ and $c_2(\alpha)$ are constants that depend on α. Letting the integrals be

$$I_1(x;\alpha) = \int_\alpha^x \frac{1}{y_1'(s)}ds,$$
$$I_2(x;\alpha) = \int_\alpha^x \frac{y_1(s)}{y_1'(s)}ds,$$

then

$$V(x) = y_1(x)\left(gI_1(x;\alpha) + c_1(\alpha)\right) - gI_2(x;\alpha) + c_2(\alpha). \tag{4.39}$$

To solve for the constant $c_2(\alpha)$, we may use the condition that $\lim_{x\to 0} V(x) = 0$ to obtain

$$g\lim_{x\to 0}\left[y_1(x)I_1(x;\alpha)\right] - gI_2(0;\alpha) + c_2(\alpha) = 0. \tag{4.40}$$

The limit may be evaluated by L'Hôpital's rule;

$$\begin{aligned}
\lim_{x\to 0}\left[y_1(x)I_1(x;\alpha)\right] &= \lim_{x\to 0}\frac{I_1(x;\alpha)}{[y_1(x)]^{-1}} \\
&= \lim_{x\to 0}\frac{1/y_1'(x)}{-[y_1(x)]^{-2}y_1'(x)} \\
&= -\lim_{x\to 0}\left(\frac{y_1(x)}{y_1'(x)}\right)^2 \\
&= -\lim_{x\to 0}\frac{x^2[S(x)]^2}{[rS(x)+xS'(x)]^2} \\
&= 0.
\end{aligned}$$

Therefore,

$$c_2(\alpha) = gI_2(0;\alpha). \tag{4.41}$$

Another condition on $V(x)$ at the origin is that $\partial V(x)/\partial x$ is zero, however, $\lim_{x\to 0} \partial V(x)/\partial x$ is always zero regardless of $c_1(\alpha)$, so this condition does not help us solve for $c_1(\alpha)$. Instead, we must use the condition that $V(x) > 0$ for all x. Splitting $I_1(x;\alpha)$ into two parts, $I_1(x;\alpha) = I_1(\infty;\alpha) - I_1(\infty,x)$, gives further insight into the behavior of $V(x)$:

$$V(x) = -gy_1(x)I_1(\infty;x) + y_1(x)\left[gI_1(\infty;\alpha) + c_1(\alpha)\right] - gI_2(x;\alpha) + c_2(\alpha). \tag{4.42}$$

From the preceding equation, $V(x)$ is greater than or equal to zero as long as

$$c1(\alpha) \geq -gI_1(\infty;\alpha). \tag{4.43}$$

Therefore, as long as $c_1(\alpha)$ is greater than a certain threshold, then $V(x)$ will be a valid cost function. If $c1(\alpha) \equiv -gI_1(\infty;\alpha)$, then the second term vanishes.

In summary, the steady state solution of the HJB equation for this system is given by

$$V(x) = -gy_1(x)I_1(\infty;x) + y_1(x)\left[gI_1(\infty;\alpha) + c_1(\alpha)\right] - gI_2(x;\alpha) + c_2(\alpha), \tag{4.44}$$

where

$$I_1(x;\alpha) = \int_\alpha^x \frac{1}{y_1'(s)} ds, \quad I_2(x;\alpha) = \int_\alpha^x \frac{y_1(s)}{y_1'(s)} ds, \tag{4.45}$$

and

$$c_1(\alpha) \geq -g \lim_{x\to\infty} I_1(x;\alpha), \quad c_2(\alpha) = gI_2(0;\alpha). \tag{4.46}$$

Linear System We can solve for the general steady state solution of a linear system in closed form. In this case, the dynamics are simply $a(x) = a_1 x$. From this, the $S(x)$ term in the Frobenius expansion is equal to 1, therefore $y_1(x) = x^r$ and $y_1'(x) = rx^{r-1}$. The integrals

$I_1(x;\alpha)$ and $I_2(x;\alpha)$ may be computed analytically:

$$I_1(x;\alpha) = \frac{1}{r(r-2)}\left(\alpha^{2-r} - x^{2-r}\right),$$
$$I_2(x;\alpha) = \frac{1}{2r}\left(x^2 - \alpha^2\right).$$

The constants c_1 and c_2 must satisfy

$$c_1(\alpha) \geq -g \lim_{x\to\infty} I_1(x;\alpha) = \frac{-g}{r(r-2)}\alpha^{2-r},$$
$$c_2(\alpha) = gI_2(0;\alpha) = \frac{-g}{2r}\alpha^2.$$

The nontrivial steady state cost function is then given by

$$V(x) = \left[\frac{g}{r(r-2)}\alpha^{2-r} + c_1\right]x^r + \frac{-g}{2(r-2)}x^2. \tag{4.47}$$

The steady state cost will always have a quadratic term, and possibly an 'x^r' term, depending on the value of c_1. If the initial $V(x)$ is quadratic, it will remain that way, and c_1 must necessarily be equal to $-g/[r(r-2)]\alpha^{2-r}$, giving

$$V(x) = \frac{-g}{2(r-2)}x^2. \tag{4.48}$$

Properties of Solution The solution,

$$V(x) = -gy_1(x)I_1(\infty;x) + y_1(x)\left[gI_1(\infty;\alpha) + c_1(\alpha)\right] - gI_2(x;\alpha) + c_2(\alpha), \tag{4.49}$$

has several properties which yield information about the nature of the solution.

1. The term $I_2(x;\alpha)$ has a valid Taylor expansion (to infinite order) about zero, and its computation does not pose a problem for any $x \geq 0$. For a finite order truncation of $S(x)$, $I_2(x;\alpha)$ grows in proportion to x^2 as $x \to \infty$.

2. The first term, $T_1(x) = -gy_1(x)I_1(\infty;x)$, also grows in proportion to x^2 as $x \to \infty$ for a finite order truncation of $S(x)$. The derivative of T_1 may be written as

$$\begin{aligned}\frac{dT_1(x)}{dx} &= -g[y_1'(x)I_1(\infty;x) - \frac{y_1(x)}{y_1'(x)}] \\ &= \frac{-gy_1'(x)y_1(x)I_1(\infty;x)}{y_1(x)} + g\frac{y_1(x)}{y_1'(x)} \\ &= \frac{y_1'(x)}{y_1(x)}T_1(x) + g\frac{y_1(x)}{y_1'(x)} \\ &= \left(\frac{r}{x} + \frac{S'(x)}{S(x)}\right)T_1(x) + \frac{gx}{r + xS'(x)/S(x)}.\end{aligned}$$

Since $T_1(x) \to \infty$ as $x \to \infty$, we may use L'Hôpital's rule to evaluate the limit

$$\lim_{x\to\infty}\frac{T_1(x)}{x^2} = \frac{1}{2}\lim_{x\to\infty}\left\{[r + xS'(x)/S(x)]\frac{T_1(x)}{x^2} + \frac{g}{r + xS'(x)/S(x)}\right\}. \tag{4.50}$$

Now, assuming that the limits

$$L_1 = \lim_{x\to\infty}\frac{T_1(x)}{x^2} \quad \text{and} \quad L_2 = \lim_{x\to\infty}[r + xS'(x)/S(x)] \tag{4.51}$$

both exist and are finite, then we obtain

$$L_1 = \frac{1}{2}\left\{L_2L_1 + \frac{g}{L_2}\right\}, \tag{4.52}$$

which gives us the result for L_1:

$$\lim_{x\to\infty}\frac{T_1(x)}{x^2} = L_1 = \frac{g}{L_2(2 - L_2)}. \tag{4.53}$$

Therefore, If $S(x)$ is truncated at order N, then $L_2 = r + N$.

3. $T_1(x)$ only has derivatives up to order $\lfloor r \rfloor$ at the origin. Assuming r is not an integer,

then $T_1(x)$ may be expanding by using integration by parts recursively to obtain

$$T_1(x) = \frac{-gS(x)}{r-2}\left\{ x^2 \sum_{n=0}^{K-2} \frac{(-1)^n \Gamma(3-r)}{\Gamma(3-r+n)} \frac{d^n U(x)}{dx^n} x^n \right. \\ \left. + \frac{(-1)^K \Gamma(3-r)}{\Gamma(1-r+K)} x^r \int_x^\infty s^{K-r} \frac{d^{K-1} U(s)}{ds^{K-1}} ds \right\}, \quad (4.54)$$

where

$$U(x) = \frac{1}{rS(x) + xdS(x)/ds}, \quad (4.55)$$

and K can be any integer greater than 2. If we choose $K = \lceil r \rceil$, then the final remaining integral has no singularity near the origin, and direct computation of $T_1(x)$ is not difficult. The last term in Equation (4.54) contributes nothing to the Taylor series (up to order $\lfloor r \rfloor$).

Deterministic System For a deterministic system, the steady state HJB equation simplifies to

$$V_t = -V_x a + \frac{1}{2}\frac{B^2}{R} V_x^2. \quad (4.56)$$

The steady state cost function may be computed directly as given by

$$V(x) = 0 \quad \text{or} \quad V(x) = \frac{2R}{B^2} \int_0^x a(s) ds. \quad (4.57)$$

Since $V(x) \geq$ for all x, we may infer that the dynamics must be unstable in order for a nontrivial solution to exist.

4.2.2 Computational Considerations

Since $I_1(\infty; x)$ diverges as $x \to 0$, even though the product $y_1(x) I_1(\infty; x)$ converges to zero, it is useful to compute the product itself instead of directly calculating $I_1(\infty; x)$ and multiplying by $y_1(x)$. Let us denote the first term of $V(x)$ as $T_1(x) = -g y_1(x) I_1(\infty; x)$. The derivative of

T_1 is then

$$\begin{aligned}\frac{dT_1(x)}{dx} &= -g[y_1'(x)I_1(\infty;x) - \frac{y_1(x)}{y_1'(x)}] \\ &= \frac{-gy_1'(x)y_1(x)I_1(\infty;x)}{y_1(x)} + g\frac{y_1(x)}{y_1'(x)} \\ &= \frac{y_1'(x)}{y_1(x)}T_1(x) + g\frac{y_1(x)}{y_1'(x)} \\ &= \left(\frac{r}{x} + \frac{S'(x)}{S(x)}\right)T_1(x) + \frac{gx}{r + xS'(x)/S(x)}.\end{aligned}$$

This is equivalent to a time-varying linear system describing the evolution of $T_1(x)$ with initial conditions $T_1(\alpha) = -gy_1(\alpha)I_1(\infty;\alpha)$. If c_1 is taken as the minimum possible value, then $T_1(\alpha) = y_1(\alpha)c_1(\alpha)$. This may be easily computed with standard ODE packages such as ode45 in MATLAB. Alternatively, we may partially solve for the state transition matrix, $\Phi(x,x_0)$. For this system,

$$\begin{aligned}\Phi(x,x_0) &= \exp\left[\int_{x_0}^{x}\left(\frac{r}{s} + \frac{S'(s)}{S(s)}\right)ds\right] \\ &= \exp\left[r(\ln x - \ln x_0) + \int_{x_0}^{x}\frac{S'(s)}{S(s)}ds\right] \\ &= \left(\frac{x}{x_0}\right)^r \exp\left[\int_{x_0}^{x}\frac{S'(s)}{S(s)}ds\right].\end{aligned}$$

The solution for $T_1(x)$, is given by

$$T_1(x) = \Phi(x,\alpha)T_1(\alpha) + \int_{\alpha}^{x}\Phi(x,s)\frac{gs}{r + sS'(s)/S(s)}ds. \tag{4.58}$$

4.2.3 Connection Between the Taylor and Frobenius Expansions

From Equation 4.44, there will generally be a term that scales as x^r as x approaches the origin. Therefore, we can only evaluate $\lfloor r \rfloor = \lfloor 1 + B^2/(2D^2a_1) \rfloor$ derivatives at the origin. This limits the order of Taylor expansions near the origin in exactly the same way as the

direct Taylor expansion.

If the general solution for $V(x)$ is expanding in a Taylor series, then the first nonzero term is

$$V(x) = \frac{-g}{2(r-2)}x^2 + \ldots, \tag{4.59}$$

which also matches the original Taylor results.

4.3 Example Implementation

Following the previous chapters, we now apply this theory to the relative equilibria of the planar H3BP, using the same parameters as the spectral method examples in Chapter 3. We compute the Taylor series coefficients of the value function for orders 2, 3, and 4. From the value function, we may then compute control values. The following figures show the root-mean-square (RMS) error, assuming the spectral results are the truth values. The errors are computed separately over two domains: the closest one-third of the nodes to the origin, and the farthest third. This gives an indication of how the accuracy of the Taylor solution degrades with increasing distance from the expansion point. Figure 4.3 shows the errors for the deterministic case. The solid lines are the RMS errors for the closest third of the nodes, and the dashed line is for the farthest third. The value function results for the stochastic case with 10% noise are shown in Figure 4.4. Each case shows similar trends; lower errors occured at higher order expansions and closer to the origin.

Figures 4.5 and 4.6 show the RMS error for the vector norm of the control over the same domain. The same trends hold – lower errors occured at higher order expansions and closer to the origin; however, the control error is much higher than the value function error. This is because the control is a function of the first and second derivatives of the value function, hence any errors become magnified. The worst case control error of 64% occurs for the second order expansion in the farthest third of the nodes. The best case error is 2%, which occurs in the fourth order expansion for the closest third of the nodes.

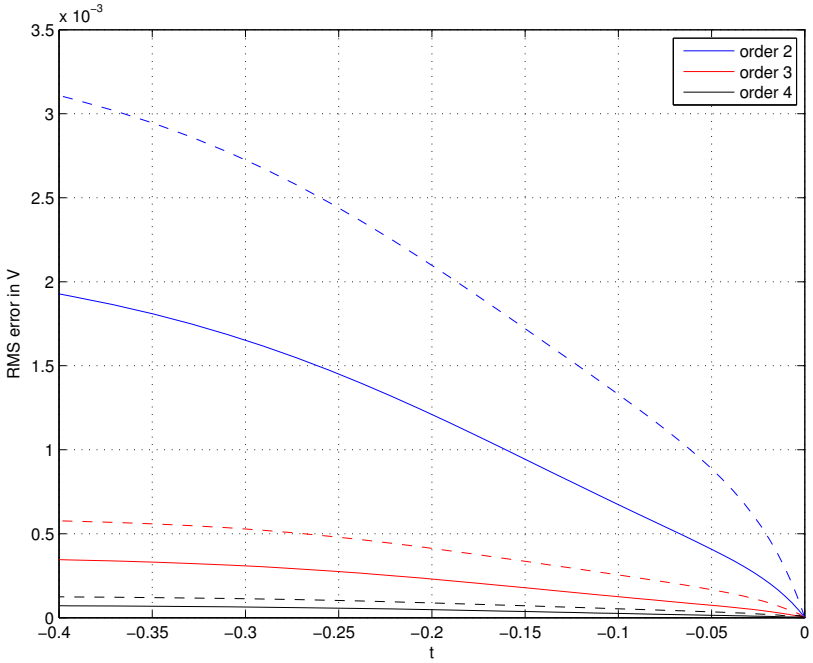

Figure 4.3 RMS Error in the value function for $\varepsilon = 0$ (deterministic). The solid lines are for the closest third of the nodes, and the dashed line is for the farthest third.

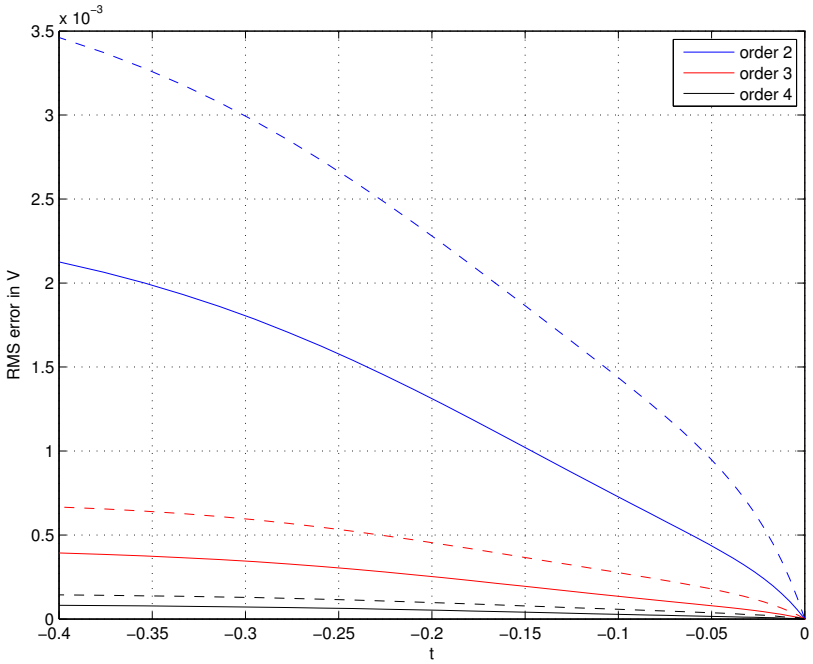

Figure 4.4 RMS Error in the value function for $\varepsilon = 0.1$. The solid lines are for the closest third of the nodes, and the dashed line is for the farthest third.

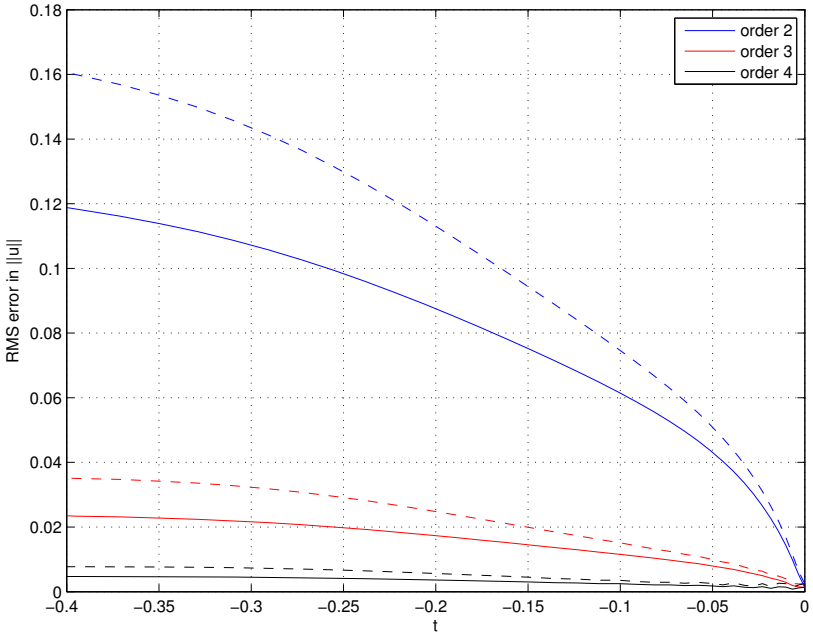

Figure 4.5 RMS Error in the control norm for $\varepsilon = 0$ (deterministic). The solid lines are for the closest third of the nodes, and the dashed line is for the farthest third.

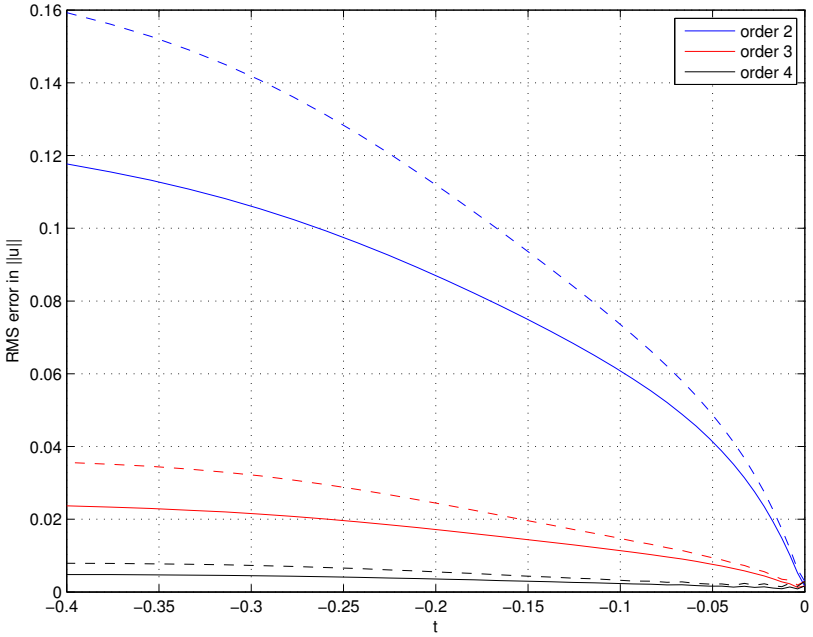

Figure 4.6 RMS Error in the control norm for $\varepsilon = 0.1$. The solid lines are for the closest third of the nodes, and the dashed line is for the farthest third.

Chapter 5
Conclusions

The primary purpose of this dissertation is to study the impact of uncertainty in spacecraft control. The uncertainty is introduced through either imperfect state measurements or stochastic dynamics. We show that consideration of uncertainty, even in the initial stages of mission planning, can be beneficial by allowing for more accurate prediction of control costs, as well as reducing the expected control cost.

5.1 Summary

The primary result from Chapter 2 is that the inclusion of uncertainty in state measurements can affect how control law updates should be performed. We show that under a common method of spacecraft measurements/updates for unstable systems, there exists an optimal time at which these updates should be performed. These results assume continuous control force, and serve as an extension of previous work done with impulsive control.

Chapter 3 deals with the numerical computation of optimal feedback control laws for stochastic systems. We use the spectral method to solve the stochastic Hamilton-Jacobi-Bellman (SHJB) equation; then we provide analysis of several systems via the Monte Carlo method.

Finally, Chapter 4 deals with the series solutions of the SHJB equation. We conclude that, under a fairly non-restrictive assumption, the SHJB equation permits solution via a Taylor series. This results in a closed system of ordinary differential equations describing the evolution of the coefficients in the power series. Also, we show that in steady-state, the

SHJB may not have a valid Taylor series expansion, and instead may be described by a Frobenius series.

5.2 Future Work

There are many interesting directions that could be pursued based on this work. In Chapter 2, we assume a fixed amount of time between control update intervals, and the problem is to find the best interval to minimize the cost function. Alternatively, a topic of future investigation could be to formulate the problem in a slightly more general way, for example finding the best way to distribute n control law updates over m periods. Another interesting topic that merits further analysis is the optimal distribution between position and velocity uncertainty to obtain optimal costs.

From Chapter 3, it would be interesting to work on expanding the domain of application for the spectral method. One could cast the dynamics of the H3BP in a different frame which would remove the singularity. In theory, it is then possible that one could solve the SHJB over the entire domain. Also, it would be interesting to investigate the benefit of discontinuous Galerkin methods, which would allow for discontinuities in the solution of the value function.

The Taylor series approach from Chapter 4, which was shown to work for the SHJB equation under certain assumptions, also works for the Fokker-Planck equation (under the same assumptions). This provides the ability to propagate probability distribution functions (PDFs) through the full nonlinear dynamics. Potentially, this could provide the basis for both optimal control and estimation. One difficulty is that the PDF must satisfy the integral constraint that the volume integral over the domain must be unity. This property of PDFs is not satisfied by a truncated power series. However, the mapping between nonlinear functions and polynomials is not one-to-one; there are many functions that can be expressed by a given polynomial. Hence, it should be possible to construct functions whose Taylor series

match to a given order, but also satisfy the integral constraint.

Other work to be done in the future is move beyond simplified uncertainty analysis. The goal is to demonstrate the techniques developed in this dissertation for actual spacecraft trajectories.

Appendices

Appendix A

Numerical Considerations for the Spectral Method with Chebyshev Polynomial Bases

A.1 Even/Odd Symmetry

Often times, the cost function possesses even symmetry, $V(\vec{x}) = V(-\vec{x})$, along with system dynamics that possess odd symmetry, $\vec{a}(\vec{x}) = -\vec{a}(-\vec{x})$. When these two conditions are met, the cost function will retain even symmetry as the solution is propagated backwards in time. Even and odd symmetry allows for more efficient storage and computation as only half of the data describing the full domain needs to be stored. For a general M dimensional problem, with n_i data points along the i-th dimension, the spectral coefficients, C are given by

$$C_{K_0 \cdots K_{M-1}} = 2^M \sum_{i_0=0}^{n_0-1} \cdots \sum_{i_{M-1}=0}^{n_{M-1}-1} V_{i_0 \cdots i_{M-1}} \cos\left(\frac{\pi(i_0+1/2)K_0}{n_0}\right) \cdots \cos\left(\frac{\pi(i_{M-1}+1/2)K_{M-1}}{n_{M-1}}\right), \quad \text{(A.1)}$$

where K_i ranges from 0 to $n_i - 1$, and $V_{i_0 \cdots i_{M-1}}$ are the values of V stored at the Chebyshev nodes. This definition matches the form of the type II discrete cosine transform (DCT), and can be computed quickly using an FFT library (see Section A.2). If V is an even or odd function, then this sum may be evaluated using only half of the data. The following formulae use the first half of the data along the last dimension, although other approaches

are possible. If V is even, then Equation (A.1) evaluates to

$$C_{K_0 \cdots K_{M-1}} = 0, \tag{A.2}$$

if

$$\sum_{j=0}^{M-1} K_j \text{ is odd},$$

and

$$C_{K_0 \cdots K_{M-1}} = 2^{M+1} \sum_{i_0=0}^{n_0-1} \cdots \sum_{i_{M-1}=0}^{n_{M-1}/2-1} V_{i_0 \cdots i_{M-1}} \cos\left(\frac{\pi(i_0+1/2)K_0}{n_0}\right) \cdots \cos\left(\frac{\pi(i_{M-1}+1/2)K_{M-1}}{n_{M-1}}\right), \tag{A.3}$$

if

$$\sum_{j=0}^{M-1} K_j \text{ is even}.$$

Alternatively, if V is an odd function, then

$$C_{K_0 \cdots K_{M-1}} = 2^{M+1} \sum_{i_0=0}^{n_0-1} \cdots \sum_{i_{M-1}=0}^{n_{M-1}/2-1} V_{i_0 \cdots i_{M-1}} \cos\left(\frac{\pi(i_0+1/2)K_0}{n_0}\right) \cdots \cos\left(\frac{\pi(i_{M-1}+1/2)K_{M-1}}{n_{M-1}}\right), \tag{A.4}$$

if

$$\sum_{j=0}^{M-1} K_j \text{ is odd},$$

and

$$C_{K_0 \cdots K_{M-1}} = 0, \tag{A.5}$$

if

$$\sum_{j=0}^{M-1} K_j \text{ is even.}$$

It is worth noting that these forms do not directly correspond to a DCT along the last dimension.

These coefficients may be packed into an array such that the zero elements are not stored. If V is even and we denote the packed form as $\widetilde{C}$, we have

$$\widetilde{C}_{K_0 \cdots K_{M-1}} = \begin{cases} C_{K_0 \cdots (2K_{M-1})}, & \sum_{j=0}^{M-2} K_j \text{ is even} \\ C_{K_0 \cdots (2K_{M-1}+1)}, & \sum_{j=0}^{M-2} K_j \text{ is odd} \end{cases} \tag{A.6}$$

where K_0 through K_{M-2} span the same range as before, but now K_{M-1} ranges from 0 to $n_{M-1}/2-1$. For the first case,

$$C_{K_0 \cdots (2K_{M-1})} = 2^{M+1} \sum_{i_0=0}^{n_0-1} \cdots \sum_{i_{M-1}=0}^{n_{M-1}/2-1} V_{i_0 \cdots i_{M-1}} \cos\left(\frac{\pi(i_0+1/2)K_0}{n_0}\right) \cdots \cos\left(\frac{\pi(i_{M-1}+1/2)K_{M-1}}{n_{M-1}/2}\right), \tag{A.7}$$

which is a DCT of type II along all dimensions. For the second case,

$$C_{K_0 \cdots (2K_{M-1}+1)} = 2^{M+1} \sum_{i_0=0}^{n_0-1} \cdots \sum_{i_{M-1}=0}^{n_{M-1}/2-1} V_{i_0 \cdots i_{M-1}} \cos\left(\frac{\pi(i_0+1/2)K_0}{n_0}\right) \cdots \cos\left(\frac{\pi(i_{M-1}+1/2)(K_{M-1}+1/2)}{n_{M-1}/2}\right), \tag{A.8}$$

which is a DCT of type II along all dimension except the last, which is a DCT of type IV.

For an odd function, the coefficients may be packed as follows:

$$\widetilde{C}_{K_0\cdots K_{M-1}} = \begin{cases} C_{K_0\cdots(2K_{M-1}+1)}, & \sum_{j=0}^{M-2} K_j \text{ is even} \\ C_{K_0\cdots(2K_{M-1})}, & \sum_{j=0}^{M-2} K_j \text{ is odd} \end{cases} \tag{A.9}$$

A.2 Discrete Cosine Transforms

The following are the 1-D forms of the four versions of the DCT, transforming input X to output Y, as defined in FFTW [26]. Multidimensional transforms are simply the separable product of the specified 1-D transforms along each dimension.

Type I: $Y_k = X_0 + (-1)^k X_{n-1} + 2\sum_{j=1}^{n-2} X_j \cos[\pi jk/(n-1)]$

Type II: $Y_k = 2\sum_{j=1}^{n-1} X_j \cos[\pi(j+1/2)k/n]$

Type III: $Y_k = X_0 + 2\sum_{j=1}^{n-1} X_j \cos[\pi j(k+1/2)/n]$

Type IV: $Y_k = 2\sum_{j=1}^{n-1} X_j \cos[\pi(j+1/2)(k+1/2)/n]$

The type II transform is the inverse of the type III and vise verse; the type I and type IV transforms are their own inverses.

Appendix B
Stochastic Maximum Principle

The stochastic maximum principle is the extension of Pontryagin's maximum principle to stochastic systems. For deterministic systems, the maximum principle leads to two coupled ODE's with initial states and terminal costates given, resulting in a boundary value problem which gives necessary conditions for optimality. The idea is similar in the stochastic case, but more involved due to the proper mathematical treatment of the probability space. The two primary complications are due to the need for second-order costates (adjoint variables) and the need for a properly adapted solution. The second order costates are necessary to obtain the correct balance between control and uncertainty. The adapted solution ensures that the non-anticipatory nature of the solution is preserved.

In a deterministic system, time is easily reversed; given a state at some time, the state at any other time (future or past) can be determined. In a stochastic system, we only have knowledge of the past. This information asymmetry complicates the time-reversal of solutions, causing the solution to backward SDEs to be a *pair* of processes. For the dynamics given in Equation (3.26) and cost function in Equation (3.27), the first order adjoint backward SDE is

$$dp(t) = -\left[b_x(t,x^*,u^*)^{\mathrm{T}} p(t) + \sum_{j=1}^{m} \sigma_x^j(t,x^*,u^*)^{\mathrm{T}} q_j(t) - f_x(t,x^*,u^*) \right] dt + q dW(t) \quad \text{(B.1)}$$

$$p(t_f) = -h_x(x^*(t_f)), \quad \text{(B.2)}$$

where x^* is the optimal trajectory, u^* is the optimal control, and $q(t)$ is the unique process

such that (p,q) is an adapted solution. The dynamics and first order adjoint equations can be written analogously to the deterministic Hamiltonian system;

$$dx(t) = H_p(t,x(t),u(t),p(t),q(t))dt + H_q(t,x(t),u(t),p(t),q(t))dW(t) \tag{B.3}$$

$$dp(t) = -H_x(t,x(t),u(t),p(t),q(t))dt + q(t)dW(t) \tag{B.4}$$

$$x(t_0) = x_0 \quad -h_x(x(t_f)), \tag{B.5}$$

where

$$H(t,x,u,p,q) = p^{\mathrm{T}}b(t,x,u) + \mathrm{Tr}\{q^{\mathrm{T}}\sigma(t,x,u)\} - f(t,x,u). \tag{B.6}$$

The second order adjoint backward SDE is

$$\begin{aligned} dP(t) = -\Big[& b_x(t,x^*,u^*)^{\mathrm{T}}P(t) + P(t)b_x(t,x^*,u^*) \\ & + \sum_{j=1}^{m} \left(\sigma_x^j(t,x^*,u^*)^{\mathrm{T}}P(t)\sigma_x^j(t,x^*,u^*) + \sigma_x^j(t,x^*,u^*)^{\mathrm{T}}Q_j(t) + Q_j(t)\sigma_x^j(t,x^*,u^*)\right) \\ & + H_{xx}(t,x^*,u^*,p,q)\Big]dt + \sum_{j=1}^{m} Q_j dW \end{aligned} \tag{B.7}$$

$$P(t_f) = -h_{xx}(x^*(t_f)), \tag{B.8}$$

where $Q(t)$ is the unique process such that (P,Q) is an adapted solution.

The maximum condition is given by

$$\mathscr{H}(t,x^*(t),u^*(t)) = \max_{u\in U} \mathscr{H}(t,x^*(t),u(t)), \tag{B.9}$$

with

$$\mathscr{H}(t,x,u) = H(t,x,u,p(t),q(t)) - \frac{1}{2}\mathrm{Tr}\left\{\sigma(t,x^*,u^*)^{\mathrm{T}}P(t)\sigma(t,x^*,u^*)\right\} + \frac{1}{2}\mathrm{Tr}\left\{[\sigma(t,x,u)-\sigma(t,x^*,u^*)]^{\mathrm{T}}P(t)[\sigma(t,x,u)-\sigma(t,x^*,u^*)]\right\}. \quad \text{(B.10)}$$

B.1 Forward-Backward SDEs and the Four-step Scheme

The stochastic maximum principle results in what is known as a forward-backward stochastic differential equation (FBSDE). A general form of an FBSDE is as follows:

$$dX(t) = b(t,X(t),Y(t),Z(t))dt + \sigma(t,X(t),Y(t),Z(t))dW(t) \quad \text{(B.11)}$$

$$dY(t) = h(t,X(t),Y(t),Z(t))dt + Z(t)dW(t) \quad \text{(B.12)}$$

$$X(0) = X_0, \quad Y(T) = g(X(T)). \quad \text{(B.13)}$$

If we assume $Y(t) = \theta(t,X(t))$, where θ is some function to be determined, then the expansion of Y by Itô's formula is

$$dY(t) = \left[\theta_t(t,X) + b^{\mathrm{T}}(t,X,\theta,Z)\theta_x(t,X) + \frac{1}{2}\mathrm{Tr}\left\{(\sigma\sigma^{\mathrm{T}})(t,X,\theta,Z)\theta_{xx}(t,X)\right\}\right]dt + \theta_x(t,X)\sigma(t,X,\theta,Z)dW(t). \quad \text{(B.14)}$$

Equating the dt and dW terms in Equations (B.12) and (B.14) yields the "four-step scheme" [28].

1. From the dW term, find $z(t,x,y,\rho)$ such that

$$z(t,x,y,\rho) = \rho\sigma(t,x,y,z(t,x,y,\rho)),\ \forall t,x,y,\rho. \quad \text{(B.15)}$$

2. From the dt term, we need to solve the following PDE for $\theta(t,x)$

$$h(t,x,\theta,z(t,x,\theta,\theta_x)) = \theta_t(t,X) + b^{\mathrm{T}}(t,X,\theta,z(t,x,\theta,\theta_x))\theta_x(t,X) + \frac{1}{2}\mathrm{Tr}\left\{(\sigma\sigma^{\mathrm{T}})(t,X,\theta,z(t,x,\theta,\theta_x))\theta_{xx}(t,X)\right\}, \quad \text{(B.16)}$$

$$\theta(T,x) = g(x). \quad \text{(B.17)}$$

3. Use θ and z, solve the SDE

$$dX(t) = b(t,x,\theta(t,X),z(t,X,\theta(t,X),\theta_x(t,X)))dt + \sigma(t,X,\theta(t,X),\theta_x(t,X)))dW(t). \quad \text{(B.18)}$$

4. Set

$$Y(t) = \theta(t,X(t)), \quad \text{(B.19)}$$

$$Z(t) = z(t,X(t),\theta(t,X(t)),\theta_x(t,X(t))). \quad \text{(B.20)}$$

B.2 System Linear in Control

When the above results are applied to a system defined Equations (3.29) and (3.30) with $C = d = 0$, the equations simplify substantially. The adjoint equations are

$$dp(t) = -\left[a_x^{\mathrm{T}} p\right] dt + qdW \quad \text{(B.21)}$$

$$dP(t) = -\left[a_x^{\mathrm{T}} P + Pa_x + \partial^2(p^{\mathrm{T}}a)/\partial x^2\right] dt + \sum_{j=1}^{m} Q_j dW^j. \quad \text{(B.22)}$$

We may solve for the optimal control from the maximum condition in terms of p and q:

$$u^* = R^{-1}(B^{\mathrm{T}}p + D^{\mathrm{T}}q). \quad \text{(B.23)}$$

Substituting this control into the dynamics gives

$$dx(t) = \left[a(t,x) + BR^{-1}B^{\mathrm{T}}p + BR^{-1}D^{\mathrm{T}}q\right]dt + \left[DR^{-1}B^{\mathrm{T}}p + DR^{-1}D^{\mathrm{T}}q\right]dW. \tag{B.24}$$

If we assume that p is some deterministic function of t and x, $p = \theta(t,x)$, then we can expand p with the Itô formula to obtain

$$\begin{aligned} dp = \Big[\theta_t + \left(a + BR^{-1}B^{\mathrm{T}}p + BR^{-1}D^{\mathrm{T}}q\right)^{\mathrm{T}}\theta_x \\ + \frac{1}{2}\mathrm{Tr}\left\{\left(DR^{-1}B^{\mathrm{T}}p + DR^{-1}D^{\mathrm{T}}q\right)\left(DR^{-1}B^{\mathrm{T}}p + DR^{-1}D^{\mathrm{T}}q\right)^{\mathrm{T}}\theta_{xx}\right\}\Big]dt \\ + \left[\theta_x^{\mathrm{T}}\left(DR^{-1}B^{\mathrm{T}}p + DR^{-1}D^{\mathrm{T}}q\right)\right]dW. \end{aligned} \tag{B.25}$$

When this is compared with Equation (B.21), the dW gives q in terms of p (this is step one of the four-step scheme):

$$q = \theta_x^{\mathrm{T}}DR^{-1}B^{\mathrm{T}}p + \theta_x^{\mathrm{T}}DR^{-1}D^{\mathrm{T}}q \tag{B.26}$$

$$\implies q = \left(I - \theta_x^{\mathrm{T}}DR^{-1}D^{\mathrm{T}}\right)^{-1}\theta_x^{\mathrm{T}}DR^{-1}B^{\mathrm{T}}p \tag{B.27}$$

$$= \left(\theta_x^{-1} - DR^{-1}D^{\mathrm{T}}\right)^{-1}DR^{-1}B^{\mathrm{T}}p, \tag{B.28}$$

assuming that the inverse exists and θ_x is symmetric. Substituting this into the control gives

$$u^* = \left[R^{-1} + R^{-1}D^{\mathrm{T}}\left(\theta_x^{-1} - DR^{-1}D^{\mathrm{T}}\right)^{-1}DR^{-1}\right]B^{\mathrm{T}}p, \tag{B.29}$$

which can be simplified with the matrix inversion lemma, Equation (B.31), to

$$u^* = \left(R - D^{\mathrm{T}}\theta_x D\right)^{-1}B^{\mathrm{T}}p. \tag{B.30}$$

The matrix inversion lemma, also know as the Woodbury identity is

$$\left(A+CBC^{\mathrm{T}}\right)^{-1} = A^{-1} - A^{-1}C\left(B^{-1}+C^{\mathrm{T}}A^{-1}C\right)^{-1}C^{\mathrm{T}}A^{-1}. \tag{B.31}$$

Comparing this form of u^* to Equation (3.33), it is clear that the first-order costate is just the gradient of the value function, just as in the deterministic case:

$$p = \theta(t,x) = -\frac{\partial V}{\partial x}, \tag{B.32}$$

$$\frac{\partial \theta}{\partial x} = -\frac{\partial^2 V}{\partial x^2}. \tag{B.33}$$

Appendix C

Stochastic Systems with Multiplicative Noise

C.1 Optimal Control of Linear System with Multiplicative Noise

In the case of linear systems with additive noise, the well-known certainty-equivalence principle states that the form of the optimal feedback control law is unchanged from the deterministic case. When multiplicative noise is considered, the certainty-equivalence principle is no longer valid, although the optimal feedback law is still linear. A continuous-time linear system with multiplicative noise is [31]

$$dX_t = A(t)X_t dt + B(t)U_t dt + D(t,X_t)dW_{1t} + F(t)dW_t. \tag{C.1}$$

The matrix D is of the form

$$D(t,x) = \sum_{i=1}^{n} x_i D_i(t), \tag{C.2}$$

where each D_i is a matrix. The cost (soft constraint) is

$$J = \mathrm{E}\left[\int_{t_0}^{T} \left(X^{\mathrm{T}}Q(t)X + U^{\mathrm{T}}R(t)U\right) dt + X^{\mathrm{T}}Q_f X\right]. \tag{C.3}$$

The optimal control is given by

$$U^* = -L(t)X, \tag{C.4}$$

where

$$L(t) = R^{-1}(t)B^{\mathrm{T}}(t)S(t), \tag{C.5}$$

$$\dot{S}(t) = -A^{\mathrm{T}}(t)S(t) - S(t)A(t) + S(t)B(t)R^{-1}(t)B^{\mathrm{T}}(t)S(t) - Q(t) + \Delta(t,S(t)) \tag{C.6}$$

$$[\Delta(t,S)]_{ij} = \mathrm{Tr}\{D_i^{\mathrm{T}}(t)SD_j(t)\}, \tag{C.7}$$

$$S(T) = Q_f. \tag{C.8}$$

In Equation (C.6), the only term differing from the deterministic case is $\Delta(t,S(t))$.

As mentioned, in the previous section, multiplicative noise can actually help stabilize a system. The following are example solutions for varying system parameters. Common parameters for all cases are $B = 1$, $F = 1$, $Q = 0$, $R = 1/2$. The remaining parameters are as follows:

1. Borderline Stable: $A = .5$, $D = 1$, $t_f = 10$, $Q_f = 10$
2. Stable: $A = .25$, $D = 1$, $t_f = 10$, $Q_f = 10$
3. Very Stable: $A = .25$, $D = 2$, $t_f = 10$, $Q_f = 10$
4. Borderline Stable with High Terminal Cost: $A = .5$, $D = 1$, $t_f = 10$, $Q_f = 1000$
5. Stable with High Terminal Cost: $A = .5$, $D = 1.5$, $t_f = 10$, $Q_f = 1000$
6. Stable with Long Horizon: $A = .5$, $D = 1.5$, $t_f = 50$, $Q_f = 10$

For all cases, the interval was divided into 20,000 time steps and numerical integration was performed using the Milstein scheme, which is strongly convergent with order 1.0. (The Milstein scheme is the proper generalization of the Euler scheme to stochastic systems.)

Notice that although all of the following systems would be unstable without noise, some of the control values are extremely small – essential zero. These are the cases where the noise actually causes sample paths to converge to zero without effort.

C.1.1 Borderline Stable

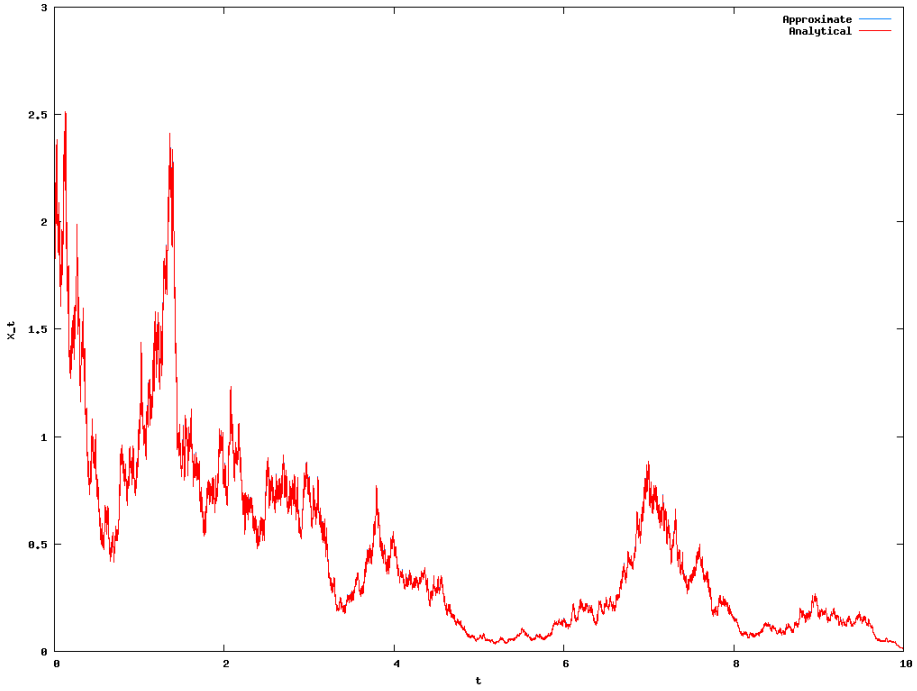

Figure C.1 Sample Path

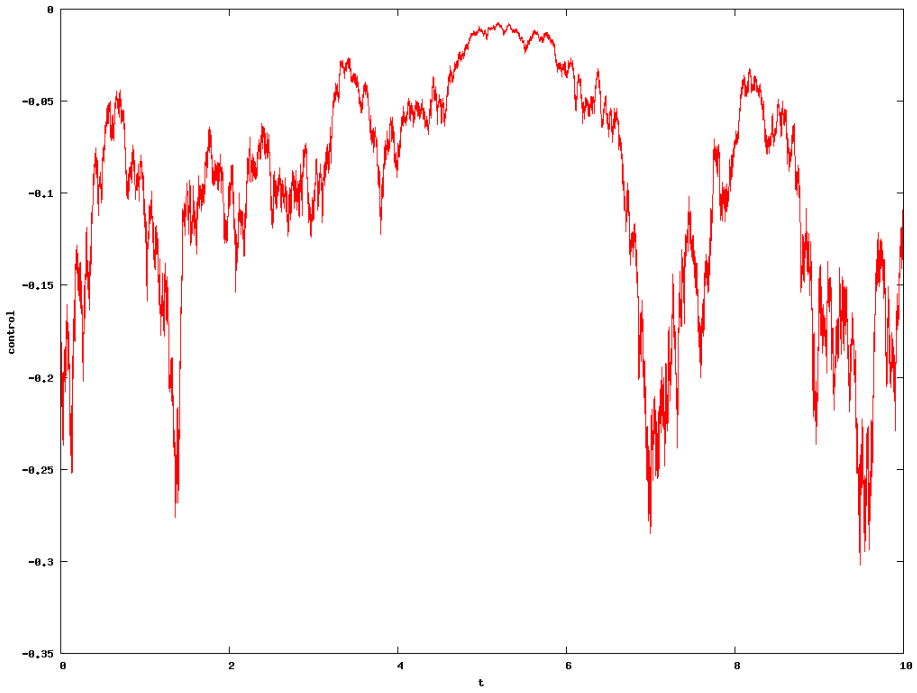

Figure C.2 Control

C.1.2 Stable

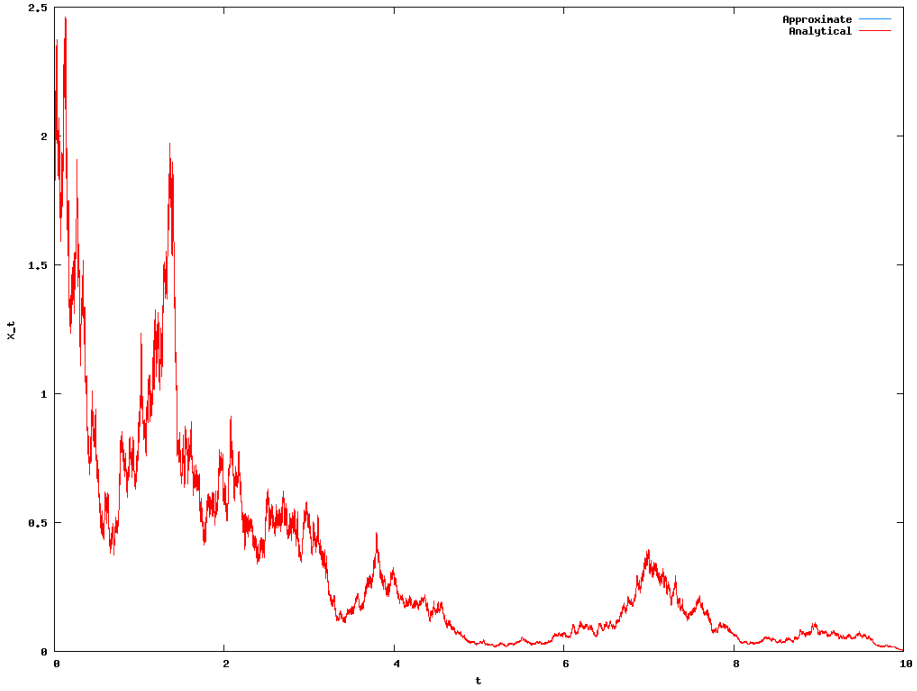

Figure C.3 Sample Path

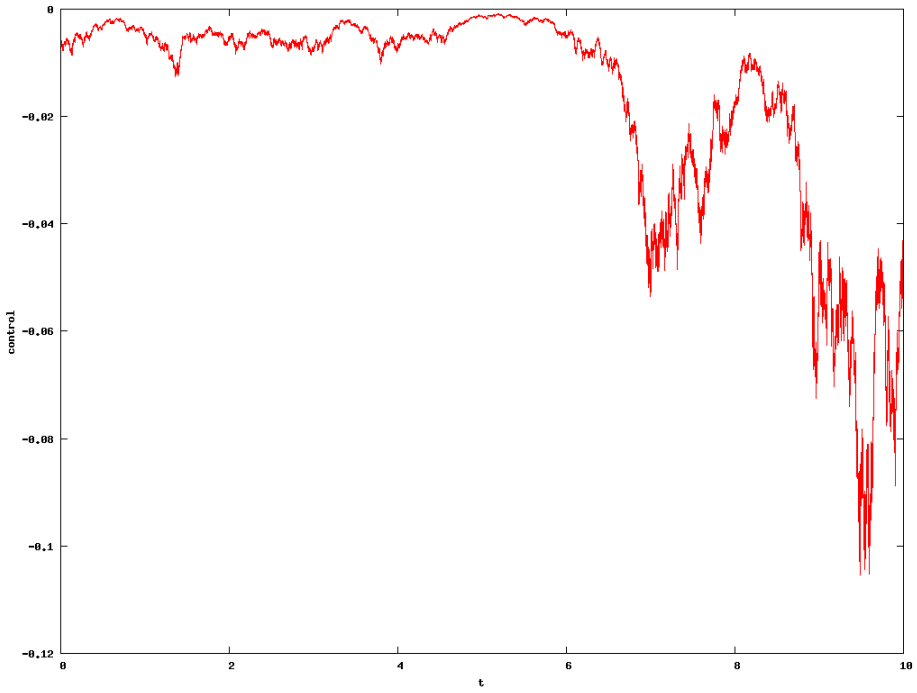

Figure C.4 Control

C.1.3 Very Stable

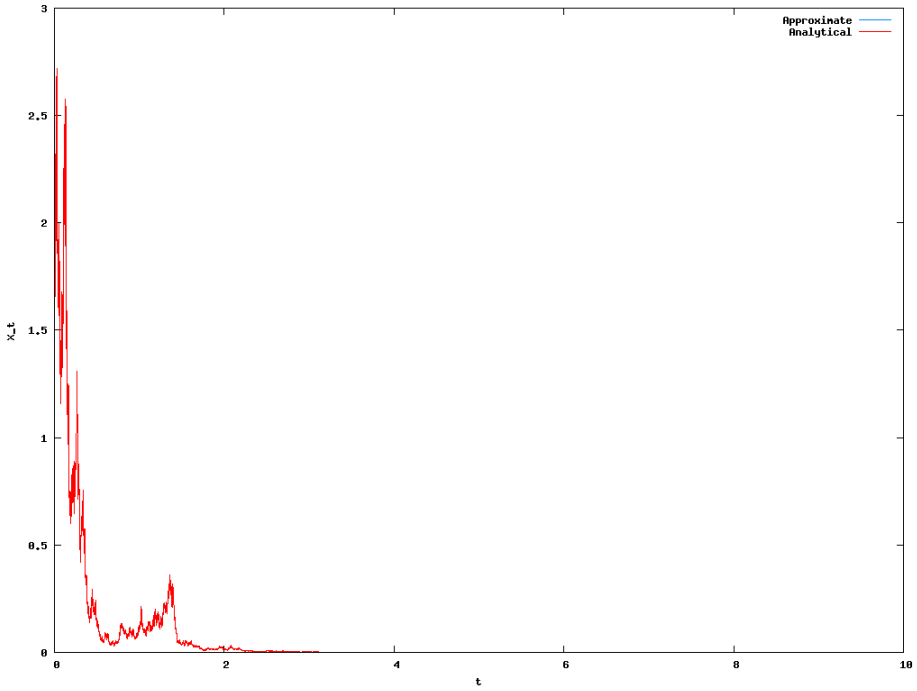

Figure C.5 Sample Path

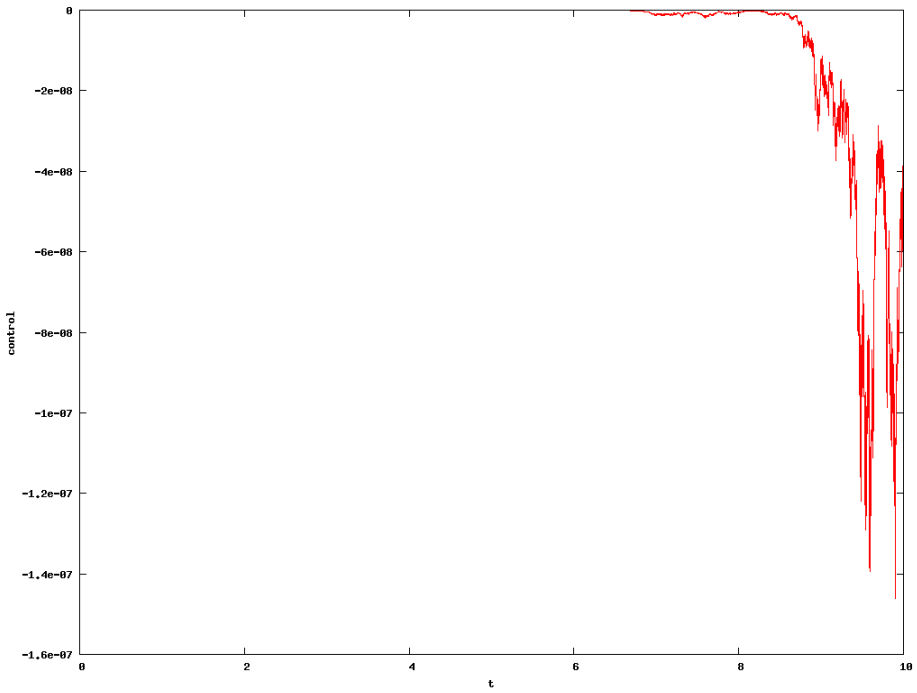

Figure C.6 Control

C.1.4 Borderline Stable with High Terminal Cost

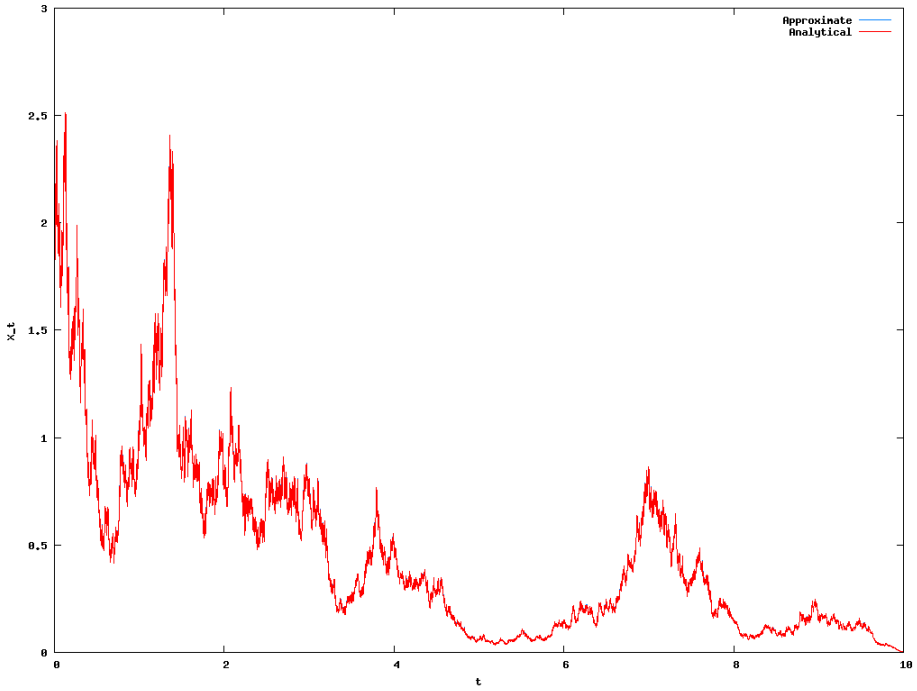

Figure C.7 Sample Path

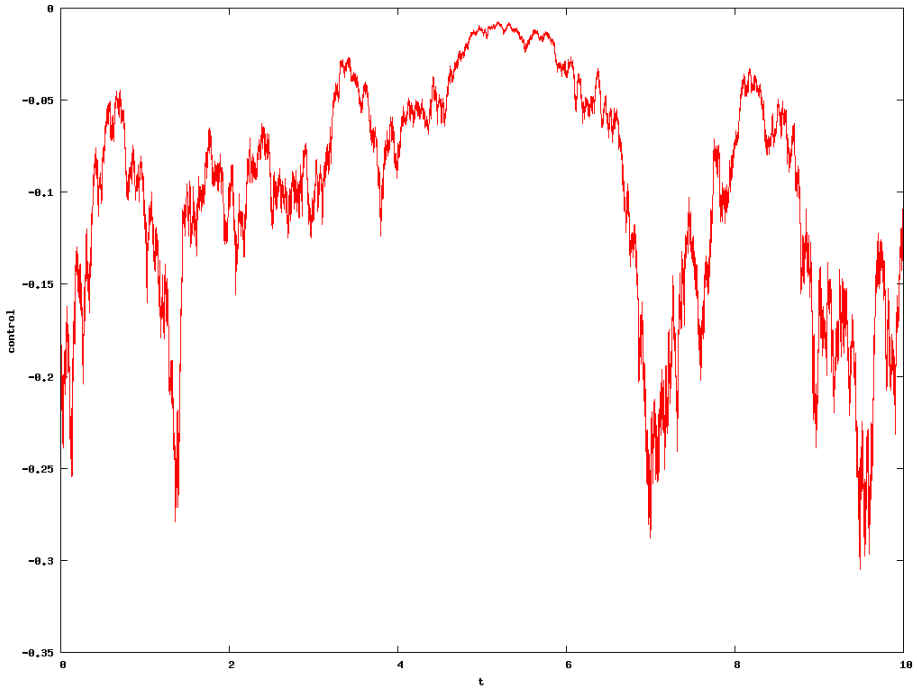

Figure C.8 Control

C.1.5 Stable with High Terminal Cost

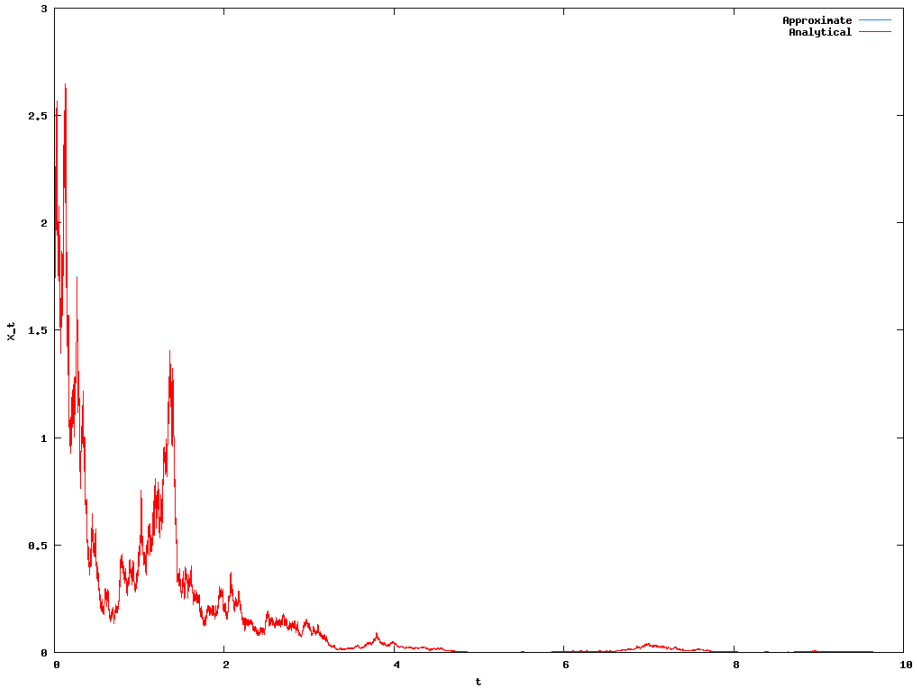

Figure C.9 Sample Path

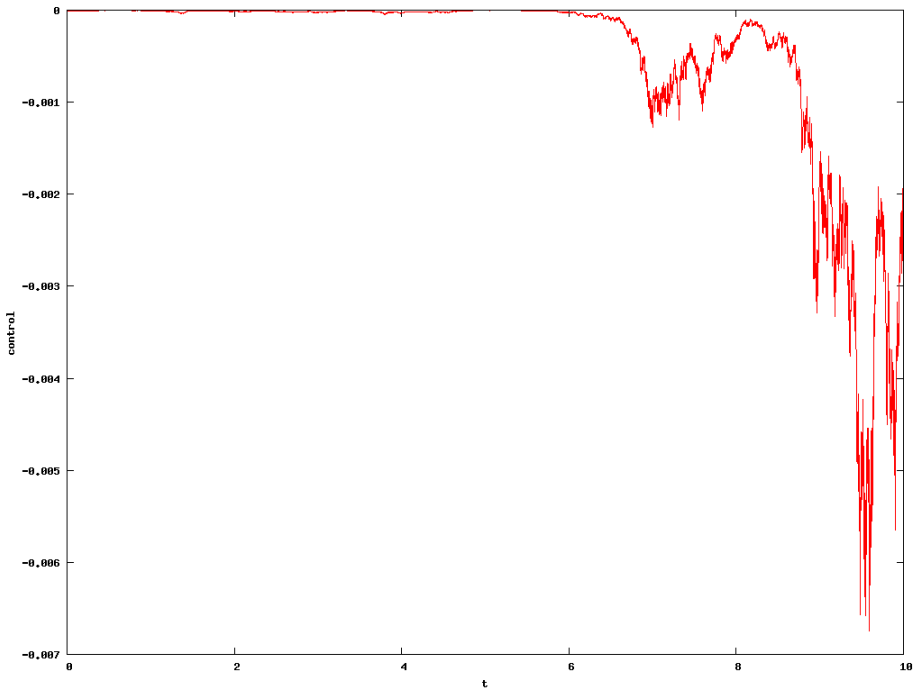

Figure C.10 Control

C.1.6 Stable with High Terminal Cost and Long Horizon

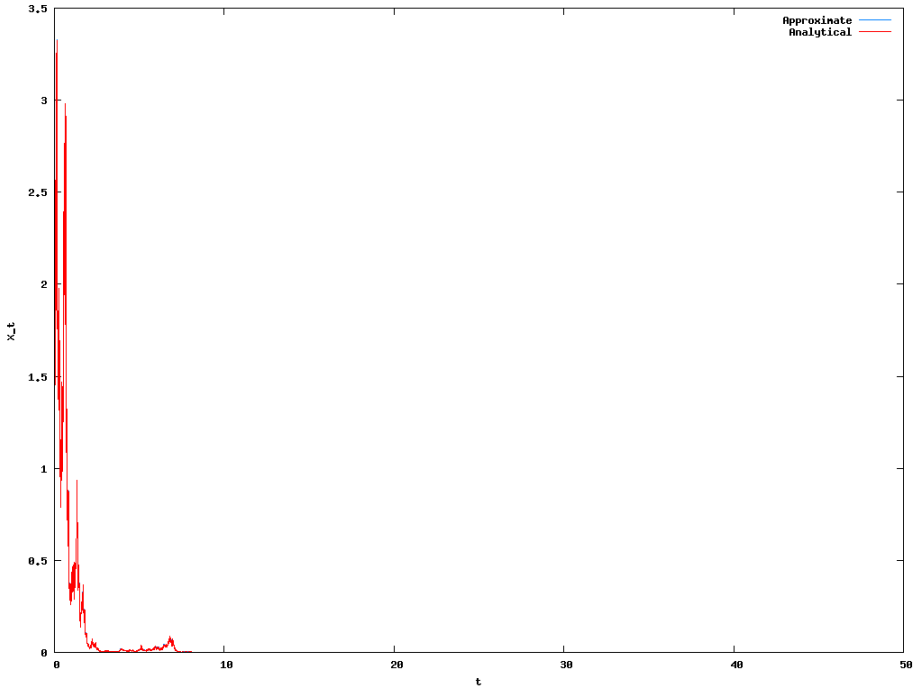

Figure C.11 Sample Path

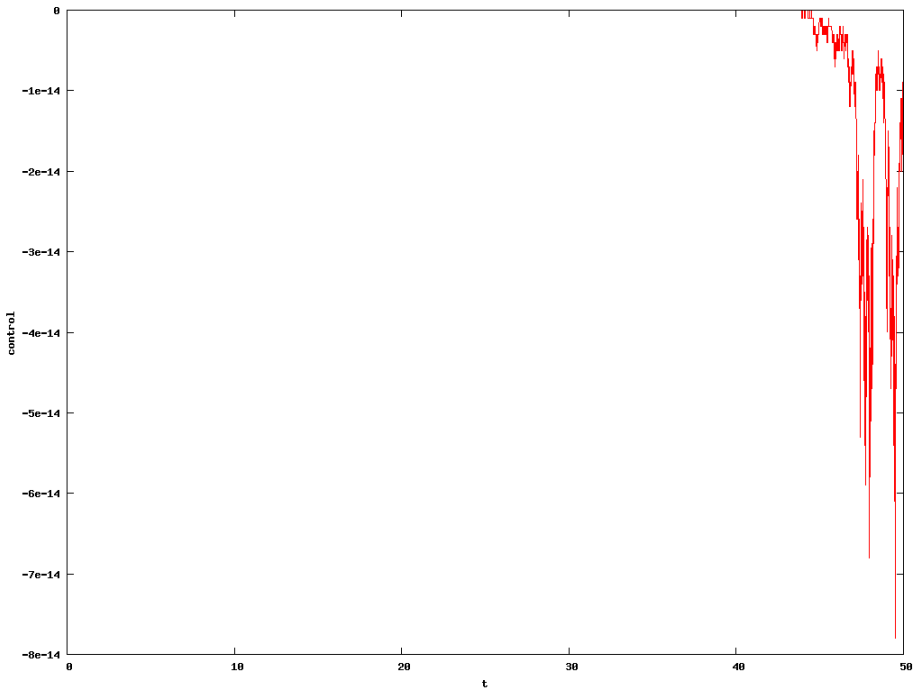

Figure C.12 Control

C.2 Multi-Dimensional Linear System with Multiplicative Noise Example

This is an example of optimal feedback control of a 1 degree of freedom linear system with scalar control and multiplicative noise in the form of Equations (C.1) through (C.3). The system is driven by scalar Brownian motion and defined by the following:

$$A = \begin{bmatrix} 0 & 1 \\ \eta\beta^2 & 0 \end{bmatrix} \quad \begin{cases} \eta = -1, & \text{oscillatory} \\ \eta = 0, & \text{double integrator} \\ \eta = 1, & \text{unstable} \end{cases}$$

$$B = \begin{bmatrix} 0 \\ 1 \end{bmatrix}, \quad D = X_2 \begin{bmatrix} 0 \\ \varepsilon \end{bmatrix}, \; \varepsilon = 0.2 \quad F = Q = 0, \quad R = 1/2, \quad Q_f = 10, \quad T = 10.$$

Note that this system is driven by noise that is proportional to the velocity (X_2). Since the noise is purely multiplicative, the system becomes smooth again as the velocity goes to zero. The following are some examples (all with the same noise realization) with initial condition $[2; 1]$.

C.2.1 Oscillatory

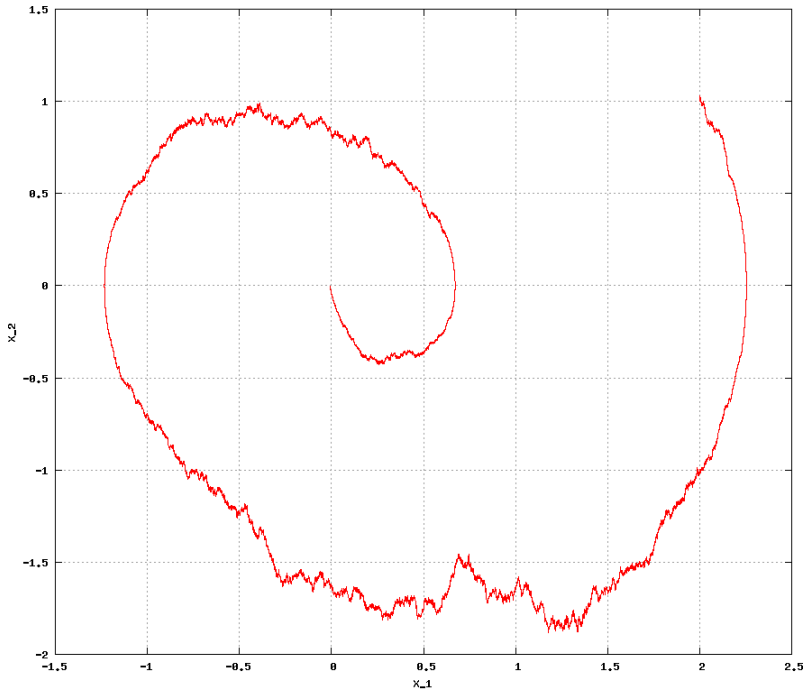

Figure C.13 Oscillatory phase-plane trajectory

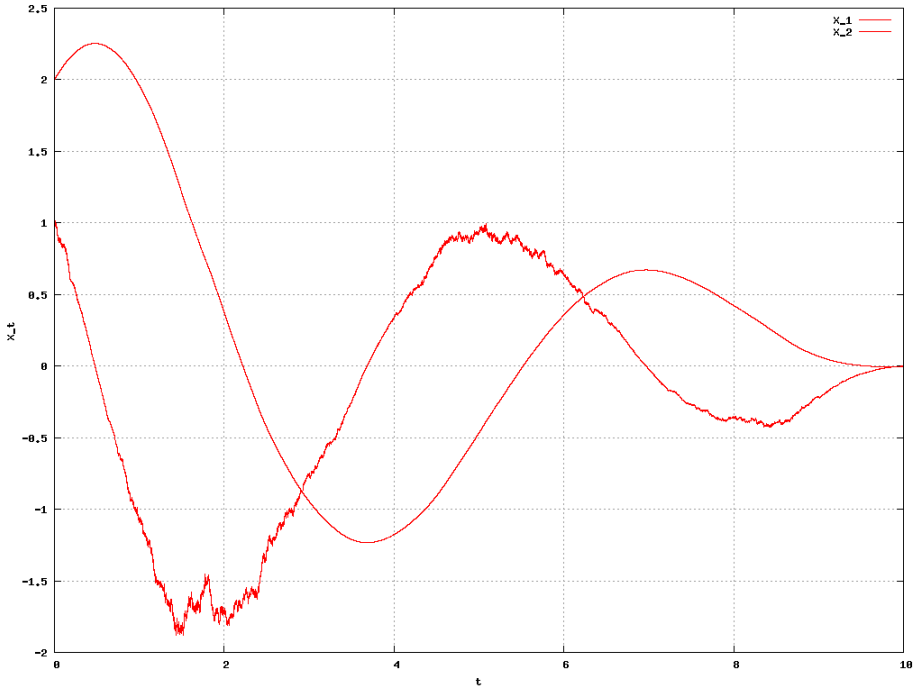

Figure C.14 Oscillatory time history of states

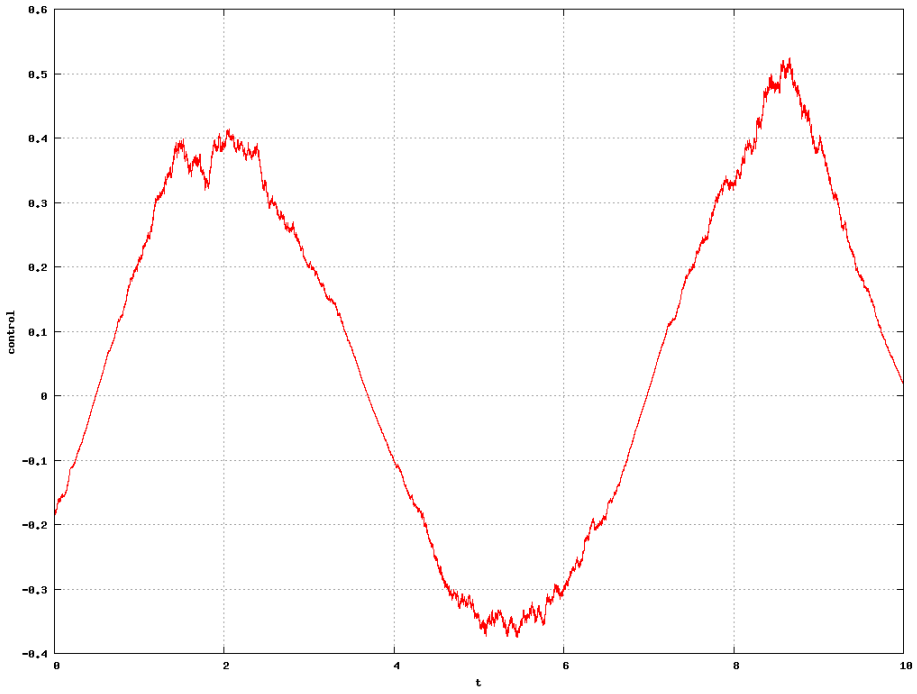

Figure C.15 Oscillatory time history of control

C.2.2 Double Integrator

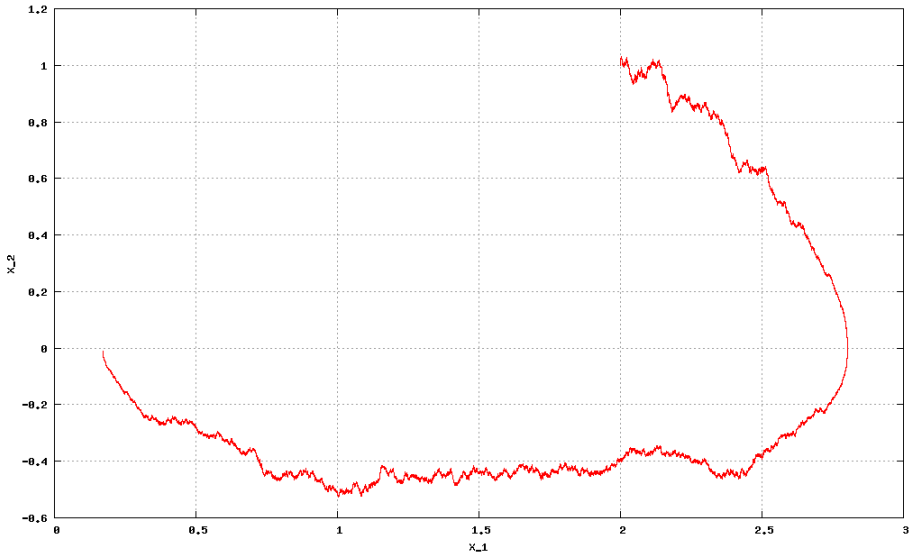

Figure C.16 Double integrator phase-plane trajectory

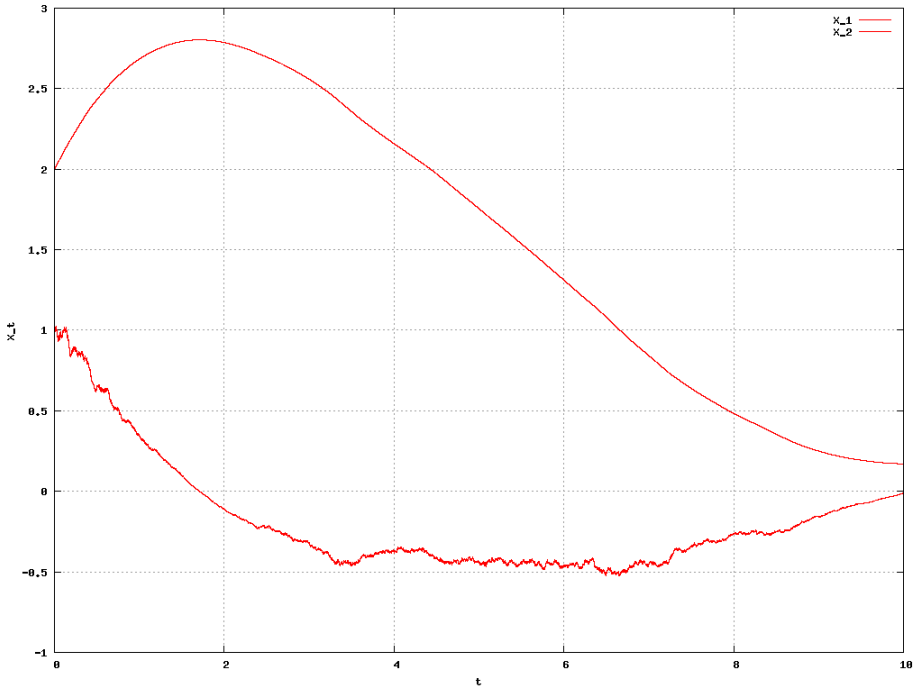

Figure C.17 Double integrator time history of states

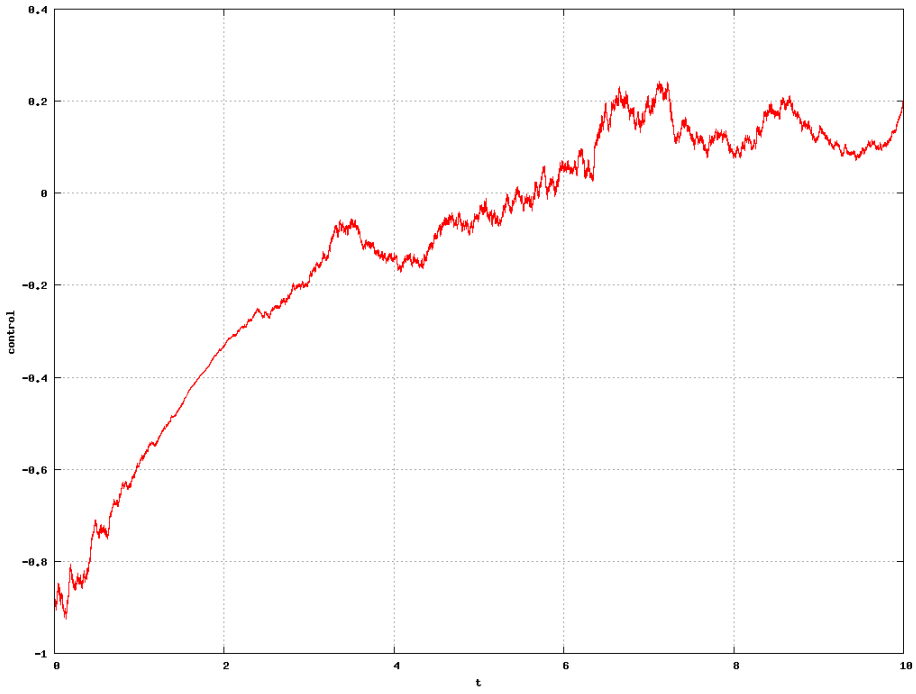

Figure C.18 Double integrator time history of control

C.2.3 Unstable

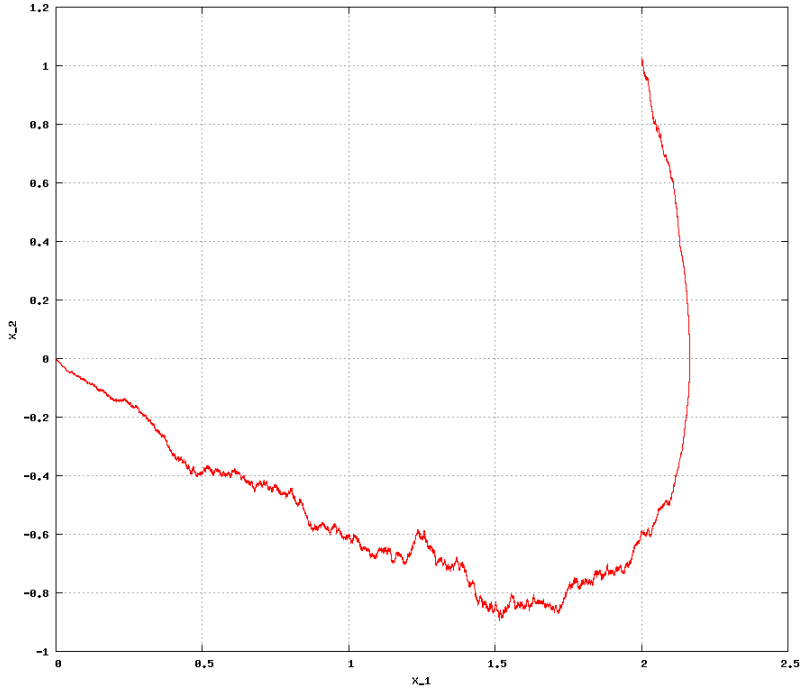

Figure C.19 Unstable phase-plane trajectory

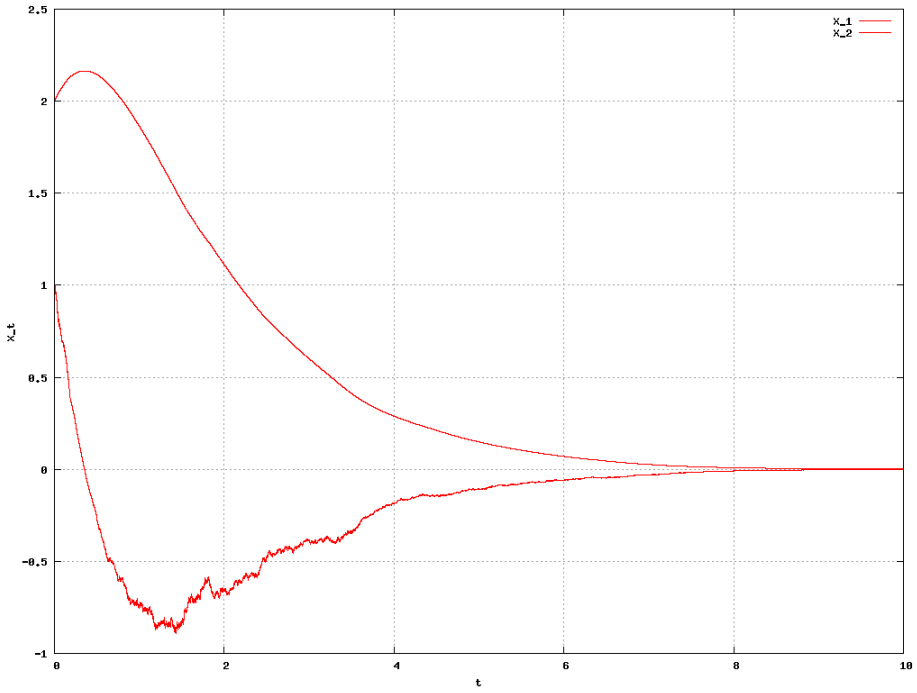

Figure C.20 Unstable time history of states

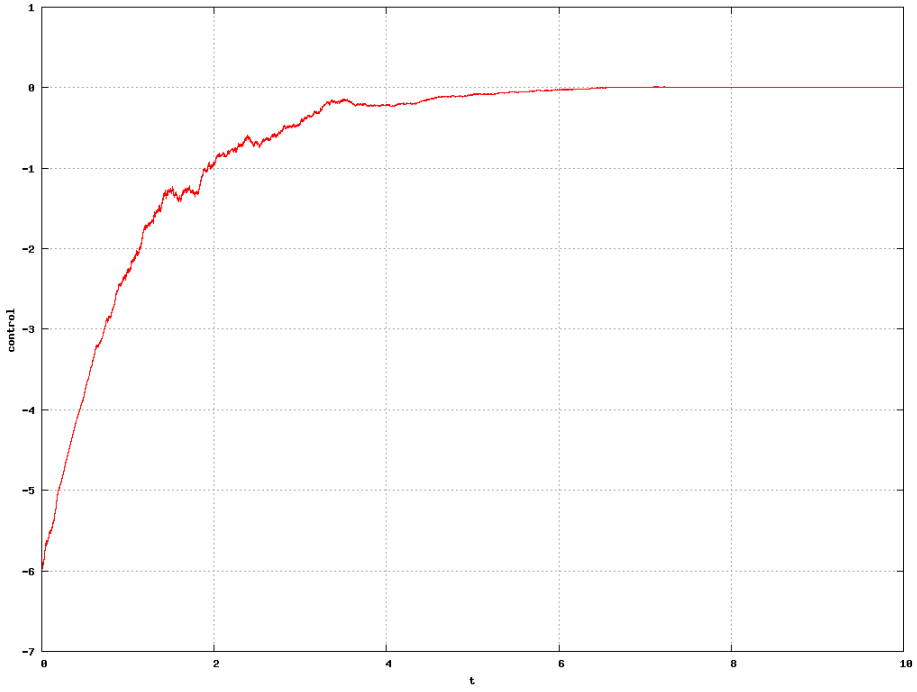

Figure C.21 Unstable time history of control

C.3 Optimal Control of a Stochastic Linear System with Control-Dependent Noise with Quadratic Cost

This section is a summary of Chapter 6 in [28]. For a general linear system with inhomogeneous terms, along with both state and control dependent noise, with multi-dimensional noise, the dynamics are given by

$$dx(t) = [A(t)x(t) + B(t)u(t) + b(t)]dt + \sum_{j=1}^{m}[C_j(t)x(t) + D_j(t)u(t) + \sigma_j(t)]dW^j(t). \quad \text{(C.9)}$$

Let the cost function be

$$J = \mathrm{E}\left[\frac{1}{2}\int_{t_0}^{T}[x^{\mathrm{T}}(t)Q(t)x(t) + 2x^{\mathrm{T}}(t)S^{\mathrm{T}}(t)u(t) + u^{\mathrm{T}}(t)R(t)u(t)]dt + \frac{1}{2}x^{\mathrm{T}}(T)Gx(T)\right]. \quad \text{(C.10)}$$

For compactness, define Z_1, Z_2, and Z_3 as

$$Z_1 = \left(B^{\mathrm{T}}P + S + \sum_{i=1}^{m} D_i^{\mathrm{T}}PC_i\right), \quad \text{(C.11)}$$

$$Z_2 = \left(R + \sum_{i=1}^{m} D_i^{\mathrm{T}}PD_i\right)^{-1}, \quad \text{(C.12)}$$

$$Z_3 = \left(B^{\mathrm{T}}\phi + \sum_{i=1}^{m} D_i^{\mathrm{T}}P\sigma_i\right). \quad \text{(C.13)}$$

The stochastic Riccati equation is

$$\dot{P} + PA + A^{\mathrm{T}}P + \sum_{j=1}^{m} C_j^{\mathrm{T}}PC_j + Q - Z_1^{\mathrm{T}}Z_2Z_1 = 0. \quad \text{(C.14)}$$

with $P(T) = G$. If the system dynamics are non-homogeneous (b or σ_j are not zero), then the following must also be integrated:

$$\dot{\phi} + [A - BZ_2Z_1]^{\mathrm{T}}\phi + \sum_{j=1}^{m}\left[C_j - D_jZ_2Z_1\right]^{\mathrm{T}}P\sigma_j + Pb = 0, \quad \text{(C.15)}$$

with $\phi(T) = 0$.

Define Ψ and ψ as

$$\Psi = Z_2 Z_1 \tag{C.16}$$

$$\psi = Z_2 Z_3. \tag{C.17}$$

The optimal feedback control is then

$$u(t) = -\Psi(t)x(t) - \psi(t). \tag{C.18}$$

The optimal cost-to-go is given by

$$V(t,x) = \frac{1}{2}x^{\mathrm{T}}Px + \phi x + f, \tag{C.19}$$

where $f(T) = 0$ and

$$\dot{f} = \frac{1}{2}\left|Z_1^{-1/2}\psi\right|^2 - \psi^{\mathrm{T}}b - \frac{1}{2}\sum_{i=1}^{m}\sigma_i^{\mathrm{T}}P\sigma_i.$$

Bibliography

[1] Renault, C. A. and Scheeres, D. J., "Statistical Analysis of Control Maneuvers in Unstable Orbital Environments," *Journal of Guidance, Control, and Dynamics*, No. 5, September-October 2003.

[2] Reid, B. M., Gallimore, A. D., Hofer, R. R., Li, Y., and Haas, J. M., "Anode Design and Verification for a 6-kW Hall Thruster," *JANNAF Journal of Propulsion and Energetics*, Vol. 2, No. 1, 2009.

[3] Gustafson, E. D. and Scheeres, D. J., "Optimal Timing of Control-Law Updates for Unstable Systems with Continuous Control," *Journal of Guidance, Control, and Dynamics*, Vol. 32, No. 3, May-June 2009, pp. 878–887.

[4] Gustafson, E. D. and Scheeres, D. J., "Spacecraft Stochastic Optimal Control," *AIAA/AAS Spaceflight Mechanics Meeting*, No. AAS 10-109, 2010.

[5] Gustafson, E. D. and Scheeres, D. J., "Optimal Timing of Control Law Updates for Unstable Systems with Continuous Control," *American Control Conference*, 2008.

[6] Gustafson, E. D. and Scheeres, D. J., "Dynamically Relevant Local Coordinates for Halo Orbits," *Astrodynamics Specialist Conference*, 2008.

[7] Gustafson, E. D. and Scheeres, D. J., "Optimal Control of Uncertain Trajectories Using Continuous Thrust," *AIAA/AAS Spaceflight Mechanics Meeting*, 2007.

[8] Danby, J., *Fundamentals of Celestial Mechanics*, Willmann-Bell, Inc., 2nd ed., 2003.

[9] Bryson, A. E. and Ho, Y.-C., *Applied Optimal Control*, Hemisphere Publishing Corporation, 1975.

[10] Park, C., Guibout, V., and Scheeres, D. J., "Solving Optimal Continuous Thrust Rendezvous Problems with Generating Functions," *AAS/AIAA Astrodynamics Specialist Conference*, No. AAS 03-575, August 2003.

[11] Park, R. S. and Scheeres, D. J., "Nonlinear Mapping of Gaussian State Uncertainties: Theory and Applications to Spacecraft Control and Navigation," *AAS/AIAA Astrodynamics Specialist Conference*, August 2005.

[12] Scheeres, D. J., "Navigation of Spacecraft in Unstable Orbital Environments," *International Conference on Libration Point Orbits and the Applications*, June 2002.

[13] Michalska, H. and Mayne, D. Q., "Robust Receding Horizon Control of Constrained Nonlinear Systems," *IEEE Transactions on Automatic Control*, Vol. 38, No. 11, Nov. 1993.

[14] Bellingham, J., Richards, A., and How, J., "Receding Horizon Control of Autonomous Aerial Vehicles," *American Control Conference*, Vol. 5, 2002, pp. 3741–3746.

[15] Park, C., Guibout, V., and Scheeres, D. J., "Solving Optimal Continuous Thrust Rendezvous Problems with Generating Functions," *Journal of Guidance, Control, and Dynamics*, Vol. 29, No. 2, 2006, pp. 321–331.

[16] Gubner, J. A., *Probability and Random Processes for Electrical and Computer Engineers*, Cambridge University Press, 2006.

[17] Howell, K., "Three-Dimensional, Periodic, 'Halo' Orbits," *Celestial Mechanics and Dynamical Astronomy*, Vol. 32, No. 1, Jan. 1984, pp. 53–71.

[18] Hairer, E., Lubich, C., and Wanner, G., *Geometric Numerical Integration: Structure Preserving Algorithms for Ordinary Differential Equations*, Springer, 2nd ed., 2004, pp. 24–34.

[19] Granlund, T., *GNU Multiple Precision Arithmetic Library*, Edition 4.2.3, July 2008.

[20] Hill, K., Parker, J., Born, G. H., and Demandantez, N., "A Lunar L_2 Navigation, Communication, and Gravity Mission," *AIAA/AAS Astrodynamics Specialist Conference*, Aug. 2006.

[21] Kuninaka, H., Nishiyama, K., Funaki, I., Yamada, T., Shimizu, Y., and Kawaguchi, J., "Powered Flight of Electron Cyclotron Resonance Ion Engines on Hayabusa Explorer," *Journal of Propulsion and Power*, Vol. 23, No. 3, May-June 2007, pp. 544–551.

[22] Kloeden, P. E. and Platen, E., *Numerical Solution of Stochastic Differential Equations*, Springer, 2nd ed., 1999.

[23] Khalil, H. K., *Nonlinear Systems*, Prentice-Hall, Inc., 3rd ed., 2002.

[24] Øksendal, B., *Stochastic Differential Equations*, Springer-Verlag, 1992.

[25] Boyd, J. P., *Chebyshev and Fourier Spectral Methods*, Dover Publications, Inc., 2nd ed., 2001.

[26] Frigo, M. and Johnson, S. G., "The Design and Implementation of FFTW3," *Proceedings of the IEEE*, Vol. 93, No. 2, 2005, pp. 216–231, Special issue on "Program Generation, Optimization, and Platform Adaptation".

[27] Versteeg, H. and Malalasekra, W., *An Introduction to Computational Fluid Dynamics: The Finite Volume Method Approach*, Prentice-Hall, Inc., 1996.

[28] Yong, J. and Zhou, X. Y., *Stochastic Controls: Hamiltonian Systems and HJB Equations*, Springer, 1999.

[29] Brophy, J. R., Marcucci, M. G., Ganapathi, G. B., Garner, C. E., Henry, M. D., Nakazono, B., and Noon, D., "The Ion Propulsion System For Dawn," *AIAA/ASME/SAE/ASEE Joint Propulsion Conference and Exhibit*, No. AIAA 2003-4542, July 2003.

[30] Riley, K. F., Hobson, M. P., and Bence, S. J., *Mathematical Methods of Physics and Engineering*, Cambridge University Press, 2nd ed., 2002.

[31] Bagchi, A., *Optimal Control of Stochastic Systems*, Prentice Hall, 1993.